



VCU

Virginia Commonwealth University
VCU Scholars Compass

Theses and Dissertations

Graduate School

2023

THE IMPACT OF HIV-1 TAT AND MORPHINE ON SPATIAL DISTRIBUTION OF DRUGS IN THE BRAIN.

Austin M. Jones
Virginia Commonwealth University

Follow this and additional works at: <https://scholarscompass.vcu.edu/etd>



Part of the [Animal Experimentation and Research Commons](#), [Immunology of Infectious Disease Commons](#), [Immunotherapy Commons](#), [Laboratory and Basic Science Research Commons](#), [Medicinal Chemistry and Pharmaceutics Commons](#), [Molecular and Cellular Neuroscience Commons](#), [Other Pharmacology, Toxicology and Environmental Health Commons](#), [Other Pharmacy and Pharmaceutical Sciences Commons](#), [Pharmaceutics and Drug Design Commons](#), and the [Pharmacology Commons](#)

© The Author (Austin Matthew Jones)

Downloaded from

<https://scholarscompass.vcu.edu/etd/7454>

This Dissertation is brought to you for free and open access by the Graduate School at VCU Scholars Compass. It has been accepted for inclusion in Theses and Dissertations by an authorized administrator of VCU Scholars Compass. For more information, please contact libcompass@vcu.edu.

THE IMPACT OF HIV-1 TAT AND MORPHINE ON SPATIAL DISTRIBUTION OF
DRUGS IN THE BRAIN.

A thesis/dissertation submitted in partial fulfillment of the requirements for the degree of
Doctor of Philosophy at Virginia Commonwealth University.

By

Austin M. Jones

Bachelor of Science, Virginia Commonwealth University, Richmond, VA, USA

Advisor: Dr. MaryPeace McRae

Assistant Professor, Department of Pharmacotherapy and Outcomes Science

Virginia Commonwealth University

Richmond, VA

May 2023

ACKNOWLEDGEMENTS

First and foremost, I want to thank my advisor **Dr. MaryPeace McRae** for accepting me into her lab and giving me the opportunity to be involved in academic research. Dr. McRae has always been there for me as an advisor/mentor and I cannot thank her enough for the constant support and encouragement both in and out of graduate school.

I also would like to thank the members of my dissertation advisory committee, **Drs. MaryPeace McRae, Kurt Hauser, Joseph McClay, Dayanjan “Shanaka” Wijesinghe, and Matt Halquist**. I sincerely appreciate everyone’s advice and assistance with my research. Thank you all for your patience and time while serving on my committee.

Dr. Eli Rosen for helping me with obtaining my mass spectrometry imaging data and for his patience as I learned how to work with the data.

Drs Sara Nass and Arianna Lark for helping me with surgery techniques and being patient with me while I worked in their lab space.

Drs. Ericka Crouse, Krista Donohoe, and Cynthia Kirkwood for guiding me through my teaching assistantship and always being so positive and kind.

Dr. Kurt Hauser for acting as a second mentor to me during my graduate research and for providing a workspace, mice, and invaluable microscopy help.

The Herb and Nina Demuth Memorial Reward from the American Foundation for Pharmaceutical Education for providing me with the funds needed to continue my research.

The **Deans Office** and **Department of Pharmacotherapy and Outcomes Science** for the administrative assistance throughout my time in graduate school.

Dr. Kara Rademeyer for being my ride-or-die throughout graduate school. Thank you for the endless silent zoom writing sessions, for helping me out during stressful experiments, and for never letting me give up.

Dr. Emily Miller for never failing to put a smile on my face and always having my back. You always inspired me to do better and to always keep moving forward. Thank you for everything you’ve done for me over the years. You inspire me to be a better scientist.

Again, I can't thank **Drs. MaryPeace McRae, Kara Rademeyer, and Emily Miller** enough for their unwavering support and guidance.

My best friend **Ryan Fedoryk** for helping me stay sane while getting my PhD. Without you, I would have pulled all my hair out and stressed myself out to an early grave. Thank you for helping me with designing images for my presentations, posters, and papers. Thanks for helping me relax with video games, for always giving me feedback, even if its not what I want to hear.

My parents, **Lynn and David Powers**, for all their encouragement and support throughout this process and always being there for me. I never would have gotten this far without your help. I love you both to the moon and back.

My sister, **Kendall Powers**, for making my crack up laughing and never letting me forget to take a break every once and a while. You helped me feel validated and confident with my research. I also want to thank my future brother-in-law, **Zack Arrington**, for helping me learn to relax and for being a loving and caring partner to my sister.

Lastly, I need to thank my 4-legged family; first **Jessie and James** for being the best dogs and for all the love, cuddles, and kisses, and then **Barkley, Lucy, Stella, Poco, Murphy, Hazel, and Bentley**. Also, **Buddy, Miller, Smokey, Felix and Susan**, and **Phillip and Joy**. I love you all!

TABLE OF CONTENTS

ACKNOWLEDGEMENTS	II
LIST OF TABLES.....	VIII
LIST OF FIGURES	IX
ABBREVIATIONS	XI
ABSTRACT	XIV
CHAPTER 1: INTRODUCTION.....	1
1A: HUMAN IMMUNODEFICIENCY VIRUS (HIV).....	3
1B: THE BLOOD-BRAIN BARRIER (BBB)	5
1C: HIV AND HIV-ASSOCIATED NEUROCOGNITIVE DISORDERS (HAND).....	9
1D: HIV IN CENTRAL NERVOUS SYSTEM (CNS).....	12
1E: OPIOIDS	15
1F: HIV-1, HIV-1 VIRAL PROTEIN, OPIOIDS, AND THE BLOOD-BRAIN BARRIER.....	17
1G: HIV NEUROPATHOLOGY MOUSE MODELS	19
<i>Tat transgenic model</i>	19
<i>gp120 transgenic model</i>	21
<i>EcoHIV model</i>	23
<i>Humanized models</i>	24
CHAPTER 2: OBJECTIVE AND SPECIFIC AIMS	27
OBJECTIVE	27
AIM 1	29
AIM 2.	29
CHAPTER 3: DEFINE THE EFFECTS OF THE HIV-1 PROTEIN TAT ± MORPHINE ON ANTIRETROVIRAL ACCUMULATION AND DISTRIBUTION WITHIN THE BRAIN	30
3A. INTRODUCTION.....	30

3B. MATERIALS AND METHODS	36
3B.1. <i>Subjects and housing</i>	36
3B.2. <i>Drug Administration</i>	37
3B.3. <i>Surgical Manipulation</i>	38
3B.4. <i>Sample Preparation</i>	39
3B.5. <i>IR-MALDESI MSI Analysis</i>	39
3B.6. <i>LC-MS/MS Analysis</i>	41
3B.7. <i>Immunohistochemistry</i>	41
3B.8. <i>Image Analysis</i>	42
3B.9. <i>Statistical Analysis</i>	43
3C. RESULTS	45
3C.1. <i>The impact of HIV-1 Tat ± morphine on antiretroviral accumulation within the anterior brain region</i>	45
Corpus Callosum	45
Caudoputamen	46
Cerebral Cortex.....	46
Nucleus Accumbens	47
3C.2. <i>The impact of HIV-1 Tat ± morphine on antiretroviral accumulation within the posterior brain region</i>	47
Hippocampal Formation.....	47
Corpus Callosum	47
Cerebral Cortex.....	48
Thalamus	48
Hypothalamus.....	49
3C.3. <i>Sex differences on antiretroviral accumulation within the anterior brain region.</i>	49
Corpus Callosum	49

Caudoputamen	50
Cerebral Cortex.....	50
Nucleus Accumbens	51
<i>3C.4. Sex differences on antiretroviral accumulation within the posterior brain region.</i>	<i>51</i>
Hippocampal Formation.....	51
Corpus Callosum	52
Cerebral Cortex.....	52
Thalamus	53
Hypothalamus	54
<i>3C.5. Antiretroviral analysis via LC-MS/MS.....</i>	<i>54</i>
<i>3C.6. Effects of HIV-1 Tat ± morphine on abacavir accumulation in areas of gliosis</i>	<i>56</i>
<i>3C.7. Sex differences and impacts of gliosis on abacavir concentrations</i>	<i>56</i>
3D. DISCUSSION.....	58
3F. FIGURES	67
CHAPTER 4: EVALUATE MORPHINE ACCUMULATION AND DISTRIBUTION IN THE PRESENCE OF HIV-1 PROTEIN TAT, ARV, AND MORPHINE CO-EXPOSURE.	91
4A. INTRODUCTION.....	91
4B. MATERIALS AND METHODS	93
<i>4B.1. Subjects and housing.....</i>	<i>93</i>
<i>4B.2. Drug Administration.....</i>	<i>94</i>
<i>4B.3. Surgical Manipulation</i>	<i>95</i>
<i>4B.4. Sample Preparation.....</i>	<i>95</i>
<i>4B.5. IR-MALDESI MSI Analysis for Morphine</i>	<i>96</i>
<i>4B.6. Immunohistochemistry.....</i>	<i>97</i>
<i>4B.7. Image Analysis</i>	<i>98</i>
<i>4B.8. Statistical Analysis.....</i>	<i>99</i>

4C. RESULTS	101
4C.1. <i>The effect of HIV-1 Tat on morphine abundance in distinct brain regions</i>	101
4C.2. <i>Sex differences in morphine abundance in the presence of antiretroviral drugs ± HIV-1 Tat</i>	101
4C.3. <i>Sex-based response to HIV-1 Tat on morphine accumulation in the brain</i>	103
4C.4. <i>Effects of HIV-1 Tat on morphine abundance in areas of gliosis</i>	104
4D. DISCUSSION.....	105
4E. FIGURES	110
CHAPTER 5: CONCLUSIONS.....	118
APPENDICES	121
APPENDIX I: MSI IONS	122
APPENDIX II: ANTERIOR AND POSTERIOR REGIONS OF INTEREST	123
APPENDIX III: ABACAVIR CONCENTRATION CODING SCRIPTS.....	124
APPENDIX IV: MORPHINE ABUNDANCE CODING SCRIPTS	138
APPENDIX V: IR-MALDESI MSI AND IHC IMAGE CO-REGISTRATION	147
REFERENCES	148

LIST OF TABLES

TABLE 1: SIGNIFICANT POST HOC TESTS DETECTED WHEN ANALYZING MORPHINE ABUNDANCE \pm HIV-1 TAT.	115
TABLE 2: SIGNIFICANT POST HOC TESTS ANALYZING MORPHINE ABUNDANCE \pm HIV-1 TAT IN MALE AND FEMALE MICE.	116
TABLE 3: ADDITIONAL SIGNIFICANT POST HOC TESTS DETECTED WHEN ANALYZING MORPHINE ABUNDANCE BETWEEN MALE AND FEMALE MICE \pm HIV-1 TAT.	117

LIST OF FIGURES

FIGURE 1: BRAIN SLICING SCHEMA ILLUSTRATING THE GEOGRAPHICAL LOCATION OF THE BRAIN SLICES OBTAINED FROM THE ANTERIOR AND POSTERIOR SECTIONS OF THE MOUSE BRAIN, AS WELL AS THE PORTION OF THE BRAIN USED FOR LC-MS/MS ANALYSIS	67
FIGURE 2: THE EFFECTS OF HIV-1 TAT AND MORPHINE ON ABACAVIR CONCENTRATIONS IN THE ANTERIOR CORPUS CALLOSUM USING IR-MALDESI MSI.....	68
FIGURE 3: THE EFFECTS OF HIV-1 TAT AND MORPHINE ON ABACAVIR CONCENTRATIONS IN THE CAUDOPUTAMEN USING IR-MALDESI MSI	69
FIGURE 4: THE EFFECTS OF HIV-1 TAT AND MORPHINE ON ABACAVIR CONCENTRATIONS IN THE ANTERIOR CEREBRAL CORTEX USING IR-MALDESI MSI	70
FIGURE 5: THE EFFECTS OF HIV-1 TAT AND MORPHINE ON ABACAVIR CONCENTRATIONS IN THE NUCLEUS ACCUMBENS USING IR-MALDESI MSI	71
FIGURE 6: THE EFFECTS OF HIV-1 TAT AND MORPHINE ON ABACAVIR CONCENTRATIONS IN THE HIPPOCAMPAL FORMATION USING IR-MALDESI MSI	72
FIGURE 7: THE EFFECTS OF HIV-1 TAT AND MORPHINE ON ABACAVIR CONCENTRATIONS IN THE POSTERIOR CORPUS CALLOSUM USING IR-MALDESI MSI	73
FIGURE 8: THE EFFECTS OF HIV-1 TAT AND MORPHINE ON ABACAVIR CONCENTRATIONS IN THE POSTERIOR CEREBRAL CORTEX USING IR-MALDESI MSI	74
FIGURE 9: THE EFFECTS OF HIV-1 TAT AND MORPHINE ON ABACAVIR CONCENTRATIONS IN THE THALAMUS USING IR-MALDESI MSI	75
FIGURE 10: THE EFFECTS OF HIV-1 TAT AND MORPHINE ON ABACAVIR CONCENTRATIONS IN THE HYPOTHALAMUS USING IR-MALDESI MSI.....	76
FIGURE 11: EFFECTS OF HIV-1 TAT AND MORPHINE ON ABACAVIR CONCENTRATIONS IN THE ANTERIOR CORPUS CALLOSUM IN MALES (A) AND FEMALES (B) USING IR-MALDESI MSI.....	77
FIGURE 12: EFFECTS OF HIV-1 TAT AND MORPHINE ON ABACAVIR CONCENTRATIONS IN THE CAUDOPUTAMEN IN MALES (A) AND FEMALES (B) USING IR-MALDESI MSI	78
FIGURE 13: EFFECTS OF HIV-1 TAT AND MORPHINE ON ABACAVIR CONCENTRATIONS IN THE ANTERIOR CEREBRAL CORTEX IN MALES (A) AND FEMALES (B) USING IR-MALDESI MSI	79
FIGURE 14: EFFECTS OF HIV-1 TAT AND MORPHINE ON ABACAVIR CONCENTRATIONS IN THE NUCLEUS ACCUMBENS IN MALES (A) AND FEMALES (B) USING IR-MALDESI MSI.....	80

FIGURE 15: EFFECTS OF HIV-1 TAT AND MORPHINE ON ABACAVIR CONCENTRATIONS IN THE HIPPOCAMPAL FORMATION IN MALES (A) AND FEMALES (B) USING IR-MALDESI MSI.....	81
FIGURE 16: EFFECTS OF HIV-1 TAT AND MORPHINE ON ABACAVIR CONCENTRATIONS IN THE POSTERIOR CORPUS CALLOSUM IN MALES (A) AND FEMALES (B) USING IR-MALDESI MSI.....	82
FIGURE 17: EFFECTS OF HIV-1 TAT AND MORPHINE ON ABACAVIR CONCENTRATIONS IN THE POSTERIOR CEREBRAL CORTEX IN MALES (A) AND FEMALES (B) USING IR-MALDESI MSI	83
FIGURE 18: EFFECTS OF HIV-1 TAT AND MORPHINE ON ABACAVIR CONCENTRATIONS IN THE THALAMUS IN MALES (A) AND FEMALES (B) USING IR-MALDESI MSI	84
FIGURE 19: EFFECTS OF HIV-1 TAT AND MORPHINE ON ABACAVIR CONCENTRATIONS IN THE HYPOTHALAMUS IN MALES (A) AND FEMALES (B) USING IR-MALDESI MSI	85
FIGURE 20: EFFECTS OF HIV-1 TAT AND MORPHINE ON ABACAVIR CONCENTRATIONS IN MALES (A) AND FEMALES (B) USING LC-MS/MS	86
FIGURE 21: EFFECTS OF HIV-1 TAT AND MORPHINE ON DOLUTEGRAVIR CONCENTRATIONS IN MALES (A) AND FEMALES (B) USING LC-MS/MS	87
FIGURE 22: EFFECTS OF HIV-1 TAT AND MORPHINE ON LAMIVUDINE CONCENTRATIONS IN MALES (A) AND FEMALES (B) USING LC-MS/MS	88
FIGURE 23: MORPHINE AND HIV-1 TAT-MEDIATED EFFECTS ON ABACAVIR CONCENTRATIONS EVALUATED USING THE RATIO OF ABACAVIR CONCENTRATIONS WITH GFAP+ AREAS TO GFAP-AREAS	89
FIGURE 24: MORPHINE-MEDIATED EFFECTS ON ABACAVIR CONCENTRATIONS EVALUATED USING THE RATIO OF ABACAVIR CONCENTRATIONS WITH GFAP+ AREAS TO GFAP- AREAS.....	90
FIGURE 25: MORPHINE ACCUMULATION AND DISTRIBUTION, USING BOTH MALE AND FEMALE MICE, IS INCREASED IN THE PRESENCE OF HIV-1 TAT WITHIN THE ANTERIOR.....	110
FIGURE 26: HIV-1 TAT STATUS IMPACTS MORPHINE LEVELS IN FEMALE, BUT NOT MALE, MICE.....	111
FIGURE 27: EFFECTS OF HIV-1 TAT ON MORPHINE ACCUMULATION WITHIN THE POSTERIOR BRAIN SECTION IN MALES (A) AND FEMALES (B) ACROSS ALL REGIONS OF INTEREST.	112
FIGURE 28: SEX DIFFERENCES IN MORPHINE ABUNDANCE WERE DETECTED IN TAT(-) AND TAT(+) MICE WITHIN THE ANTERIOR (A,B) AND POSTERIOR (C,D) BRAIN SECTIONS	113
FIGURE 29: CHANGES IN MORPHINE ACCUMULATION DEMONSTRATES INTERACTIVE EFFECTS BETWEEN HIV-1 TAT AND SEX WITHIN AREAS OF GLIOSIS IN THE ANTERIOR (A) BUT NOT POSTERIOR (B) BRAIN SECTIONS	114

ABBREVIATIONS

HIV = Human Immunodeficiency Virus

cART = Combination antiretroviral therapy

HAND = HIV-associated neurocognitive disorders

CNS = Central nervous system

BBB = Blood-brain barrier

PLWH = People living with HIV

AIDS = Acquired immunodeficiency syndrome

IDU = Injection drug users

JAM = Junctional adhesion molecules

ZO = Zonula occludens

P-gp = P-glycoprotein

BCRP = Breast Cancer Resistance Protein

OCT1 = Organic Cation Transporter 1

OCT2 = Organic Cation Transporter 2

SLC = Solute carrier

ANI = Asymptomatic neurocognitive impairment

HAD = HIV-associated dementia

CSF = Cerebrospinal fluid

NF- κ B = Nuclear factor-kappa B

MDM = monocyte-derived macrophages

BMEC = Brain microvascular endothelial cell

SIV = Simian immunodeficiency virus

MLCK = Myosin light chain kinase

FAK = focal adhesion kinase

MOR = Mu (μ) opioid receptor

DOR = Delta (δ) opioid receptor

KOR = Kappa (κ) opioid receptor

Tat = Transactivator of transcription

gp120 = HIV envelope glycoprotein

ROS = Reactive oxygen species

RNS = Reactive nitrogen species

GFAP = Glial fibrillary acidic protein

TNF α = Tumor necrosis factor alpha

IL-6 = Interleukin-6

CAT-1 = Cationic acid transporter 1

PWID = People who inject drugs

IR-MALDESI MSI = Infrared matrix-assisted laser desorption electrospray ionization
mass spectrometry imaging

LC-MS/MS = Liquid chromatography-tandem mass spectrometry

cAMP = Cyclic AMP

MAPK = Mitogen-activated protein kinase

rtTA = Reverse tetracycline transactivator

TRE = Tetracycline-responsive element

IHC = immunohistochemistry

ANOVA = Analysis of variance

ABC = ATP-binding cassette

DTG = Dolutegravir

3TC = Lamivudine

ABSTRACT

Despite combination antiretroviral therapy effectively suppressing HIV within the periphery, the central nervous system (CNS) remains affected by the virus. Approximately half of people living with HIV will experience HIV-associated neurocognitive disorders (HAND) or neuroHIV. Concurrent opioid use exacerbates neuroHIV by promoting neuroinflammation, viral replication, and potentially altering the antiretroviral concentrations within the brain.

Using a transgenic mouse that expresses the HIV-1 Tat protein, we examined the effects of Tat and morphine on antiretroviral accumulation and distribution and the effects of Tat on morphine accumulation within the brain using infrared matrix-assisted laser desorption electrospray ionization with mass spectrometry imaging (IR-MALDESI-MSI). After Tat induction, antiretrovirals (abacavir, dolutegravir, and lamivudine) \pm morphine were continuously delivered for 5 days. Brains were harvested and cryosectioned and slices were imaged using IR-MALDESI-MSI. Multiple brain regions were examined.

The present study revealed that morphine exposure resulted in significantly decreased antiretroviral concentrations in the anterior and posterior brain sections. Interestingly, male mice experienced greater morphine-associated decreases in antiretroviral concentrations than females. The study also assessed whether changes in both antiretroviral and morphine concentrations were associated with areas of activated glia, using GFAP as a marker for glial activation. Differences in antiretroviral concentrations within areas of glial activation differed among treatments based on sex.

The findings from this study highlight the importance of monitoring opioid use in patients with HIV, as antiretroviral medications may become less efficacious within the CNS when co-exposed with opioids, which may contribute to the worsening of neuroHIV.

CHAPTER 1: Introduction

Currently there are roughly 38.4 million people in the world living with HIV (UNAIDS, 2022). Although combination antiretroviral therapy (cART) can effectively reduce the virus to non-detectable levels and improve health outcomes, still half of HIV-infected people will experience HIV-associated neurocognitive disorders (HAND) (Rumbaugh & Tyor, 2015; Sacktor et al., 2002). Even though severe cases of HAND have decreased due to cART, the more mild forms of HAND continue to negatively affect patients, such as learning and memory deficits, and decreased executive functioning (Alfahad & Nath, 2013). Studies have also indicated high persisting rates of mild-to-moderate neurocognitive impairment in patients undergoing cART (R. Ellis et al., 2007). HAND may persist due to several reasons, including persistent HIV replication in the brain, the effects of aging on the brain, and central nervous system (CNS) toxicity from long-term antiretroviral (ARV) therapy (Gannon et al., 2011). Neuroinflammation from HIV infection, which leads to neurodegeneration, may also contribute to the development of HAND (Fauci & Marston, 2015; Saylor et al., 2016). Another reason why HAND may persist is due to insufficient viral control within the brain due to poor penetration of ARVs across the blood-brain barrier (BBB) (Spudich & González-Scarano, 2012). While cART has proven to decrease viral loads primarily peripherally, HIV 'hides' in certain areas of the body called reservoir sites, notably the brain, and can later reactivate and contribute to systemic infection (Nath, 2015; Saylor et al., 2016; Valcour et al., 2013). Other HIV reservoir sites include the lungs, kidney, liver, and gut (Nath, 2015; Saylor et al., 2016; Valcour et al., 2013).

Opioid misuse worsens the negative effects of HIV infection, including the progression of HIV into AIDS, and increasing the severity/incidence of HAND (D. Byrd et al., 2012; Kumar et al., 2006; McArthur et al., 2010; Peterson et al., 1990). Furthermore, people who inject drugs are at an increased risk of getting HIV, either by sharing HIV-infected needles or by risky sexual behavior, with a large population of people infected with HIV ($\frac{1}{3}$) claiming to have abused opioids (J. E. Bell et al., 1998; Reddy et al., 2012). People living with HIV (PLWH) who abuse opioids have reportedly higher viral loads compared to people with HIV who do not abuse opioids (Kerr et al., 2012; J. Kim et al., 2021; Lu & Wang, 2020). Exposure to both HIV and opioids can weaken the immune system and increase the rate and replication of HIV (Hauser et al., 2012; Kumar et al., 2006; Roy et al., 2011). Evidence even suggests PLWH who receive cART, yet continue abusing opioids, are more likely to experience increased rates and severity of HAND compared to those not abusing opioids (D. Byrd et al., 2012; Lu & Wang, 2020; Murphy et al., 2019; Robinson-Papp et al., 2012). While neurocognitive deficits have been reported in PLWH, people who abuse opioids experience increased deficits, such as the worsening of memory (D. Byrd et al., 2012; Fitting et al., 2020; Meyer et al., 2013). Specifically the μ -opioid receptor agonist, morphine, has been shown to increase HIV viral loads and viral progression (Kumar et al., 2006; McLane et al., 2014).

Opioid abuse can increase the incidence of both HAND and HIV encephalitis (J. E. Bell et al., 1998; D. A. Byrd et al., 2011; Roberts & Goralski, 2008), while also exacerbating cognitive impairment (J. E. Bell et al., 2006; Bruce-Keller et al., 2008; Fitting et al., 2010; Hauser et al., 2012; Heaton et al., 2004; Leibrand et al., 2019;

McLane et al., 2018; Robinson-Papp et al., 2012; Roy et al., 2011) and CNS inflammation (Anthony et al., 2008; Bruce-Keller et al., 2008; D. Byrd et al., 2012; Chen et al., 2020; El-Hage et al., 2006; Hauser et al., 2007; Peng et al., 2000) and HIV progression into acquired immunodeficiency syndrome (AIDS) (Kumar et al., 2006). In fact, studies have demonstrated that opioids, particularly morphine, can increase viral replication in infected macrophages and microglia (Fitting et al., 2010; Hauser et al., 2012; Kumar et al., 2006; Peterson et al., 1990), glial activation (Bruce-Keller et al., 2008; El-Hage et al., 2006, 2008; Persidsky et al., 1999; Persidsky & Gendelman, 2003), and cytokine production (J. E. Bell et al., 2006; D. Byrd et al., 2012; El-Hage et al., 2006, 2008; Fitting et al., 2010; McLane et al., 2018; Peng et al., 2000). While much is known about the negative impact of opioid and HIV co-exposure on several aspects of brain function, less is known about the impact of opioids on the ability of ARVs to effectively penetrate into the brain.

1A: Human Immunodeficiency Virus (HIV)

Human immunodeficiency virus (HIV) is a lentivirus, a type of retrovirus, that infects cells of the human immune system such as CD4-positive T-cells and macrophages, which are key components of the cellular immune system, and destroys or impairs their function (Okoye & Picker, 2013; UNAIDS, 2022). HIV infection results in the progressive depletion of the immune system, leading to immunodeficiency. The immune system is considered immunodeficient when it can no longer fulfill its role of fighting off infection and diseases (Okoye & Picker, 2013; UNAIDS, 2022). People suffering with immunodeficiency are much more vulnerable to a wide range of infections, such as tuberculosis and *Pneumocystis* pneumonia, and cancers, including

Kaposi sarcoma, aggressive B-cell non-Hodgkin lymphoma, and cervical cancer (*HIV Infection and Cancer Risk - NCI, 2017; Opportunistic Infections | Living with HIV | HIV Basics | HIV/AIDS | CDC, 2022; UNAIDS, 2022*). Since these diseases take advantage of a weakened immune system, they are commonly referred to as opportunistic infections. HIV infection overtime leads to the development of acquired immunodeficiency syndrome (AIDS), the collection of symptoms and infections associated with acquired deficiency of the immune system (*UNAIDS, 2022*). Without treatment, HIV infection can advance to AIDS in approximately 10 years (*The Stages of HIV Infection | NIH, n.d.; UNAIDS, 2022*). Furthermore, people diagnosed with AIDS, who remain untreated, typically have a survival rate of 2-3 years (*About HIV/AIDS | HIV Basics | HIV/AIDS | CDC, 2022; Poorolajal et al., 2016*).

HIV was first discovered in the United States in early 1980s, with higher infection rates seen in young, gay and bisexual men, African American and Latino populations, an injection drug users (IDU) (*Adler, 2001; High-Impact HIV Prevention: CDC's Approach to Reducing HIV Infections in the United States, n.d.; Sharp & Hahn, 2011*). The number of AIDS-related deaths continued to rise until the introduction of combination antiretroviral therapy (cART) in 1996. As cART quickly became established within clinical care, the degree of deaths due to AIDS sharply decreased by 60-80% (*Global HIV & AIDS Statistics — Fact Sheet, n.d.; R. D. Moore & Chaisson, 1999; Parashar et al., 2016*). People on antiretroviral therapy start their regimen by taking a combination of typically 3 HIV medications from at least 2 different HIV drug classes, often combined into one pill. The different classes of HIV medication include entry

inhibitors, nucleoside/nucleotide reverse transcriptase inhibitors, non-nucleoside reverse transcriptase inhibitors, integrase inhibitors, and protease inhibitors.

Increased access and availability to cART, coupled with advances in cART regimens, have allowed people living with HIV to live longer lives, thus changing HIV into a life-long chronic condition. People living with HIV and receiving effective cART, have been shown to have a significantly increased survival rate where the life expectancy can reach that of non-infected individuals (May et al., 2014). As of 2021, 38.4 million [33.9 million–43.8 million] people globally were living with HIV, 1.2 million residing in the United States (UNAIDS, 2022). While the mortality rate has greatly decreased since the advent of cART, people living with HIV reportedly have increased comorbidities. Studies have shown that people living with HIV have a higher prevalence of comorbidities compared to the general population due to aging, side effects of ARVs, and biological effects of HIV infection (Esser et al., 2013; Gallant et al., 2017; Guaraldi et al., 2014; Triant et al., 2007). The comorbidities most commonly observed in patients with HIV are non-AIDS cancers, cardiovascular diseases, diabetes, dyslipidemia, chronic renal disease, hepatitis B and C, and neurocognitive disorders (Lorenco et al., 2014; Roomaney et al., 2022; UNAIDS, 2022).

1B: The Blood-Brain Barrier (BBB)

The blood-brain barrier (BBB) functions as a protective barrier that maintains homeostasis in the brain by allowing specific substances into the brain, while restricting access to toxic substances (Abbott, 2013). The blood-brain barrier (BBB) is composed of brain microvascular endothelial cells held together by tight junctions and surrounded

by other cells in the neurovascular unit (Abbott & Friedman, 2012; Kadry et al., 2020). The neurovascular unit is composed of neurons, astrocytes, cerebral endothelial cells, microglia and pericytes (R. D. Bell et al., 2010; McCarty, 2005; Zlokovic, 2010). During periods of infection, activation of any component of the neurova can result in the disturbance of brain homeostasis and functioning (Fattakhov et al., 2021; Huang et al., 2021). The ability for compounds to cross the BBB is dependent upon its physical and chemical properties, such as molecular weight, protein binding, and lipophilicity (Banks, 2009; Tajes et al., 2014). Tight junctions form a seal between the endothelial cells, effectively limiting paracellular permeability from the blood into the brain. The major molecular components of tight junctions include the structural proteins occludin, junctional adhesion molecules (JAM), claudins, and the cytoplasmic scaffolding protein zonula occludens (ZO) (Heinemann & Schuetz, 2019). In addition to tight junctions, the endothelial cells are also held together by adherens junctions (Stamatovic et al., 2016). In adherens junctions, cadherin proteins span the intercellular cleft and are linked into the cell cytoplasm by the scaffolding proteins alpha, beta and gamma catenin (Abbott et al., 2010; Stamatovic et al., 2016). Adherens junctions hold the cells together, providing structural support to the tissue and are essential in forming tight junctions (Abbott et al., 2010; Stamatovic et al., 2016). Disruption of adherens junctions leads to weakening of the BBB by altering tight junction protein formation (Abbott et al., 2010; Stamatovic et al., 2016). Tight/adherens junctions effectively form a physical barrier, limiting the amount of ions and other small hydrophilic molecules from crossing the intercellular cleft and reaching the brain (Abbott et al., 2010; Bors & Erdő, 2019; Heinemann & Schuetz, 2019; Stamatovic et al., 2016; Tajes et al., 2014).

The BBB also contains transporter proteins that influences the uptake and efflux of drug molecules into the brain. Uptake drug transporters help facilitate molecules crossing the BBB, while efflux transporters are responsible for expelling molecules back into the blood (Abbott, 2013). Several transporters, both efflux and uptake, are located within the BBB, including the efflux transporters P-glycoprotein (P-gp), Breast Cancer Resistance Protein (BCRP), and the uptake transporters Organic Cation Transporter 1 (OCT1) and Organic Cation Transporter 2 (OCT2) (Agarwal et al., 2011; Bartels & Meissner, 2017; Elmeliegy et al., 2011). The neurovascular unit surrounding the BBB may also help regulate properties of the BBB, including the expression and upregulation of tight junction proteins, and the expression of drug transporters like P-gp and BCRP (Abbott et al., 2006; Ronaldson & Davis, 2015).

The ability for compounds to cross the BBB is dependent upon its physical and chemical properties, such as molecular weight, protein binding, and lipophilicity (Ene et al., 2011). Compounds capable of diffusing across the barrier may do so via paracellular transport. Paracellular transport, or transport between brain microvascular endothelial cells is primarily regulated by tight junctions located between the endothelial cells (Abbott et al., 2010). Tight junctions form a seal between the endothelial cells, effectively limiting paracellular permeability. The major molecular components of tight junctions include the structural proteins occludin, junctional adhesion molecules (JAM), claudins, and zonula occludens (ZO) (Bazzoni et al., 2000).

Transcellular transport is a mechanism by which drug transport proteins facilitate the movement of specific molecules across the BBB (Wolburg et al., 2005). While small, lipophilic molecules passively diffuse across the barrier, such as essential nutrients and

ions (Abbott & Friedman, 2012), large water-soluble molecules primarily require active mechanisms (Abbott, 2013). Astrocytes help induce and maintain barrier properties, promote tight junction protein expression, and increase drug transporter expression (Abbott et al., 2006).

Additional routes for crossing the BBB exist, such as passive diffusion, carrier-mediated transport, receptor-mediated and adsorptive-mediated endocytosis and transcytosis, mononuclear cell migration, and ATP-binding cassette transporter efflux (Abbott, 2013; Abbott et al., 2010). Lipid soluble, non-polar molecules with low molecular weight are more inclined to passively diffuse across the barrier (Abbott et al., 2010). Solutes may also cross the BBB using solute carriers (SLCs) as carrier-mediated influx and can carry a variety of important molecules into the CNS, such as glucose, amino acids and nucleosides (Abbott et al., 2010). Alternatively, receptor-mediated transcytosis enables the transport of macromolecules, including peptides and proteins, into the CNS. These macromolecular ligands then bind to specific receptors on the cell surface, where they form a caveolus which transports both the receptors and ligands across the endothelial cell. Similarly, adsorptive-mediated transcytosis uses vesicles for transporting molecules but requires an excess positive charge on the molecule (Abbott, 2013; Abbott et al., 2010). In addition, leukocytes are able to migrate across the BBB using modified tight junctions or by penetrating close to the tight junctional regions (diapedesis). Certain molecules attempting to cross the BBB may be intercepted by ATP-binding cassette (ABC) transporters, such as P-gp and BCRP, which actively pump the molecule out of the endothelial cell.

1C: HIV and HIV-Associated Neurocognitive Disorders (HAND)

HIV-associated neurocognitive disorders, otherwise known as HAND, is a term that has been collectively used to describe the neurological deficits and associated with HIV infection (Saylor et al., 2016). Prior to the advent of potent combination antiretroviral therapy (cART), severe cognitive impairments reportedly affected up to 50% of people living with HIV (Alford et al., 2019, 2021; Wang et al., 2020). But due to the effectiveness of the cART era, the more severe forms of neurocognitive impairment have decreased, although milder forms remain (Clifford & Ances, 2013). These milder forms of HAND include deficits in learning and memory, as well as executive functioning, which may result in poor medication adherence and difficulty maintaining employment (Alfahad & Nath, 2013; McArthur, 2004; D. J. Moore et al., 2018). Cross sectional studies continue to report around half of all treated HIV patients demonstrating some form of cognitive impairment (Clifford & Ances, 2013). Recently, studies have reported the prevalence of HAND to be as high as 52% despite being on cART, with low level of education, older age, advanced stage of HIV, CD4 count of 500 cells/dL or less, and comorbidity of depression all associated with HAND (Alford et al., 2019, 2021; Heaton et al., 2010; Wang et al., 2020; Zenebe et al., 2022). As previously mentioned, chronic opioid abuse can increase the incidence of HAND and can even worsen CNS inflammation in patients treated with cART (Anthony et al., 2008; J. E. Bell et al., 1998; D. A. Byrd et al., 2011; Roberts & Goralski, 2008). Opioid abuse can also increase the severity of the symptoms of HAND, including significant impairment in verbal memory, problem solving, multitasking, visual-motor coordination, and cognitive flexibility (Kennedy & Zerbo, 2014; Meyer et al., 2013; Murphy et al., 2019).

In 2006, the varying degrees of severity commonly seen in patients diagnosed with HAND were categorized into three sub-classifications: the least severe asymptomatic neurocognitive impairment (ANI), mild neurocognitive disorder, and the most severe HIV-associated dementia (HAD) (Antinori et al., 2007). Patients with ANI reportedly have little to no impairment in daily living activities with ~30% prevalence in cART-treated HIV+ individuals, while those with mild neurocognitive disorder demonstrate a mild to moderate interference in daily functioning, with a prevalence of ~20-30% (Antinori et al., 2007; Clifford & Ances, 2013; Saylor et al., 2016). Patients diagnosed with HAD show marked signs of interference in daily functioning, with a prevalence of 2-8% (Clifford & Ances, 2013; Saylor et al., 2016). Despite the several advancements made in HIV treatment therapy, there have been no clinical trials to demonstrate effective protection against HAND (Bougea et al., 2019; McArthur et al., 2010). Evidence suggests that a lack of ARV penetration into the CNS may not only result in incomplete viral suppression in the brain, but may also contribute to the continued prevalence of neurocognitive impact seen in patients with HAND (Danta & Piplani, 2020; Kolson, 2022; S. Letendre, 2008; S. L. Letendre et al., 2004; Nabha et al., 2013; Rumbaugh & Tyor, 2015; Scanlan et al., 2022).

Patients with HAND also experience disruption of the BBB (Calcagno et al., 2014; Caligaris et al., 2021). Several studies have reported that HIV is able to disrupt the BBB. A study by Chaganti et al. examined the degree of BBB disruption using modern MRI techniques and discovered that patients with HIV demonstrated increased capillary permeability compared to patients without HIV (Chaganti et al., 2019). Another study sought to analyze BBB permeability by using the serum albumin quotient, a well-

established clinical fluid marker for BBB permeability, and found that HIV-infected patients exhibited higher levels of albumin in the cerebrospinal fluid (CSF) compared to uninfected patients, even when receiving effective treatment for one year (Rahimy et al., 2017). HIV was also shown to infect astrocytes, though only low levels of viral replication was detected (Eugenin et al., 2011). Although astrocytes have been shown to play a vital role in maintaining BBB function and integrity, once infected with HIV these cells reportedly disrupt the BBB via a gap junction-dependent mechanism (Eugenin et al., 2011). HIV can further disrupt the BBB by the release of its viral protein, Tat. Studies have reported that Tat enhances the release of pro-inflammatory cytokines from CNS cells, as well as altering the molecular permeability across the BBB (Hauser et al., 2012; Leibrand et al., 2017; Mahajan et al., 2008).

Additionally, several studies have discovered increased BBB disruption as a result of HIV infection in specific brain regions, namely the prefrontal cortex, basal ganglia, and hippocampus (Aylward et al., 1993; Chaganti et al., 2019; Leibrand et al., 2019; Ntshangase et al., 2019; P. M. Thompson et al., 2005). Not surprisingly, these regions of the brain are primarily responsible for concepts such as working memory, attention, risky decision-making, and executive functioning tasks, which lends further evidence to why we see neurocognitive impairment in patients with HIV even during periods of viral suppression (J. Kelschenbach et al., 2019; Nass et al., 2020; R. X. Smith et al., 2018).

1D: HIV in Central Nervous System (CNS)

HIV infection in the central nervous system (CNS) is a major complicating factor in the treatment of HIV. The majority of patients with systemic infection experience HIV infection in the CNS even in the presence of combination antiretroviral therapy (cART) (Ene, 2018; Fauci & Marston, 2015; Spudich & González-Scarano, 2012). Shortly after systemic infection, HIV can enter the CNS in as early as 15 days (Davis et al., 1992). HIV viral entry into the CNS is believed to be mediated through a “Trojan horse” mechanism, whereby HIV-infected monocytes cross the blood–brain barrier and then release virus into the CNS (Hazleton et al., 2010; Spudich & González-Scarano, 2012). The subsequent HIV released from these infected cells causes infection in the brain that results in significant inflammation and eventually neuronal damage and loss (Hazleton et al., 2010). HIV primarily infects CNS macrophages and microglia and may infect astrocytes at low levels (Eugenin & Berman, 2007; Persidsky et al., 1999). Additionally, perivascular macrophage accumulation occurs during HIV infection and is primarily observed in patients with HIV-associated dementia or HIV encephalitis (Fischer-Smith et al., 2001; Gannon et al., 2011; Rappaport & Volsky, 2015). Patients suffering from HIV-associated dementia experience pathological changes in the brain that correlate with an increase in activated bone-marrow-derived cells, including macrophages (Fischer-Smith et al., 2001; Li et al., 2020). Several studies have also indicated that accumulation of phagocytic macrophages and microglia, as well as increased recruitment and/or activity within the brain has been associated with a worsening prognosis (Yadav & Collman, 2009; Yu et al., 2022). HIV viral proteins such as Tat (transactivator of transcription) increase the recruitment of perivascular macrophages

and microglia into the brain (Leibrand et al., 2022). Tat also increased the transmigration of peripheral monocytes in an *in vitro* blood-brain barrier model, through the increased production of CCL2 and upregulation of CCR5 (a chemokine receptor) on monocytes (Bozzelli et al., 2019; Eugenin et al., 2005; Weiss et al., 1999). CCL2 is a chemokine responsible for the recruitment of monocytes, memory T cells, and dendritic cells to sites of inflammation, while CCL5 recruits leukocytes to inflammatory sites (Weiss et al., 1999).

HIV infection results in morphological changes within the brain, including an increase in diameter of cortical vessels, surface area density, and volume fractions (Toborek et al., 2005). These changes are frequently associated with thinning of the basal lamina and decreased immunoreactivity of collagen IV (Toborek et al., 2005). When infected with HIV, the virus is able to infect monocytes in the periphery but cannot replicate effectively until after the monocyte has crossed the BBB and differentiated into macrophages (Ivey et al., 2009). Macrophages and microglia possess unique transcriptional properties, serving as a latent HIV reservoir and capable of reactivating in the presence of pro-inflammatory mediators, leading to the activation of nuclear factor kappa B (NF- κ B) which then binds to the long terminal repeat triggering HIV transcription and the release of viral proteins, thereby suggesting their involvement in HIV neuropathogenesis (Hauser et al., 2005). Perivascular macrophages and microglia can differ functionally and phenotypically in their response to HIV (DePaula-Silva et al., 2019; Grassivaro et al., 2020; Prinz et al., 2021). As microglia are located within the brain, the virus must first enter the brain in order to infect the microglia. Initially, the virus is able to reach the CNS by infecting perivascular macrophages which originate from

monocyte-derived macrophages (MDMs) (El-Hage et al., 2005; Gurwell et al., 2001; Peterson et al., 1990; Zou et al., 2011). These macrophages are able to bidirectionally traverse between the blood and perivascular sites within the CNS parenchyma.

Monocyte migration across the BBB is a critical component to sustaining neuroinflammation in the setting of HIV. The passage of monocytes across the BBB involves a series of complex interactions between monocytes and brain microvascular endothelial cells (Ivey et al., 2009). These complex interactions are mediated by adhesion molecules, chemokines, and cytokines which enables the transmigration through the BBB without compromising the integrity and selectivity of the barrier (Ivey et al., 2009). Importantly, this rate of recruitment can increase greatly during inflammatory states such as neuroAIDS (Ivey et al., 2009; Persidsky et al., 1999). The interaction between monocytes within the blood and brain microvascular endothelial cells (BMECs) also results in the activation of integrin receptors and adhesion molecules, which initiates the intracellular signaling cascades seen within BMECs. Consequently, these signals may result in the temporary opening of tight junctions located between BMEC which enables the passage of monocytes into the CNS (Ivey et al., 2009). Infected monocytes/perivascular macrophages begin actively releasing the virus, as well as multiple proinflammatory mediators which impact the function of surrounding cells and increase future monocyte recruitment (Ivey et al., 2009; Toborek et al., 2005). Furthermore, studies have demonstrated that the dysregulation of tight junction proteins within microvessels is correlated with increased BBB permeability in simian immunodeficiency virus (SIV) (MacLean et al., 2005). This dysregulation of tight junctions may involve cytokine signaling via receptors located on BMECs, which leads

to the phosphorylation of myosin light chain kinase (MLCK) and focal adhesion kinase (FAK), thereby increasing barrier permeability and facilitating monocyte binding (Ivey et al., 2009; McKenzie & Ridley, 2007).

1E: Opioids

The use of opioid medications has steadily increased in the U.S since the late 1990s (C. M. Parker et al., 2019). Opioid are classified as alkaloids that are derived from the opium poppy plant *Papaver somniferum*, and include drugs such as morphine, codeine, and heroin (Hauser et al., 2012; Hauser & Knapp, 2014). Opioids are capable of binding at specific opioid receptors where they elicit an analgesic-like response. Opioid drugs with abuse liability mainly act on μ -opioid receptors (MOR) with lesser effects on δ -opioid receptors (DOR) and κ - opioid receptors (KOR) (Hauser et al., 2012; Hutchinson et al., 2011; McCarthy et al., 2001). Heroin quickly becomes deacetylated within the CNS forming the main bioactive metabolite morphine (Hauser et al., 2012; Nath et al., 2002; Pasternak, 2014).

Medical prescriptions for opioids began to drastically increase in the mid-to-late 1990s, with non-prescription opioid medications increasing shortly after, reaching a peak of 2.7 million new users in 2002 (Kolodny et al., 2015). A primary cause of the opioid epidemic has been attributed to pharmaceutical companies pushing for increased prescribing of opioids, while claiming such medications were not addictive (J. H. Marks, 2020; Van Zee, 2009). Thus, healthcare providers across the United States began increasing the number of opioid prescriptions they would prescribe, eventually leading to the diversion and misuse of opioid medications before their highly addictive potential

was realized (Morone & Weiner, 2013; Van Zee, 2009). Other causes of the opioid epidemic can be associated with the illicit marketing of opioids through pill mills (clinics prescribing medications for non-medical purposes), as well as the focus on treating pain with medications instead of non-pharmacologic measures like physical therapy (Rosenblum et al., 2008). In fact, drug overdose was reported to be the leading cause of accidental death in the United States, with 52,404 lethal drug overdoses in 2015 (Rudd, 2016). Of those lethal overdoses, 20,101 deaths were due to prescription opioids and 12,990 deaths were due to heroin (Rudd, 2016). Additionally, 4 out of 5 new heroin users reportedly began misusing prescription opioids prior to attempting heroin (C. M. Jones, 2013). Heroin users also revealed a stronger preference for heroin over prescription opioids, largely due to the lower cost and greater availability, which is likely due to increased illegal distribution of heroin in rural and suburban communities (Cicero et al., 2014; National Academies of Sciences et al., 2017).

HIV and opioid abuse are oftentimes interconnected due to the common mode of HIV transmission via injection drug use. In states, like New York, with needle exchange programs, initiation of these programs reduces the transmission of blood borne infections, including HIV, by people who inject drugs (Broz et al., 2021; Programs et al., 1995). According to the CDC, adults and adolescents who inject drugs accounted for 10% of the new HIV diagnoses in the United States in 2018 (*HIV Among People Who Inject Drugs | HIV by Group | HIV/AIDS | CDC*, 2022). Globally, around 11 million people reportedly inject drugs, with approximately 1.4 million of this population living with HIV and 39.4% having viral hepatitis C (World Health Organization, 2016).

1F: HIV-1, HIV-1 viral protein, Opioids, and the Blood-Brain Barrier

HIV-1 viral protein Tat (transactivator of transcription) is expressed early in HIV-1 infection and is required for efficient HIV replication. The viral protein Tat enhances the release of pro-inflammatory cytokines from CNS cells and alters molecular permeability across the BBB (Heaton et al., 2004). As the virus enters the CNS via the trafficking of infected cells across the BBB, the migration of infected cells into the CNS, such as peripheral monocytes, is increased (Hauser et al., 2007; Persidsky et al., 1999; Williams et al., 2013). Infected monocytes cross into the CNS, leading to the activation of microglia and release of proinflammatory agents that continue to recruit monocytes/macrophages to the brain (Hauser et al., 2007; Hauser & Knapp, 2014; Heaton et al., 2010; Robinson-Papp et al., 2012) creating a positive feedback loop further activating proinflammatory responses.

Sex differences have been reported in the pathogenesis of HIV (Scully, 2018). Women possess an increase in CD8+ T cell activation, resulting in lower HIV viral loads compared to men (Griesbeck et al., 2016; Scully, 2018). Women also respond more favorably to ARV treatment than men as measured by CD4+ T cell recovery (R. T. Gandhi et al., 2006; Mosha et al., 2013; Scully, 2018). Sex differences have also been reported using a mouse Tat transgenic model, in which males demonstrate increased vulnerability to behavioral deficits in several standard rodent tests of motor and social/cognitive skills (Hahn et al., 2015).

Opioid drugs worsen HIV-1 pathology through direct interactions with glia, particularly microglia and astroglia (Hauser et al., 2007; Hauser & Knapp, 2014). In the

CNS, microglia support productive infection of HIV-1 whereas astroglia are not productively infected (Hauser et al., 2007, 2012). Infected cells can release viral proteins such as the HIV envelope glycoprotein (gp120) and Tat. HIV infection and viral protein release triggers the production of reactive oxygen species (ROS), reactive nitrogen species (RNS), pro-inflammatory cytokines promoting spiraling inflammation, and cytotoxicity in bystander neurons and glia (Hauser et al., 2012). Opioid abuse in HIV-1-infected individuals exacerbates many pathophysiological effects of HIV—especially in the CNS (Hauser et al., 2007). For example, morphine's unique interaction with HIV-1-exposed astroglia demonstrates a spiraling, intercellular feedback loop of microglia and perivascular macrophages which increases and sustains inflammation (El-Hage et al., 2008; Fitting et al., 2010; Hauser & Knapp, 2014). HIV-1 Tat and morphine co-exposure has been associated with decreased expression of tight junctions (ZO-1, occludin, and JAM-2), increased P-gp expression, and increased production of proinflammatory cytokines (Hauser et al., 2012; Leibrand et al., 2017, 2019; Mahajan et al., 2008). Previous research has shown that morphine can result in decreased brain concentrations of select ARVs, particularly ones that are substrates for efflux drug transporters like P-gp, and does so in a region-specific manner (Leibrand et al., 2017, 2019). These findings demonstrate how morphine exposure leads to the decrease of P-gp substrate, ARV concentrations in the striatum and hippocampus of mice. Interestingly, not all ARVs exposed to morphine resulted in decreased brain concentrations, suggesting that morphine can also increase P-gp function. While the association between HIV-1 Tat and morphine has been studied in-depth, the

mechanism in which the interaction of HIV-1/HIV-1 Tat and morphine alters the spatial distribution of ARV concentrations within the brain remains largely unknown.

1G: HIV Neuropathology Mouse Models

Although the introduction of combination antiretroviral therapy (cART) transformed HIV from a deadly infection to a chronic disease, HIV still persists in the latent viral reservoir sites, leaving the viral infection incurable. Currently, 1.5 million new cases of HIV infection are reported each year, and approximately half of the HIV-infected individuals experience some form of neurocognitive impairment despite receiving cART (Rumbaugh & Tyor, 2015; Sacktor et al., 2002). Additional research is required to advance the current state of HIV management and further understand the mechanisms of HIV pathogenesis and prevention strategies. The use of animal models capable of portraying fundamental features of human disease are vital in the investigation and discovery of disease pathogenesis, and the development of innovative therapies (Tyor & Bimonte-Nelson, 2018). Animal models allow for the systematic evaluation of questions since viral and other relevant exposures can be methodically manipulated, while controlling for variables that can impact and interact with outcomes that may be misinterpreted in human studies.

Tat transgenic model

The Tat transgenic is a well-described model used to mimic the effects of neuroHIV, particularly neurodegeneration and glial cell activation. This model provides valuable information regarding the acute toxicity of viral proteins released during HIV infection and reflects the current HIV-infected population. Despite people living with HIV

reporting low viral loads with modern antiretroviral therapy, high levels of Tat remain, which has both direct and indirect neurotoxic effects in the CNS and is thought to contribute to the development of HIV-associated neurocognitive disorders (HAND) (Ajasin & Eugenin, 2020; Ellis et al., 1997). In fact, research suggests that approximately 33% of HIV-infected individuals have detectable levels of Tat in serum, ranging from 0.1 to 40 ng/mL (Xiao et al., 2000). Tat exposure is capable of directly altering neuronal integrity, homeostasis, neuroexcitatory properties, endoplasmic reticulum calcium load, and oxidative state (Brailoiu et al., 2006; Caporello et al., 2006; Kruman et al., 1998; Norman et al., 2007; Xiaojie et al., 2020). Indirectly, Tat has been shown to decrease neuronal integrity by recruiting infected monocytes/ macrophages, which can lead to the release of several proinflammatory cytokines (Hauser et al., 2007, 2012; Hauser & Knapp, 2014; Heaton et al., 2010; Mahajan et al., 2008).

While early Tat transgenic models were unable to detect the Tat protein in the animal brain or develop any obvious neurological deficiencies, later models were more brain-specific where mice were able to express the Tat protein using a glial fibrillary acidic protein (GFAP) promoter with a doxycycline-inducible component (Bruce-Keller et al., 2008; Fitting et al., 2010; B. O. Kim et al., 2003). Additionally, several behavioral studies using the GFAP-driven Tat transgenic model have reported multiple cognitive deficits, validating the use of Tat transgenic mice as a model for HAND (Hahn et al., 2015; Joshi et al., 2020; W. D. Marks et al., 2016; Nass et al., 2020). Thus, the use of the Tat transgenic model is believed to provide deeper insight into the role viral proteins play in the development of HAND.

While this model is effectively able to model HAND, there are some limitations. The most obvious limitation is that the mice used in this model are not able to support robust viral replication due to not being natural hosts of HIV. Additionally, due to the GFAP promoter, the Tat transgenic model is only able to express Tat within glial cells, while the primary cell type supporting productive brain infection of HIV is the macrophage. An alternative approach could be to use a promoter that signals the expression of viral proteins with macrophages rather than astrocytes (Jaeger & Nath, 2012). Similarly, the use of doxycycline in the Tat transgenic model may also be considered a limitation due to potential neuroprotective effects, thereby increasing the risk of false negatives (Jantzie et al., 2006).

gp120 transgenic model

The HIV envelope glycoprotein (gp120) plays a vital role in mediating viral entry into the host cell and has been demonstrated to induce a variety of neurotoxic effects (Avdoshina et al., 2017; Bansal et al., 2000; Dawson & Dawson, 1994; Hart et al., 1991; Scorziello et al., 1998). In addition to mediating viral infection, gp120 is reportedly released by infected cells such as macrophages and microglia (Kaul, 2008; Kaul & Lipton, 1999). HIV-infected macrophages can also shed gp120 into the extracellular space as a soluble protein, where it may potentially interact with uninfected neurons (Jaeger & Nath, 2012; Yadav & Collman, 2009).

The gp120 transgenic mouse model was created by inserting the portion of the HIV *env* gene responsible for encoding gp120 into the murine genome, under the control of a glial fibrillary acidic protein (GFAP) promoter, resulting in gp120 protein

expression by brain astrocytes (Toggas et al., 1994). The gp120 transgenic mice experience neuropathological changes in the neocortex and hippocampus in response to the secretion of gp120, thereby suggesting that gp120 is neurotoxic (Toggas et al., 1994). The transgene is also highly expressed within the olfactory bulb, tectum, selected white matter tracts, and along the glia limitans (Toggas et al., 1994). Interactions between gp120 and the chemokine receptor CXCR4 has also been shown to upregulate the nicotinic acetylcholine receptor resulting in the dysregulation of Ca^{2+} signaling in neurons, particularly in the striatum (Ballester et al., 2012). While only expressing the gp120 protein, these transgenic mice exhibit a neuropathology similarly found in a human AIDS brain, including decreased synaptic and dendritic density, neuronal loss, and increased numbers of activated microglia (Thaney et al., 2018; Toggas et al., 1994). The gp120 transgenic model has also been used to assess behavioral performance. The transgenic mice, compared to non-transgenic controls, demonstrated an increase in anxiety-like behavior in 6 month old mice using an open field test, as well as compromised spatial learning and retention (Bachis et al., 2016; Hoefler et al., 2015; Maung et al., 2014).

Some limitations to the gp120 transgenic model is that mice are capable of only expressing one viral protein and may overlook the pathological effects originating from the combined action of different viral proteins. This concern can be addressed through the cross-breeding of transgenic models expressing different viral proteins. Gp120 transgenic mice, like Tat transgenic mice, are unable to acquire HIV infection and thus cannot truly model the early stages of infection or the AIDS progression, which are important in the development of HAND (Ru & Tang, 2017).

EcoHIV model

Another model used in the study of HIV neuropathology is the EcoHIV model. EcoHIV is a chimeric virus constructed by replacing the gp120 coding region of HIV with gp80, limiting viral replication and infection to rodents rather than primates (Potash et al., 2005). The gp80 gene was obtained from the ecotropic murine leukemia virus which restricts viral replication to rodents and not primates (Potash et al., 2005). A major benefit to using the EcoHIV model is that it is able to establish infection in immunocompetent mice after a single inoculation, with detectable viral loads in the spleen, peritoneal macrophages, and brain between 2- and 12-weeks post inoculation (Potash et al., 2005). In the brains of EcoHIV-infected mice there is evidence of frequent perivascular infiltrates of mononuclear cells, increased macrophage, microglia and astrocyte activation, and an increase in related inflammatory and cellular gene induction (He et al., 2014; Potash et al., 2005). EcoHIV infection has demonstrated high levels of inflammatory cytokines, such as tumor necrosis factor alpha (TNF α) and interleukin 6 (IL-6), within the brain (Sindberg et al., 2015). EcoHIV mice have an early peak viral replication which is controlled, at least in part, by adaptive immune responses. Yet, chronically infected mice show persistent viral expression in macrophages and demonstrate memory and learning impairment similarly seen in HIV-infected individuals on effective antiretroviral therapy (Gu et al., 2018; J. Kelschenbach et al., 2019; Potash et al., 2005). The neurocognitive impairment observed in EcoHIV-infected mice reflects those seen in HIV-infected individuals, as a result of synaptodendritic injury and non-necrotic functional changes in the hippocampus (He et al., 2014; B.-H. Kim et al., 2019). Another advantage of the EcoHIV model involves increased BBB permeability 2 weeks

post infection and decreased expression of the tight junction protein, claudin-5 (L. D. Jones et al., 2016).

However, the EcoHIV model does have some limitations. EcoHIV binds to a different receptor, known as cationic acid transporter 1 (CAT-1), than HIV, which uses the CD4 receptor; this may alter the neuropathogenesis of the virus in unforeseen ways (Potash et al., 2005). Furthermore, in order to generate the EcoHIV virus, the gp120 protein was replaced with gp80 in order to establish infection in mice. The lack of gp120 results in additional complexity as it is unclear to what degree the chimeric virus mimics the HIV infection. However, the EcoHIV virus has been shown to persistently infect conventional mice targeting CD4+ T cells, macrophages, and microglia (He et al., 2014; J. L. Kelschenbach et al., 2012; Potash et al., 2005). Finally, since gp120 is an important HIV neurotoxic protein, the EcoHIV model may not accurately reflect some of the neuropathological phenotypes related to HAND (Ru & Tang, 2017).

Humanized models

Researchers have also studied HIV neuropathogenesis using humanized mice. Humanized mouse models are created by transplanting specific human cells or tissues into an immunodeficient mouse (Shultz et al., 2012). For example, to model the human peripheral blood lymphocyte line in a mouse, researchers would inject peripheral lymphoid cells into the mouse. As with any animal model, there are certain advantages and disadvantages. The main advantage of humanized mice is that it allows experimental interventions and sampling that are not feasible in clinical studies of infected people (Marsden, 2020). Other examples of effective humanized mouse

models involve the transplantation of CD34+ stem cells into immunodeficient mice thereby supporting both a sustained HIV infection and an antiviral immune response within a single physiological system (Shultz et al., 2012). Additionally, humanized mice are generated with an extensive set of human immune cells in several tissues throughout the mouse, enabling the interaction between wild-type HIV and human host cells, such as CD4+ T cells and macrophages, to be studied in vivo without the need for genetic modification to overcome virus species barriers (Marsden, 2020). As a result, clinically relevant antiretroviral drugs, antibodies, and other reagents specific to HIV can be directly tested (Marsden, 2020).

However, the humanized mouse model also has limitations. In particular, one of the main limitations of this model is the lack of consistency from mouse to mouse due to the high variability in human immune cells from person to person, resulting in differences in timing and level of HIV infection (Jaeger & Nath, 2012). In terms of breeding, humanized mice are not able to be bred the same as mice that are genetically modified to encode specific human genes and must therefore be transplanted with human cells and/or tissues (Marsden, 2020). As a result, trained investigators are required to conduct microsurgeries and maintain suitable isolation and biohazard containment conditions for housing immunodeficient mice which will then be infected with HIV (Marsden, 2020).

Despite the effective cART regimens of today, approximately half of all people diagnosed with HIV will report some degree of neurocognitive impairment, or HAND (Rumbaugh & Tyor, 2015; Sacktor et al., 2002). People experiencing HAND will exhibit

deficits in learning and memory, as well as decreased executive functioning (Alfahad & Nath, 2013). Both HIV and HAND remain incurable due to the brain serving as a reservoir for the latent virus, which is capable of being reactivated resulting in systemic infection (Saylor et al., 2016). Injection drug use is also of concern in people living with HIV, with people who inject drugs accounting for 10% of all new HIV cases in 2018 (*HIV Among People Who Inject Drugs | HIV by Group | HIV/AIDS | CDC, 2022*). Opioid abuse can exacerbate HIV neuropathology and contribute to the sustained neuroinflammation seen in patients with HIV, as well as worsening the penetration of select antiretroviral drugs into the brain in a region-specific manner (Hauser et al., 2012; Leibbrand et al., 2017, 2019). This dissertation research will further explore the regional accumulation and spatial distribution on select antiretroviral drugs and morphine to address several important questions in the area of HIV and opioid co-exposure.

CHAPTER 2: Objective and Specific Aims

Objective

Over 38 million people are living with human immunodeficiency virus (HIV) infection worldwide, with over half experiencing symptoms attributed to HIV-associated neurocognitive disorders (HAND), despite the development of combination antiretroviral therapy (cART) (Bandera et al., 2019; Rumbaugh & Tyor, 2015; Sacktor et al., 2002). While cART has effectively decreased incidences of the more severe forms of neurocognitive impairment in people living with HIV, such as HIV-associated dementia, other less severe forms of HAND still remain, including mild neurocognitive disorder and asymptomatic neurocognitive impairment (ANI) (Antinori et al., 2007). These milder forms of HAND include deficits in learning and memory, as well as executive functioning (Alfahad & Nath, 2013). Unfortunately, despite the beneficial effects of modern HIV therapy, there continues to be a lack of effective treatment options to cure the neurocognitive deficits seen in patients with HAND (Heaton et al., 2011; McArthur & Brew, 2010). Several factors are believed to contribute to the development and persistence of HAND, including the effects of aging, persistent HIV replication in the brain, and long-term CNS toxicity of antiretroviral therapy (Gannon et al., 2011; Heaton et al., 2010), as well as poor antiretroviral drug penetration across the blood-brain barrier (Ghosh et al., 2017; Spudich & González-Scarano, 2012). The total eradication of the HIV virus has proven to be more challenging as HIV enters the brain early during infection, and thus serves as a reservoir for latent HIV capable of reactivating and contributing to systemic infection (Saylor et al., 2016).

Drug abuse, specifically opioid drug abuse, exacerbates the progression of HIV into AIDS and can increase the incidence and severity of HAND (D. Byrd et al., 2012;

Kumar et al., 2006; McArthur et al., 2010; Peterson et al., 1990). People who inject drugs (PWID) are particularly susceptible to contracting HIV, with up to one-third of people infected with HIV reporting opioid abuse (J. E. Bell et al., 1998; Des Jarlais et al., 2016; Reddy et al., 2012). Multiple studies have demonstrated how morphine exposure can increase viral loads and neuropathological progression of HIV (Bokhari et al., 2011; Cernasev et al., 2020; Kumar et al., 2006). Individuals who abuse opioids and are living with HIV have noticeably worse virologic suppression compared to patients with HIV who do not abuse opioids (Kumar et al., 2006; Roy et al., 2011). People infected with HIV and who also abuse opioids experience HAND at a higher rate and severity than those with HIV who do not abuse opioids, even with both receiving effective antiretroviral therapy (D. Byrd et al., 2012; Lu & Wang, 2020; Murphy et al., 2019; Robinson-Papp et al., 2012).

Opioids can perpetuate HIV neuropathology by further exacerbating neuroinflammation through the release of pro-inflammatory cytokines, can decrease tight junction protein expression, and lead to poor ARV penetration into the brain (Hauser et al., 2012; Leibrand et al., 2017, 2019; Mahajan et al., 2008). However, not much is known about the impact of opioids on HIV drug penetration into the brain, with recent studies demonstrating how morphine decreases ARV concentrations in the brain for select ARVs and does so in a region-specific manner. Thus, the overall objective of this research is to better understand how HIV and morphine impact ARV accumulation and spatial distribution with the brain. Secondly, the dissertation will also measure the impact of HIV-1 Tat on the central accumulation and regional distribution of morphine.

Additional work was performed to establish an infection HIV model within the lab to be used for future studies.

Aim 1: Define the effects of the HIV-1 protein Tat \pm morphine on ARV accumulation and distribution within the brain.

The regional effects on ARV concentrations and distribution within the brain \pm morphine was assessed using Tat transgenic mice. Tat transgenic mice received ARVs \pm morphine via a subcutaneous osmotic pump. ARV concentrations and distribution were quantitatively evaluated using LC-MS/MS and infrared matrix-assisted laser desorption electrospray ionization (IR-MALDESI) mass spectrometry imaging (MSI).

Aim 2: Evaluate morphine accumulation and distribution in the presence of HIV-1 protein Tat, ARV, and morphine co-exposure.

The impact of Tat expression on morphine accumulation and distribution within the brain was measured in the Tat transgenic mice. Morphine was administered via a subcutaneous osmotic pump containing ARVs. Morphine abundance was assessed using qualitative IR-MALDESI MSI in conjunction with quantitation within the anterior, posterior, and midbrain by LC-MS/MS.

CHAPTER 3: Define the effects of the HIV-1 protein Tat ± morphine on antiretroviral accumulation and distribution within the brain

3A. Introduction

Although combination antiretroviral therapy (cART) effectively suppresses HIV within the periphery and improves health outcomes, up to one-half of people with HIV still experience HIV-associated neurocognitive disorders (HAND) (Arentoft et al., 2022; Clifford & Ances, 2013; Etherton et al., 2015; Gannon et al., 2011). HAND, which is also sometimes called neuroHIV, is a term encompassing a spectrum of disorders ranging from asymptomatic neurocognitive impairment (ANI), mild neurocognitive disorder to HIV associated dementia (HAD) (Clifford & Ances, 2013). Several underlying mechanisms have been implicated in contributing to the neuropathology of HAND (neuroHIV). Some of the most studied mechanisms related to neuroHIV include neuroinflammation, persistent HIV replication in the brain, CNS toxicity from viral proteins and long-term antiretroviral (ARV) therapy and opioid drug abuse (Gannon et al., 2011; Ghosh et al., 2017; Heaton et al., 2010, 2011; Hong & Banks, 2015; Mahajan et al., 2021).

Since the beginning of the HIV crisis, HIV and opioid epidemics have been interlinked; with up to 50% of initial HIV infection attributable to injection drug use (Dutta & Roy, 2012; Hauser et al., 2012; Mathers et al., 2008). Drugs of abuse, specifically opioids, enhance neurotoxicity and contribute to neuroHIV through several mechanisms including the release of proinflammatory cytokines, worsening CD4 counts, decreasing ARV adherence, and exacerbating cognitive deficits observed in people with HIV (Bruce-Keller et al., 2008; D. A. Byrd et al., 2011; Denis et al., 2019; Fitting et al., 2010,

2020; Hauser & Knapp, 2014; Meijerink et al., 2014; Murphy et al., 2019; Ryan et al., 2004; Zou et al., 2011).

At high doses and with chronic use, in the absence of HIV, morphine induces neuronal apoptosis in the brain and spinal cord, and contributes to cerebral dysfunction (Hauser et al., 2012; Hauser & Knapp, 2014; Zhang et al., 2008). The neurotoxic effects of opioids have been related to the various opioid receptor-mediated intracellular pathways including modulation of neurotransmitter release, regulation of ion channels, regulation of cyclic AMP (cAMP), activation of mitogen-activated protein kinase (MAPK), and G-protein coupled receptor activity (Zhang et al., 2008). By acting through opioid receptors and working in synergy with neurotoxic viral proteins, morphine may potentiate neuroHIV through aggravating CNS inflammation (Byrd et al., 2011; Chen et al., 2020; Leibrand et al., 2022; Reddy et al., 2012), increasing viral replication and viral loads (Guo et al., 2002; Hauser et al., 2012; Kumar et al., 2006), and altering cell signaling in the CNS ultimately leading to cellular dysfunction and death (Hu et al., 2002; Murphy et al., 2019; Reddy et al., 2012).

Early in HIV infection, the HIV-1 viral protein Tat (transactivator of transcription) is expressed and is required for efficient HIV replication. Tat is capable of increasing the release of pro-inflammatory cytokines from CNS cells and altering the molecular permeability across the BBB (Heaton et al., 2004). Infected monocytes cross into the CNS, leading to the activation of microglia and release of proinflammatory agents that continue to recruit monocytes to the brain (Hauser et al., 2007; Hauser & Knapp, 2014b; Heaton et al., 2010; Persidsky et al., 1999; Robinson-Papp et al., 2012; Williams et al.,

2013), thereby creating a positive feedback loop, which further activates proinflammatory responses.

In addition to exacerbating neuroHIV, both the HIV-1 Tat viral protein and morphine, can alter the BBB and limit ARV accumulation within the brain. The BBB, composed of brain microvascular endothelial cells held together by tight junctions and surrounded by astrocytes, microglia, and pericytes, exists to separate the neurons from circulating blood while also mediating the entry of specific molecules into the brain based on molecular size and charge to maintain homeostasis (Abbott, 2013; Abbott et al., 2006, 2010; S. L. Letendre et al., 2004). Both morphine and Tat exposure have been reported to alter the function and the integrity of the BBB, through increased leakage of fluorescently labeled dextrans into the brain as well as alterations in tight junction related proteins, like ZO-1 (Bruce-Keller et al., 2008; Fitting et al., 2010b; Leibrand et al., 2017, 2019). Regional differences in the response of the BBB to Tat expression and the involvement of Tat in glial activation, neuroinflammation, and neuronal injury have previously been reported (Hauser & Knapp, 2014; Niu et al., 2021; Toborek et al., 2005). We have also reported that morphine exposure can alter the overall accumulation of antiretroviral drugs within the brain. Using the Tat transgenic mouse model, it was demonstrated that morphine exposure resulted in a significant decrease in the tissue-to-plasma ratio for dolutegravir and abacavir within the striatum and dolutegravir within the hippocampus, irrespective of Tat (Leibrand et al., 2019).

The Tat protein and other neurotoxic viral byproducts are implicated in neuroHIV (Eugenin et al., 2011; Leibrand et al., 2017, 2022; Lindl et al., 2010). The role of Tat in mediating neurotoxicity has been described in the literature (Ajasin & Eugenin, 2020;

Carey et al., 2012; Fitting et al., 2010; Hauser et al., 2009; King et al., 2006). The Tat transgenic mouse model, used to study neuroHIV and Tat-induced toxicity, is well characterized and mimics key aspects of the HIV-opioid interplay (Bruce-Keller et al., 2008; Fitting et al., 2010; Hauser et al., 2009; Langford et al., 2018; Leibrand et al., 2017; Toggas et al., 1994). Importantly, clinical studies demonstrate that even in virally suppressed patients on chronic ARV therapy, active Tat viral proteins remain elevated in the cerebrospinal fluid (CSF) of these patients and that a history of drug abuse is associated with elevated Tat protein levels in the CSF (Henderson et al., 2019).

Infection with HIV is also associated with enhanced trafficking of infected monocyte-derived macrophages into the brain and the subsequent viral reservoirs formed in these cells (Eugenin et al., 2011; Leibrand et al., 2017, 2022; Lindl et al., 2010). HIV preferentially infects brain regions such as the striatum (basal ganglia) and the hippocampus (Berger et al., 1999; Haughey & Mattson, 2002; D. J. Moore et al., 2006; Nath, 2015; Nath et al., 2000). It is widely accepted that the hippocampus plays an important role in both declarative (memory of facts and events) and spatial memory. The dorsolateral striatum provides the basis for habits that are assessed in stimulus–response types of tasks (Ferbinteanu, 2020). As both these regions are heavily involved in learning, memory, and executive functions, HIV infection in these brain regions have been implicated in the pathogenesis of the clinical manifestations of neuroHIV (Anand & Dhikav, 2012; D. J. Moore et al., 2006; Nath et al., 2000).

The introduction of combination antiretroviral therapy, which combines first-line ARV therapies into one regimen, has provided potent and effective control of HIV (Arentoft et al., 2022). While combination antiretroviral therapy is highly effective at

decreasing viral loads within the periphery, HIV hides and continues to persist in reservoir sites, where the virus largely evades the host immune system (Arentoft et al., 2022; Hauser et al., 2012; Lambotte et al., 2006). HIV reservoirs include the brain, lungs, kidney, liver, gut-associated lymphoid tissue, and both male and female genital tracts (Marban et al., 2016; Saylor et al., 2016; K. A. Thompson et al., 2011; Wong & Yukl, 2016). The viral reservoirs formed within the brain remain the largest barrier to eradicating the virus (Castro-Gonzalez et al., 2018). Even with combination antiretroviral therapy, a majority of the viral reservoirs persist because of poor penetration into these sites (Castro-Gonzalez et al., 2018; S. Letendre, 2008; Ntshangase et al., 2019).

Because of the inability to sample human brain tissue, a full characterization of antiretroviral penetration into the brain and its viral reservoirs is not well known. To date, there are only two published studies of antiretroviral penetration in human brain tissue using postmortem samples (Ferrara et al., 2020; Nicol et al., 2019). Yet there are limitations associated with using postmortem brain tissue to estimate drug penetration into the brain. The interval from death to sample collection can vary widely, the time since last dose of antiretroviral drug to sample collection will often be unknown, and postmortem drug redistribution can occur (Butzbach, 2010; Ferner, 2008; Ferrer et al., 2008; Peters & Steuer, 2019). Additionally, often little is known about concomitant medication use or past medical history of these individuals, which could further complicate the interpretation of drug concentration data.

Drug penetration into the CNS can be estimated using cerebrospinal fluid CSF, however this method also has limitations. CSF drug concentrations are used as surrogate markers for unbound brain concentrations, yet may not be an accurate

measurement of drug penetration into the brain for highly protein bound drugs, such as non-nucleoside reverse transcriptase inhibitors and protease inhibitors (Shen et al., 2004; Van den Hof et al., 2018). While using CSF concentrations to measure drug exposure in the brain is common, there can be significant differences in drug concentrations between CSF and the brain. Drug penetration into the brain is mediated through the blood-brain barrier (BBB), while drug penetration into the CSF is regulated by the blood-CSF-barrier (BCSFB). Transport proteins at the BBB and BCSFB help facilitate drug flux, either through the uptake or efflux of a drug across the respective barrier. However, there are differences between the BBB and BCSFB regarding the localization and expression of transport proteins (Morris et al., 2017; Nicol & McRae, 2021), which may explain why the CSF tends to over-predict drug exposure in the brain, especially in drugs with high efflux potential (Fridén et al., 2009; Kodaira et al., 2011, 2014). While the CSF can be measured using computed tomography (CT) scans or magnetic resonance imaging (MRI), a spinal tap/lumbar puncture remains the most direct and accurate way to obtain CSF measurements despite being invasive and often painful for patients (Bruce, 2014; Nau et al., 2010). Animal models can provide useful information when investigating drug penetration into the brain. Preclinical models allow researchers to design more controlled studies with larger sample sizes and more robust pharmacokinetic variables, which can provide a better understanding of the effects of a particular treatment or intervention (Nicol & McRae, 2021).

Quantitative methods for evaluating CNS concentrations include liquid chromatography-tandem mass spectrometry (LC-MS/MS) of tissue homogenates and the more recently developed infrared-matrix assisted laser desorption electrospray

ionization (IR-MALDESI) mass spectrometry imaging (MSI). LC-MS/MS is performed on brain tissue homogenates in order to determine brain drug concentrations. LC-MS/MS can also evaluate broad regional differences, but lacks the ability to detect the more discreet regional differences. IR-MALDESI MSI, on the other hand, is capable of visualizing the spatial distribution of select molecules by their molecular masses from discreet locations across an entire tissue slice (Caprioli et al., 1997). The use of IR-MALDESI MSI to visually evaluate the distribution of drugs in tissue is of particular interest in the field of HIV. Understanding the distribution of antiretrovirals in HIV tissue reservoirs, where low-level viral replication may still be occurring in the face of clinically effective antiretroviral therapy may help form the foundation of successful eradication strategies (Barry et al., 2014; M. Z. Smith et al., 2012).

The purpose of the present study was to examine the impact of HIV-1 Tat and morphine on antiretroviral penetration and distribution within the brain, across several structures including and surrounding the anterior and posterior regions of the brain. We also examined the impact of sex on overall antiretroviral penetration and if there were any subsequent differences in the response to Tat or morphine exposure on drug penetration or distribution.

3B. Materials and Methods

3B.1. Subjects and housing

The doxycycline-inducible HIV-1 Tat-1 transgenic mice, and their appropriate controls, were used for the present studies (39 mice in total; 20 males, 19 females). Tat transgenic mice are on a C57 background and express HIV-1 Tat₁₋₈₆ controlled by an

reverse tetracycline transactivator(rtTA)-driven, glial-specific GFAP promoter. The tetracycline responsive element (TRE) promoter triggers Tat expression by a specially formulated chow containing 6 mg/g doxycycline. Tat(+) transgenic mice express both GFAP-rtTA and TRE-tat genes, while control Tat(-) transgenic mice express only the GFAP-rtTA genes. In all experiments using Tat transgenic mice (~4 months of age, ~25 g, males and females), genotype-confirmed Tat(+) and Tat(-) mice were placed on doxycycline chow to induce HIV-1 Tat transcription, if applicable.. The Tat transgenic model is well characterized and mimics key aspects of the HIV-opioid interplay (Bruce-Keller et al., 2008; Fitting et al., 2010a; Hauser et al., 2009; Langford et al., 2018; Leibrand et al., 2017). Importantly, recent evidence demonstrated that even in virally suppressed patients on chronic antiretroviral therapy, active Tat viral proteins remain elevated in the CSF of these patients and that there is a significant association between a history of drug abuse and Tat levels (Henderson et al., 2019).

For these studies, Tat(+) and Tat(-) mice were placed on doxycycline chow for 14 days (to induce Tat expression), followed by a 5-day washout (no doxycycline) to minimize potential doxycycline-ARV-morphine drug interactions. Long lasting effects (up to 1 month) of Tat on learning and memory after doxycycline completion has previously been demonstrated (Carey et al., 2012).

3B.2. Drug Administration

Triumeq®, a combination tablet containing abacavir (600 mg), dolutegravir (50 mg), and lamivudine (300 mg) was purchased from the VCU Health System Pharmacy. The dosing for mice was calculated based on interspecies allometric scaling from the

recommended dose in humans to mice (McArthur et al., 2010; Nair & Jacob, 2016; ViiV Healthcare, 2014), based on an average 25 g mouse and was as follows: abacavir 2.5 mg/day (123.5 mg/kg/day), dolutegravir 0.2 mg/day (10.3 mg/kg/day) and lamivudine 1.2 mg/day (61.7 mg/kg/day) and drugs were prepared as previously described (Leibrand et al., 2019). Briefly, Triumeq® tablets were crushed into a fine powder and resuspended in normal saline. After centrifugation to pellet tablet excipients at 1000 rpm for 5 min, the supernatant was sterile filtered twice using a 0.45 µm followed by a 0.22 µm filter. After filtration, 210 µL was loaded into the ALZET® osmotic pump (Model 2001, 1 µL/hr delivery). For morphine groups, morphine salt pentahydrate powder was directly diluted into the antiretroviral solution prior to loading the osmotic pump at a concentration sufficient to deliver 2.5 mg/day. Drug preparations were made in batches to minimize dosing variability.

3B.3. Surgical Manipulation

Mice were anesthetized with isoflurane (4% induction, 2% maintenance). A small mid-scapular entry was made in the skin and the osmotic pump, containing the antiretroviral drugs and morphine (or placebo) delivering 2.5 mg morphine per day or placebo was subcutaneously implanted. Bupivacaine was applied to all surgical sites immediately post-operation to provide local anesthesia. During sample collection, the tissues were minimally handled to maintain tissue morphology. Mice were briefly perfused with cold 1x PBS to flush the blood from within the brain vasculature. All flushing of the tissue was performed for approximately 5 minutes to minimize the leaching of drugs from tissue cells. After perfusions, the mice were decapitated, and brain tissue was harvested. The tissue was then carefully transferred to a protective

barrier made of foil and placed atop dry ice to freeze. Once frozen (~5 minutes) the samples were placed in a fresh protective barrier made of foil, properly identified, and stored at -80°C until the time of IR-MALDESI MSI analysis.

3B.4. Sample Preparation

Mouse brain samples were placed in a brain matrix (Zivic Instruments, BSMAS001-1) to reproducibly access coronal regions that included the anterior and posterior regions. A clinical cryostat (Leica CM1950, Leica Biosystems, Nussloch, Germany) was used to section tissue from each of these two regions. Serial sections of 10 µm thickness were thaw-mounted onto glass slides and stored at -86°C until analysis by IR-MALDESI MSI and immunohistochemistry. A diagram of the sectioning plan is found in Figure 1.

3B.5. IR-MALDESI MSI Analysis

Conducting MSI analyses using an IR-MALDESI source has been described in detail elsewhere (Bokhart et al., 2015; C. G. Thompson et al., 2015, 2019), and will be briefly summarized. Prepared tissue sections were placed on a thermally controlled stage (a thermoelectric cooler TE Technology, Inc., Traverse City, MI) in the source chamber. Dry nitrogen was introduced to the closed chamber to reduce humidity, after which samples were cooled to -9°C. The source was then opened to ambient environment to increase the relative humidity to ~50% and allow an ice film to form on the surface of the sample, after which the source was closed and a low flow of nitrogen was re-introduced to maintain a relative humidity of ~15 % during sample analysis allowing for constant ice thickness. An IR OPO laser (Opotek, Carlsbad, CA) tuned to

2.94 μm was used for sample ablation. The plume of volatilized material from each sampling location was ionized by a perpendicular electrospray. Resulting ions were sampled into the Orbitrap QE Plus mass spectrometer (ThermoFisher Q Exactive Plus, Bremen, Germany), which was triggered to start data acquisition simultaneously with the laser shot and ion injection time was fixed to allow ion transience from the pulsed laser to the Orbitrap. A table of the resulting ions, both identified and unidentified, is listed in Appendix I. Following acquisition, the sample stage was translated in 100 μm step increments. Laser, stage, and mass spectrometer signaling was controlled by a microcontroller and custom software (Robichaud et al., 2013).

Analysis was conducted in positive mode, with resolving power set to 140,000 at m/z 200. The mass accuracy of better than 1 part per million (ppm) was confirmed by weekly calibration of the mass spectrometer with the calibration solution recommended by the manufacturer. Antiretrovirals (ARV) were evaluated in a single tissue section using full-scan MS mode, with mass spectra acquired with a mass range m/z 150 – 600, with an electrospray solvent of water and methanol (50:50 v/v) and 0.2% formic acid. A subjacent section was used to measure morphine in LC-MS/MS acquisition, using a m/z 4 isolation window centered at m/z 286.00 and a normalized collision energy NCE = 10 with an electrospray solvent of water and acetonitrile (50:50 v/v) and 0.2% formic acid. Automatic gain control (AGC) function was turned off to match trapping conditions required by IR-MALDESI MSI, and ion injection time was fixed at 11 ms. Calibration of antiretroviral response on brain tissue was performed by spiking 100 nL of standards directly onto mouse brain tissue sections collected in the same region from mice not dosed with drug.

3B.6. LC-MS/MS Analysis

For LC-MS/MS analysis of ARV concentrations, tissues were homogenized in 1 mL of 70:30 acetonitrile:1 mM ammonium phosphate (pH 7.4) using a Precellys 24 tissue homogenizer (Bertin Technologies, Montigny-le-Bretonneux, France). A Shimadzu HPLC system performed chromatographic separation and an AB SCIEX API 5000 mass spectrometer (AB SCIEX, Foster City, CA, USA) equipped with a turbo spray interface was used as the detector. The samples were analyzed with a set of calibration standards (0.025 - 50.0 ng) and quality control samples. Precision and accuracy of the calibration standards and quality control samples was within acceptance criteria of 15%.

3B.7. Immunohistochemistry

Chromogenic immunohistochemistry (IHC) was performed on OCT-embedded tissue sections mounted on positively charged slides. This IHC was carried out using the Leica Bond III Autostainer system. Slides were first hydrated in Bond Wash solution (AR9590). Heat induced antigen retrieval was performed at 100° C in Bond-Epitope Retrieval solution 1 pH-6.0 (AR9961) for 20 minutes. The antigen retrieval was followed with a 5 min peroxide blocking step (Biocare, IPB5000L). After pretreatment, slides were incubated with a GFAP primary antibody (Dako, Z0334) at 1:1500 for 60 minutes followed with Novolink Polymer (Leica, RE7260-CE) secondary. Antibody detection with 3,3'-diaminobenzidine (DAB) and hematoxylin counterstain were performed using the Bond Intense R detection system (Leica, DS9263). Stained slides were dehydrated and coverslipped with Cytoseal 60 (23-244256, Fisher Scientific). Positive controls were

included for this assay. Slides were digitally imaged with the Aperio AT2 (Leica Biosystems) using a 20x objective.

3B.8. Image Analysis

Following immunohistochemistry, brain regions within the anterior and posterior sections were histologically annotated by hand using the Allen Mouse Brain Atlas for reference. For the anterior sample sections, coronal images 44 - 53 of the Allen Mouse Brain Atlas were used to identify four regions of interest: the corpus callosum, caudoputamen, cerebral cortex, and nucleus accumbens [Appendix IIa]. For the posterior sample sections, coronal images 66 - 85 of the Allen Mouse Brain Atlas were used to identify five regions of interest: the hippocampal formation, corpus callosum, cerebral cortex, thalamus, and hypothalamus [Appendix IIb]. MSConvert (Race et al., 2012) was used to convert raw signal intensity data to .mzXML files, which were then loaded into the mass spectrometry imaging program MSiReader (MATLAB application; Mathworks, Natick, MA) to generate ion distribution maps. MSiReader was used to export pixel intensity matrices for ARVs, morphine, and endogenous ions of interest across the entire tissue slice into Matlab. IHC microscopy data and annotations were downsampled to match the resolution of the IR-MALDESI MSI data (pixel size: 100x100 m) and color thresholded to isolate staining from counterstain. Using Matlab, several series of coding were performed to co-localize both IR-MALDESI MSI and IHC images to generate drug concentrations in several regions of interest [Appendix III]. Image co-localization was performed by manually selecting a minimum of 8 control points between the IR-MALDESI MSI and IHC images [Appendix V]. Once selected the control

points were used to align the images atop one another in order to generate regionally specific ion intensities.

After image co-registration was performed, a secondary analysis was conducted to determine if glial activation (measured by GFAP immunoreactivity) was associated with antiretroviral signal. This was done by masking antiretroviral signal onto the distribution of GFAP and was used to determine the proportion of drug that was colocalized with both GFAP(+) and GFAP(-) cell populations.

3B.9. Statistical Analysis

Antiretroviral IR-MALDESI MSI

Abacavir concentrations were the only antiretroviral concentrations quantifiable by way of IR-MALDESI MSI as both lamivudine and dolutegravir were below the lower limit of quantitation. A primary analysis was conducted to determine the mean abacavir concentrations of all mice (male and female mice combined) in each brain region within the anterior (corpus callosum, caudoputamen, cerebral cortex, nucleus accumbens) and posterior (hippocampal formation, corpus callosum, cerebral cortex, thalamus, hypothalamus) sections using a two-way analysis of variance (ANOVA) to address the main effects between drug treatment and Tat status, followed by a Tukey's post-hoc test for pairwise comparisons. Secondary analyses were performed on male versus female mice to determine if there were sex differences in antiretroviral accumulation and distribution. A significance level of $\alpha = 0.05$ was used for all statistical analyses, and results were considered statistically significant if the p -value was less than α . GraphPad Prism Version 9.4.0 (GraphPad Software, LLC.) was used for all statistical analyses

Antiretroviral LC-MS/MS

For the antiretroviral concentrations obtained from the LC-MS/MS analysis, data was separated by sex, such that a separate analysis was performed for males and females, respectively. A two-way analysis of variance (ANOVA) was used to identify significant main effects for drug treatment and Tat status on the antiretrovirals of interest (abacavir, dolutegravir, lamivudine), as well as interactions between drug treatment and Tat status. A Tukey's post-hoc test was then conducted to perform pairwise comparisons where the group means and the antiretroviral concentration of interest for each sex was assessed. A significance level of $\alpha = 0.05$ was used for all statistical analyses, and results were considered statistically significant if the p -value was less than α . GraphPad Prism Version 9.4.0 (GraphPad Software, LLC) was used for all statistical analyses

Changes in abacavir concentrations within areas of gliosis

In order to evaluate whether abacavir concentrations were preferentially localized to regions of activated glial cells and whether Tat and/or morphine exposure influenced drug accumulation in these areas, abacavir concentrations within areas of gliosis were analyzed. Glial activation was evaluated using immunohistochemistry, where brain slices immediately adjacent to the slices used for MSI were stained for glial fibrillary acidic protein (GFAP), a marker for detecting areas of astrogliosis. Morphine and HIV-1 Tat effects on abacavir accumulation within areas of gliosis were determined by comparing abacavir concentrations in both GFAP+ and GFAP- cells. Statistical analyses were performed on the ratio of antiretroviral concentrations within GFAP(+) to abacavir

concentrations in GFAP(-) areas. A primary analysis was conducted using male and female mice whole brain slices from the anterior and posterior brain sections using a two-way analysis of variance (ANOVA) to identify significant main effects and interactions between drug treatment and Tat status in both brain areas. A secondary analysis was conducted to evaluate if there were sex differences in this response. Both primary and secondary analyses were followed with a Tukey's post-hoc test to assess pairwise comparisons. A significance level of $\alpha = 0.05$ was used for all statistical analyses, and results were considered statistically significant if the p -value was less than α . GraphPad Prism Version 9.4.0 was used for all statistical analyses.

3C. Results

Only abacavir concentrations were above the limit of quantitation for the mass spectrometry imaging experiments. Therefore, the results from the IR-MALDESI MSI experiments will report the impact of Tat, morphine and sex on abacavir regional concentrations. Traditional LC-MS/MS concentrations for dolutegravir, lamivudine, and abacavir from brain tissue lysates will also be reported below.

3C.1. The impact of HIV-1 Tat \pm morphine on antiretroviral accumulation within the anterior brain region

Corpus Callosum

When males and female mice were tested together, there was a main effect of treatment in the corpus callosum [$F_{(1,30)} = 21.31, p < 0.0001$]. Morphine treated mice showed significantly lower abacavir concentrations compared to placebo mice. Post-hoc

analysis revealed that, within the corpus callosum, both Tat(-) and Tat(+) morphine mice had significantly lower abacavir concentrations than Tat(-) placebo mice [$p = 0.0004$, $p = 0.0035$, respectively]. Tat(-) and Tat(+) morphine mice had significantly lower abacavir concentrations than Tat(+) placebo [$p = 0.0435$, $p = 0.0004$, respectively] [Figure 2].

Caudoputamen

There was a main effect of treatment in the caudoputamen [$F_{(1,30)} = 19.48$, $p = 0.0001$] such that morphine-treated mice had significantly lower concentrations of abacavir as compared to mice not treated with morphine. Post-hoc analysis revealed that Tat(-) placebo mice had significantly higher abacavir concentrations in the caudoputamen compared to both Tat(-) and Tat(+) morphine mice [$p = 0.0007$, $p = 0.0021$, respectively]. Additionally, Tat(+) morphine mice had significantly lower abacavir concentrations in the caudoputamen compared to Tat(+) placebo mice [$p = 0.0007$] [Figure 3].

Cerebral Cortex

When combining the sexes, the main effect of treatment was significant in the cerebral cortex [$F_{(1,30)} = 18.76$, $p = 0.0002$] such that placebo-treated mice had overall higher concentrations of abacavir compared to morphine mice. Post-hoc analysis revealed that Tat(-) placebo mice had significantly higher abacavir concentrations in the cerebral cortex compared to both Tat(-) and Tat(+) morphine mice [$p = 0.0008$, $p = 0.0036$, respectively]. Tat(+) placebo mice had significantly higher abacavir concentrations in the cerebral cortex compared to Tat(+) morphine mice [$p = 0.0008$]

[Figure 4].

Nucleus Accumbens

There were no significant differences in abacavir concentrations among any of the experimental groups in the nucleus accumbens [Figure 5].

3C.2. The impact of HIV-1 Tat ± morphine on antiretroviral accumulation within the posterior brain region

Hippocampal Formation

When combining the sexes, the main effect of treatment was significant in the hippocampal formation [$F_{(1,28)} = 33.14, p < 0.0001$] such that placebo mice had overall higher concentrations of abacavir compared to morphine mice. Post-hoc analysis revealed that Tat(-) placebo mice had significantly higher abacavir concentrations in the hippocampal formation compared to both Tat(-) and Tat(+) morphine mice [$p < 0.0001, p = 0.0033$, respectively]. Tat(+) placebo mice had significantly higher abacavir concentrations in the hippocampal formation compared to both Tat(-) and Tat(+) morphine mice [$p = 0.0008, p < 0.0001$, respectively] [Figure 6].

Corpus Callosum

When combining the sexes, the main effect of treatment was significant in the corpus callosum [$F_{(1,28)} = 36.00, p < 0.0001$] such that placebo mice had overall higher concentrations of abacavir compared to morphine mice. Post-hoc analysis revealed that Tat(-) placebo mice had significantly higher abacavir concentrations in the corpus

callosum compared to both Tat(-) and Tat(+) morphine mice [$p < 0.0001$, $p = 0.0010$, respectively]. Tat(+) placebo mice had significantly higher abacavir concentrations in the corpus callosum compared to both Tat(-) and Tat(+) morphine mice [$p = 0.0013$, $p < 0.0001$, respectively] [Figure 7].

Cerebral Cortex

When combining the sexes, the main effect of treatment was significant in the cerebral cortex [$F_{(1,27)} = 33.55$, $p < 0.0001$] such that placebo mice had overall higher concentrations of abacavir compared to morphine mice. Post-hoc analysis revealed that Tat(-) placebo mice had significantly higher abacavir concentrations in the cerebral cortex compared to both Tat(-) and Tat(+) morphine mice [$p < 0.0001$, $p = 0.0035$, respectively]. Tat(+) placebo mice had significantly higher abacavir concentrations in the cerebral cortex compared to both Tat(-) and Tat(+) morphine mice [$p = 0.0010$, $p < 0.0001$, respectively] [Figure 8].

Thalamus

When combining the sexes, the main effect of treatment was significant in the thalamus [$F_{(1,27)} = 36.56$, $p < 0.0001$] such that placebo-treated mice had overall higher concentrations of abacavir compared to morphine mice. Post-hoc analysis revealed that Tat(-) placebo mice had significantly higher abacavir concentrations in the thalamus compared to both Tat(-) and Tat(+) morphine mice [$p < 0.0001$, $p = 0.0010$, respectively]. Tat(+) placebo mice had significantly higher abacavir concentrations in the cerebral cortex compared to both Tat(-) and Tat(+) morphine mice [$p = 0.0014$, $p < 0.0001$, respectively] [Figure 9].

Hypothalamus

When combining the sexes, the main effect of treatment was significant in the hypothalamus [$F_{(1,25)} = 32.19, p < 0.0001$] such that placebo-treated mice had overall higher concentrations of abacavir compared to morphine mice. Post-hoc analysis revealed that Tat(-) placebo mice had significantly higher abacavir concentrations in the hypothalamus compared to both Tat(-) and Tat(+) morphine mice [$p < 0.0001, p = 0.0105$, respectively]. Tat(+) placebo mice had significantly higher abacavir concentrations in the hypothalamus compared to both Tat(-) and Tat(+) morphine mice [$p = 0.0007, p < 0.0001$, respectively] [Figure 10].

3C.3. Sex differences on antiretroviral accumulation within the anterior brain region.

To better understand the complexities of antiretroviral accumulation and distribution within the CNS, a secondary analysis was performed to examine sex differences in abacavir concentrations. The effects of HIV-1 Tat and/or morphine exposure on abacavir accumulation within the CNS for males versus females are reported below.

Corpus Callosum

For males, the main effect of treatment was significant in the corpus callosum [$F_{(1,12)} = 8.846, p = 0.0116$] such that male placebo mice had overall higher concentrations of abacavir compared to male morphine mice. Post-hoc analysis revealed that male Tat(-) placebo mice had significantly higher abacavir concentrations than male Tat(-) morphine mice [$p = 0.0495$]. Abacavir concentrations were significantly

higher in male Tat(+) placebo mice compared to male Tat(+) morphine mice [$p = 0.0495$] [*Figure 11a*].

For females, the main effect of treatment was significant in the corpus callosum [$F_{(1,16)} = 6.492, p = 0.0215$] such that placebo female mice had overall higher concentrations of abacavir compared to female morphine mice. No significant differences between the means were revealed with the post-hoc analysis [*Figure 11b*].

Caudoputamen

For males, the main effect of treatment was significant in the caudoputamen [$F_{(1,12)} = 9.626, p = 0.0091$] such that male placebo mice had overall higher concentrations of abacavir compared to male morphine mice. Post-hoc analysis revealed that male Tat(-) placebo mice had significantly higher abacavir concentrations than male Tat(-) morphine mice [$p = 0.0397$]. Abacavir concentrations were significantly higher in male Tat(+) placebo mice compared to male Tat(+) morphine mice [$p = 0.0397$] [*Figure 12a*].

For females, there were no observed significant effects in either the treatment or Tat status groups. [*Figure 12b*].

Cerebral Cortex

For males, the main effect of treatment was significant in the cerebral cortex [$F_{(1,12)} = 6.948, p = 0.0217$] such that male placebo mice had overall higher concentrations of abacavir compared to male morphine mice. No significant differences between the means were revealed with the post-hoc analysis [*Figure 13a*].

For females, no significant effects were observed. [Figure 13b].

Nucleus Accumbens

For males, the main effect of treatment was significant in the nucleus accumbens [$F_{(1,10)} = 6.143, p = 0.0326$] such that male placebo mice had overall higher concentrations of abacavir compared to male morphine mice. No significant differences between the means were revealed with the post-hoc analysis [Figure 14a].

For females, no significant effects were observed in the nucleus accumbens [Figure 14b].

3C.4. Sex differences on antiretroviral accumulation within the posterior brain region.

Hippocampal Formation

For males, the main effect of treatment was significant in the hippocampal formation [$F_{(1,13)} = 24.92, p = 0.0002$] such that male placebo-treated mice had overall higher concentrations of abacavir compared to male morphine mice. Post-hoc analysis revealed that Tat(-) placebo mice had significantly higher abacavir concentrations compared to both Tat(-) and Tat(+) morphine mice [$p = 0.0012, p = 0.0288$, respectively]. Tat(+) placebo mice had significantly higher abacavir concentrations compared to both Tat(-) and Tat(+) morphine mice [$p = 0.0099, p = 0.0012$, respectively] [Figure 15a].

For females, the main effect of treatment was significant in the hippocampal formation [$F_{(1,13)} = 6.134, p = 0.0278$] such that female placebo-treated mice had overall higher concentrations of abacavir compared to female morphine mice. No significant

differences between the means were revealed with the post-hoc analysis [Figure 15b].

Corpus Callosum

For males, the main effect of treatment was significant in the corpus callosum [$F_{(1,13)} = 33.98, p < 0.0001$] such that male placebo mice had overall higher concentrations of abacavir compared to male morphine mice. Post-hoc analysis revealed that Tat(-) placebo mice had significantly higher abacavir concentrations compared to both Tat(-) and Tat(+) morphine mice [$p = 0.0003, p = 0.0077$, respectively]. Tat(+) placebo mice had significantly higher abacavir concentrations compared to both Tat(-) and Tat(+) morphine mice [$p = 0.0042, p = 0.0003$, respectively] [Figure 16a].

For females, the main effect of treatment was significant in the corpus callosum [$F_{(1,12)} = 10.99, p = 0.0062$] such that female placebo mice had overall higher concentrations of abacavir compared to female morphine mice. Post-hoc analysis revealed that Tat(-) placebo mice had significantly higher abacavir concentrations compared to Tat(-) morphine mice [$p = 0.0273$]. Tat(+) placebo mice had significantly higher abacavir concentrations compared to Tat(+) morphine mice [$p = 0.0273$] [Figure 16b].

Cerebral Cortex

For males, the main effect of treatment was significant in the cerebral cortex [$F_{(1,13)} = 28.89, p = 0.0001$] such that male placebo mice had overall higher concentrations of abacavir compared to male morphine mice. Post-hoc analysis

revealed that Tat(-) placebo mice had significantly higher abacavir concentrations compared to both Tat(+) and Tat(-) morphine mice [$p = 0.0006$, $p = 0.0097$, respectively]. Tat(+) placebo mice had significantly higher abacavir concentrations compared to both Tat(+) and Tat(-) morphine mice [$p = 0.0101$, $p = 0.0006$] [Figure 17a].

For females, no significant effects were observed in the cerebral cortex [Figure 17b].

Thalamus

For males, the main effect of treatment was significant in the thalamus [$F_{(1,13)} = 27.16$, $p = 0.0002$] such that male placebo-treated mice had overall higher concentrations of abacavir compared to male morphine mice. Post-hoc analysis revealed that Tat(-) placebo mice had significantly higher abacavir concentrations compared to both Tat(+) and Tat(-) morphine mice [$p = 0.0008$, $p = 0.0108$, respectively]. Tat(+) placebo mice had significantly higher abacavir concentrations compared to both Tat(+) and Tat(-) morphine mice [$p = 0.0138$, $p = 0.0008$] [Figure 18a].

For females, the main effect of treatment was significant in the thalamus [$F_{(1,12)} = 9.032$, $p = 0.0110$] such that female placebo-treated mice had overall higher concentrations of abacavir compared to female morphine mice. Post-hoc analysis revealed that Tat(-) placebo mice had significantly higher abacavir concentrations compared to Tat(-) morphine mice [$p = 0.0470$]. Tat(+) placebo mice had significantly higher abacavir concentrations compared to Tat(+) morphine mice [$p = 0.0470$] [Figure

18b].

Hypothalamus

For males, the main effect of treatment was significant in the hypothalamus [$F_{(1,13)} = 23.76$, $p = 0.0003$] such that male placebo-treated mice had overall higher concentrations of abacavir compared to male morphine mice. Post-hoc analysis revealed that Tat(-) placebo mice had significantly higher abacavir concentrations compared to both Tat(+) and Tat(-) morphine mice [$p = 0.0015$, $p = 0.0299$, respectively]. Tat(+) placebo mice had significantly higher abacavir concentrations compared to both Tat(+) and Tat(-) morphine mice [$p = 0.0128$, $p = 0.0015$] [Figure 19a].

For females, no significant effects were observed in the hypothalamus [Figure 19b].

3C.5. Antiretroviral analysis via LC-MS/MS

All mice in the present study received a combination of abacavir, lamivudine, and dolutegravir. Of those drugs, only abacavir concentrations were above the limit of quantitation (>102.25 ng/g) for IR-MALDESI MSI. Lamivudine and dolutegravir concentrations were below the limit of quantitation (<1534.27 and <11732.44 ng/g, respectively) for IR-MALDESI MSI analysis. In order to understand the impact of HIV-1 Tat and morphine on the concentrations for all antiretrovirals in this study, traditional LC-MS/MS was also performed. For these analyses, brain tissue lysate located between the anterior and posterior sections were used, as illustrated in Figure 1.

Therefore, concentrations for these drugs within discrete brain regions were not able to be determined.

Abacavir Concentrations from brain tissue

For males, there were no significant main effects or interactions between treatment and Tat status detected [Figure 20a].

For females, no significant main effects or interactions between treatment and Tat status were detected [Figure 20b].

Dolutegravir Concentrations from brain tissue

For males, there was a significant main effect of treatment [$F_{(1,16)} = 5.188, p = 0.0368$], as well as a significant interaction between treatment and Tat status [$F_{(1,16)} = 5.641, p = 0.0304$]. Additionally, post-hoc analysis revealed that Tat(+) placebo mice had significantly higher dolutegravir concentrations compared to Tat(+) morphine mice [$p = 0.0230$] [Figure 21a].

For females, there were no significant main effects or interaction between treatment and Tat status detected [Figure 21b].

Lamivudine Concentrations from brain tissue

For males, no significant main effects or interactions between treatment and Tat status were detected [Figure 22a].

For females, there were no significant main effects or interactions between treatment and Tat status detected [Figure 22b].

3C.6. Effects of HIV-1 Tat ± morphine on abacavir accumulation in areas of gliosis

In order to evaluate whether the morphine-mediated effects on abacavir concentrations were observed primarily within areas of gliosis, a ratio of abacavir concentrations within GFAP(+) areas (representing reactive astrogliosis) to abacavir concentrations within GFAP(-) areas was calculated. These ratios were then compared statistically to determine whether morphine treatment (or Tat exposure) significantly influenced the amount of abacavir accumulation within areas of gliosis.

An analysis of the effects of morphine and/or Tat exposure on abacavir concentrations within areas of gliosis, when males and females were combined, revealed no significant effects of morphine treatment or Tat status in the anterior and posterior brain [*Figure 23a and 24a*].

3C.7. Sex differences and impacts of gliosis on abacavir concentrations

A secondary analysis was performed to examine whether abacavir concentrations were more associated with areas of gliosis in males as compared to females. To make this comparison, the ratio of abacavir concentrations in GFAP(+) to abacavir concentrations in GFAP(-) areas was compared across experimental groups (Tat and morphine) and between males and females using a two-way ANOVA.

Analysis of Anterior Brain Region

For males, there was a significant main effect for treatment [$F_{(1, 11)} = 7.369, p = 0.0201$] such that in morphine-treated mice, irrespective of Tat status, there was a significantly higher ratio of abacavir in GFAP(+) cells versus GFAP(-) cells compared to

placebo-treated mice, suggesting greater abacavir accumulation in areas of gliosis. A post-hoc analysis revealed no significant differences between group means [Figure 23b].

In females, there was a significant main effect for Tat status [$F(1, 15) = 5.504, p = 0.0331$] such that Tat-exposed mice, irrespective of morphine exposure status, had a significantly higher ratio of abacavir in GFAP(+) cells versus GFAP(-) cells as compared to Tat- mice. A post-hoc analysis revealed no significant differences between group means [Figure 23c].

Analysis of Posterior Brain Region

For male mice, there were no significant main effects for treatment or Tat status and no significant differences between the means were revealed following the post-hoc analysis [Figure 24b].

For female mice, the two-way ANOVA revealed a significant main effect for treatment [$F(1, 12) = 8.200, p = 0.0143$] and a significant interaction between treatment and Tat status [$F(1, 12) = 9.020, p = 0.0110$]. The multiple comparison post-hoc analysis revealed a significant interaction between Tat(-) placebo and Tat(+) morphine female mice in areas of glial activation compared to both Tat(-) and Tat(+) placebo mice ($p=0.0160$ and $p=0.0098$, respectively) and Tat(-) morphine mice ($p=0.0095$) [Figure 24c].

3D. Discussion

The study examined the effects of HIV-1 Tat and morphine exposure on antiretroviral concentrations in the brain. This experiment was multifaceted, where we examined 1) morphine- and/or Tat-mediated effects on abacavir concentrations at several regions of interest within the anterior and posterior brain using IR-MALDESI MSI, 2) morphine and Tat exposure on abacavir, dolutegravir, and lamivudine concentrations located between the anterior and posterior sections using LC-MS/MS, and 3) morphine- and/or Tat-mediated effects on abacavir concentrations within areas of gliosis.

Morphine decreases abacavir concentrations in most brain regions examined

The initial analysis, for which males and females were included in the sample, examined abacavir concentrations when exposed to HIV-1 Tat and morphine in the anterior and posterior brain. Results from this analysis revealed significantly reduced abacavir concentrations across all brain regions examined, except for the nucleus accumbens where significant changes in abacavir concentrations were observed only in males. This is consistent with prior findings in our lab, where abacavir concentrations within the striatum were significantly decreased in morphine-exposed mice (Leibrand et al., 2019). A secondary analysis was conducted to determine if there were sex differences in morphine- and/or Tat-mediated effects on abacavir concentrations. Results from the secondary analysis revealed that the morphine-mediated reduction in abacavir concentrations is more pronounced in male mice. There could be several explanations for the observed sex differences within the current study. Of note, visual inspection of the data suggests that the female mice have increased variability in

abacavir concentrations as compared to the male mice. This variability could be due to the individual females being in different stages of their estrous cycle, which was not controlled for within the study (Doyle et al., 2017; Loyd et al., 2008). Changes in estrogen levels can alter hepatic enzyme activity, which may result in increased drug accumulation or decreased drug elimination (O. P. Soldin et al., 2011). Other potential reasons for the observed differences in abacavir concentrations in response to morphine could be body weight, plasma volume, gastric emptying time, plasma protein levels, hepatic enzyme activity, and drug transporter function (M. Gandhi et al., 2004; O. Soldin & Mattison, 2009; O. P. Soldin et al., 2011). There have been reports of sex differences in the pharmacokinetics of other antiretroviral drugs. One study reported that women have consistently higher (two- to eight-fold) levels of carbovir triphosphate, the active metabolite of abacavir, compared to men after receiving 600 mg of abacavir orally (Harris et al., 2002). Women also had significantly higher intracellular zidovudine triphosphate and lamivudine triphosphate concentrations compared to men, leading to faster times to achieve viral suppression (less than 50 copies/mL of HIV RNA) (Anderson et al., 2003). Additionally, another study demonstrated that women had 45% higher exposure (measured by area under the curve) of mean total zidovudine phosphates as compared to men (Stretcher et al., 1994). A study conducted by Doyle et al (2017) determined that the observed differences in male and female opioid abuse may be due to females desensitizing to the analgesic effects of morphine more quickly than males thereby developing a drug tolerance more quickly (Doyle et al., 2017; Lopresti et al., 2020). While the exact mechanism(s) in which sex effects morphine pharmacokinetics is unclear, there is evidence morphine metabolism is partially

mediated by steroid hormones, as seen from the significant decrease in morphine-3-glucuronide:morphine ratio in female rats after receiving a gonadectomy (Baker & Ratka, 2002). These results highlight the importance of sex when considering antiretroviral therapy and opioid use.

While HIV-1 Tat exposure in the present study was not significantly associated with changes in abacavir concentrations, female mice demonstrated an interactive effect between morphine and HIV-1 Tat exposure within areas of gliosis, such that abacavir concentrations were increased during morphine and HIV-1 Tat co-exposure. These findings highlight the interactive effects of morphine and Tat exposure, where studies have shown that the combination of morphine and Tat leads to increases in intracellular Ca^{2+} and the release of proinflammatory cytokines/chemokines (El-Hage et al., 2005; Zou et al., 2011). The modulatory effects of morphine and HIV-1 Tat on abacavir concentrations could potentially impact the effectiveness of antiretroviral therapy in suppressing HIV replication within the brain.

The impact of Tat and morphine on abacavir, dolutegravir, and lamivudine in the tissue lysates

Of the three antiretroviral drugs administered to the mice (abacavir, dolutegravir, and lamivudine), only abacavir concentrations were above the limit of quantitation by IR-MALDESI MSI. The lower sensitivity of IR-MALDESI MSI, which is a limitation of the method, prevented a full evaluation of Tat and morphine effects on the regional accumulation of the other two antiretrovirals in this study. In order to more fully evaluate the impact of tat and morphine on the concentrations of all antiretrovirals administered

to the mice, the middle portion of the brain (located between the anterior and posterior brain sections, see Figure 1) was measured using traditional LC-MS/MS. Using MS/MS, the only antiretroviral drug that was significantly impacted by Tat or morphine exposure was dolutegravir. Specifically, Tat(+) placebo male mice had significantly greater amounts of dolutegravir compared to Tat(+) morphine male mice. These findings are mostly consistent with previous work conducted in our lab, where morphine exposure decreased dolutegravir in the striatum and hippocampus and decreased abacavir concentrations in the striatum of HIV-1 Tat transgenic mice (Leibrand et al., 2019). Previous studies conducted in our lab have also discovered that the decreases in dolutegravir and abacavir concentrations within the CNS were likely associated with morphine-induced increases in the expression and function of the efflux transporter, P-glycoprotein (P-gp) (Leibrand et al., 2019). While abacavir concentrations were decreased in the presence of morphine using IR-MALDESI MSI, using tissue lysates for LC-MS/MS collected from between the anterior and posterior brain sections did not reveal any significant Tat or morphine effects. The lack of results using LC-MS/MS suggests the region-specific nature of morphine effects, as the IR-MALDESI MSI samples were able to detect morphine-mediated effects in abacavir concentrations when analyzing discrete brain regions. However, the tissue lysate sample used for the LC-MS/MS analysis comprised several brain regions in one sample, which reduces the ability of LC-MS/MS to detect any region-specific effects. In order to test this theory, IR-MALDESI MSI-derived abacavir concentrations from across entire whole brain slices were analyzed. When using non-region-specific IR-MALDESI MSI data, no significant differences in abacavir concentrations were detected in response to HIV-1 Tat or

morphine exposure (data not shown). This provides further evidence for assessing the regionally specific effects of HIV-1 Tat and opioids on abacavir concentrations in the brain, as whole brain tissue lysates were unable to detect these differences.

HIV-1 Tat and morphine effects on abacavir concentrations at areas of gliosis

During periods of neuroinflammation, astrocytes quickly become activated (Brahmachari et al., 2006) and this astrogliosis may facilitate inflammatory responses, resulting in neuronal injury and death (Tani et al., 1996). Upon activation, astrocytes secrete various neurotoxic substances, such as nitric oxide and several pro-inflammatory cytokines/chemokines, and have enhanced levels of glial fibrillary acidic protein (GFAP), a common marker protein for astrogliosis (Brahmachari et al., 2006; Eng & Ghirnikar, 1994). Morphine and HIV-morphine co-exposure are known to activate astrocytes (and increase GFAP immunoreactivity) (Anderson et al., 2003; Bruce-Keller et al., 2008; Chen et al., 2020; El-Hage et al., 2006; Persidsky et al., 1996). In the current study, we examined whether abacavir concentrations were more commonly associated with areas of gliosis. We would expect more activated astrocytes in mice treated with morphine or with Tat-morphine co-exposure, as this has been described previously (Anderson et al., 2003; Bruce-Keller et al., 2008; Chen et al., 2020; El-Hage et al., 2006). Therefore, we hypothesized that morphine or Tat + morphine mice would have lower antiretroviral concentrations in areas of gliosis (areas where the ratio of abacavir concentration in GFAP+ / abacavir concentration in GFAP- is less than one). When the male and female groups were not differentiated, there was no significant difference in abacavir accumulation regardless of experimental group. Interestingly,

however, a secondary analysis of potential sex effects revealed that for the anterior brain slice (the slice that contained the corpus callosum, caudoputamen, cerebral cortex, and nucleus accumbens), morphine treatment, irrespective of Tat status, resulted in a greater accumulation of abacavir within areas of gliosis than mice not treated with morphine. This finding is particularly interesting because the primary MSI analysis of abacavir concentrations consistently revealed that morphine treated mice had lower concentrations of abacavir. These data examined concentrations without consideration of the activation state of astrocytes and were focused on discrete brain regions. Collectively, these data suggest that even though overall abacavir concentrations may be decreased within the brain (primarily within male mice), there may be differential accumulation within areas of gliosis versus other less damaged areas, which contribute to variable effects on viral suppression across different regions and activation states within the brain.

In contrast, in the females, there was no effect of morphine on gliosis-mediated abacavir accumulation for the anterior slice. There was, however, a main effect for Tat whereby the Tat(+) mice had significantly higher accumulation of abacavir in areas of gliosis than Tat(-) mice. The lack of a morphine effect on abacavir concentrations was also a pattern with the MSI data for most of the anterior sections of female mice, except for the corpus callosum, where there was a main effect of morphine to decrease abacavir concentrations. In the posterior sections, there was only one experimental group in which there was a significant effect. In the female mice, there was an interaction term such that Tat(+) morphine treated mice had higher concentrations of abacavir in areas of gliosis than did all other groups. Another study by our group

examined the impact of Tat and/or morphine on antiretroviral intracellular concentrations within different primary human brain cell types, including astrocytes, brain microvascular endothelial cells, pericytes and microglia. The investigators found that Tat as well as Tat plus morphine treatment resulted in a decrease in intracellular antiretroviral concentrations, whereas no significant change in drug concentrations were observed in other cell types (Patel et al., 2019). In this present study, Tat and/or morphine treatment had an opposite effect on abacavir concentrations, they were increased with treatment depending on the brain section and sex of the animal being examined. However, some key differences between the studies exist. The prior study was in human cells, was in vitro, it measured intracellular concentrations and it did not examine abacavir specifically. This present study, as well as some of our prior work (Leibrand et al., 2019), has demonstrated that Tat and/or morphine can have different effects on drug accumulation, depending on the specific antiretrovirals being used. Despite these differences, the prior study does support the idea that Tat and/or morphine can impact drug concentrations in astrocytes more so than for other cell types.

These data, which examined whether abacavir concentrates in areas of gliosis, also reinforces the sex dependent effects observed with the MSI abacavir data. Male mice appear to be more susceptible to morphine-mediated effects on drug accumulation within the brain. Additionally, females are perhaps more susceptible to HIV-1 Tat mediated effects at least in the posterior region of the brain. Although this exact question has not been experimentally tested before, others report sex differences in several types of outcomes, specifically the number, morphology, gene expression, and function of astroglia in different regions of the developing and adult CNS (Acaz-Fonseca

et al., 2016; Amateau & McCarthy, 2002; Arias et al., 2009; Beyer et al., 1990; Chowen et al., 1995; Chowen & Garcia-Segura, 2021). It has also been reported that sex differences in glial activation may be related to phagocytosis; an in vitro study demonstrated that inflammation stimulated phagocytosis in male, but not female, astroglia, possibly suggesting sex specific differences in the role of astroglia to reestablish tissue homeostasis (Crespo-Castrillo et al., 2020).

The present study examined abacavir concentrations in the brain when exposed to HIV-1 Tat and morphine. Morphine, but not HIV-1 Tat, was found to significantly alter abacavir concentrations in the brain. As these findings highlight morphine's ability to reduce antiretroviral concentrations in the brain, special attention needs to be given to individuals living with HIV receiving antiretroviral therapy who use/abuse drugs, specifically those suffering from opioid use disorder. Individuals living with HIV may experience reduced efficacy in antiretroviral therapy when using morphine. While this current study examined morphine's effect on antiretroviral concentrations in the brain, future experiments should incorporate additional opioids into the study targeting other opioid receptors, such as delta- and kappa-opioid receptor agonists, to better understand the underlying mechanisms in which opioids suppress antiretroviral concentrations in the CNS. Additionally, future studies may wish to evaluate neurocognitive function in people with HIV who misuse drugs by incorporating behavioral assays into the experiment. Furthermore, future studies may wish to utilize an infectious mouse model to investigate whether the changes in antiretroviral concentrations are associated with the decreased ability to suppress viral replication.

Lastly, to better understand potential sex differences, our future experiments should use larger sample sizes for each sex to ensure the studies are powered to detect sex differences.

3F. Figures

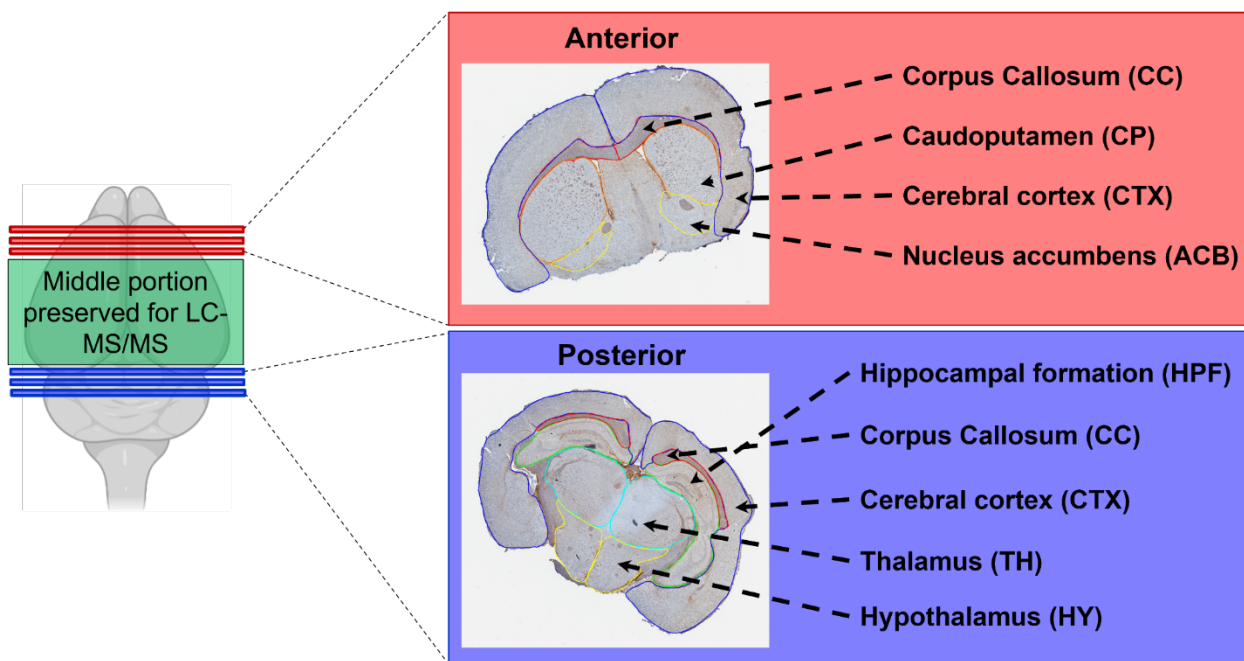


Figure 1: Brain slicing schema illustrating the geographical location of the brain slices obtained from the anterior and posterior sections of the mouse brain, as well as the portion of the brain used for LC-MS/MS analysis.

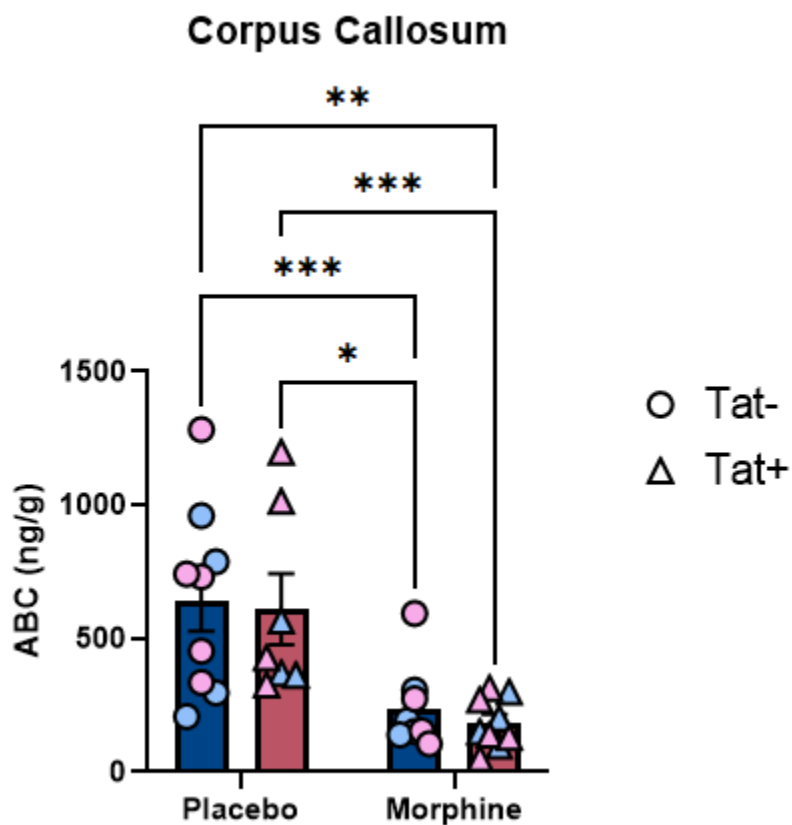


Figure 2: The effects of HIV-1 Tat and morphine on abacavir concentrations in the anterior corpus callosum using IR-MALDESI MSI. In the bar graph, Tat(-) mice are depicted by dark blue bars and circles, while Tat(+) mice are depicted by red bars and triangles. Post-hoc significant differences at $\alpha < 0.05$ are denoted by * $p < 0.0032$, ** $p < 0.0021$ and *** $p < 0.0002$. The mean abacavir concentrations \pm SEM were sampled from $n = 9$ Tat(-) placebo, $n = 7$ Tat(+) placebo, $n = 8$ Tat(-) morphine, $n = 9$ Tat(+) morphine; both sexes are included in this analysis, where female mice are represented using pink circles or triangles and male mice are represented using light blue circles or triangles.

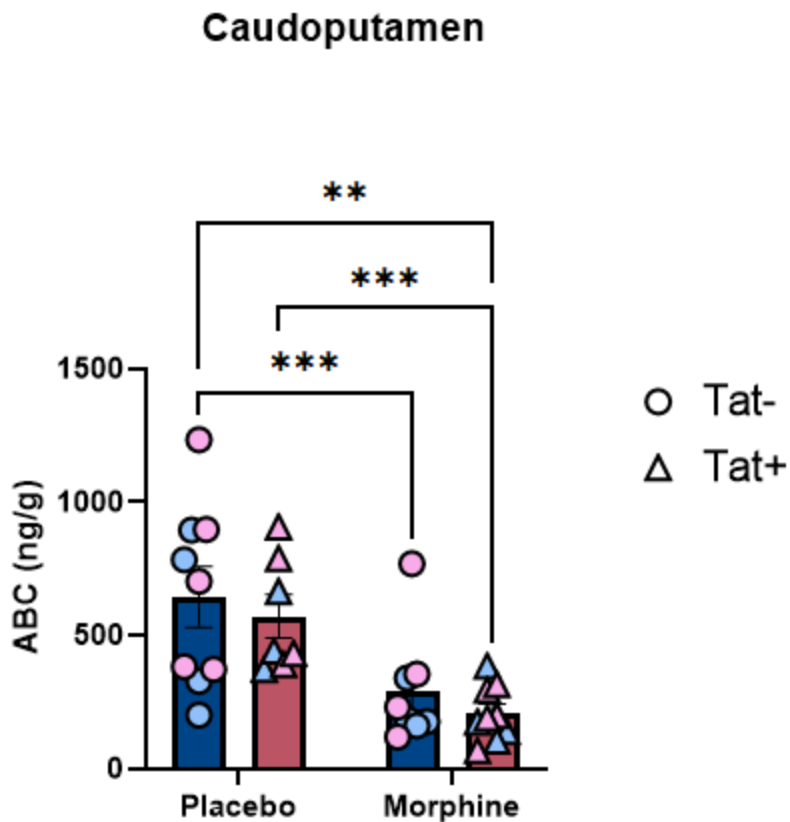


Figure 3: The effects of HIV-1 Tat and morphine on abacavir concentrations in the caudoputamen using IR-MALDESI MSI. In the bar graph, Tat(-) mice are depicted by dark blue bars and circles, while Tat(+) mice are depicted by red bars and triangles. *Post-hoc* significant differences at $\alpha < 0.05$ are denoted by $**p < 0.0021$ and $***p < 0.0002$. The mean abacavir concentrations \pm SEM were sampled from $n = 9$ Tat(-) placebo, $n = 7$ Tat(+) placebo, $n = 8$ Tat(-) morphine, $n = 9$ Tat(+) morphine; both sexes are included in this analysis, where female mice are represented using pink circles or triangles and male mice are represented using light blue circles or triangles.

Cerebral Cortex

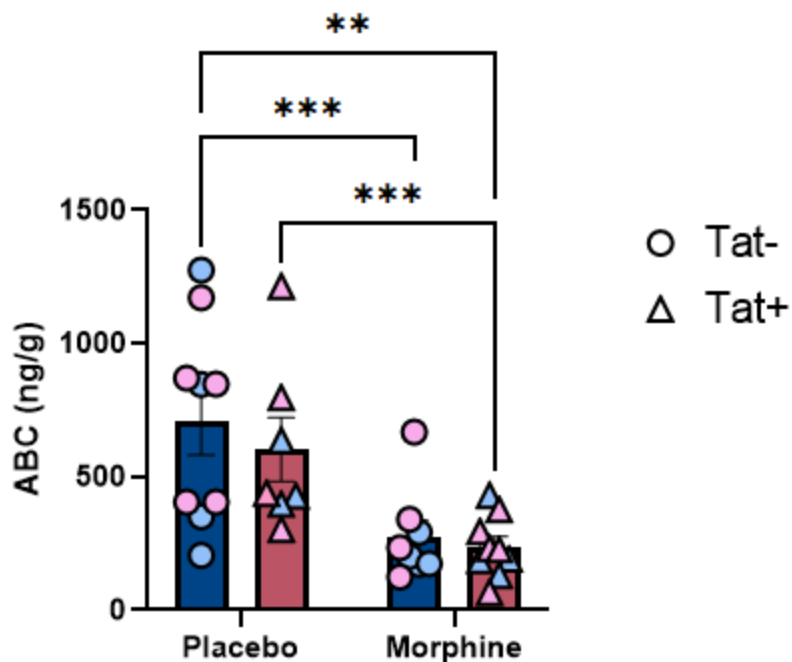


Figure 4: The effects of HIV-1 Tat and morphine on abacavir concentrations in the anterior cerebral cortex using IR-MALDESI MSI. In the bar graph, Tat(-) mice are depicted by dark blue bars and circles, while Tat(+) mice are depicted by red bars and triangles. Post-hoc significant differences at $\alpha < 0.05$ are denoted by $**p < 0.0021$ and $***p < 0.0002$. The mean abacavir concentrations \pm SEM were sampled from $n = 9$ Tat(-) placebo, $n = 7$ Tat(+) placebo, $n = 8$ Tat(-) morphine, $n = 9$ Tat(+) morphine; both sexes are included in this analysis, where female mice are represented using pink circles or triangles and male mice are represented using light blue circles or triangles.

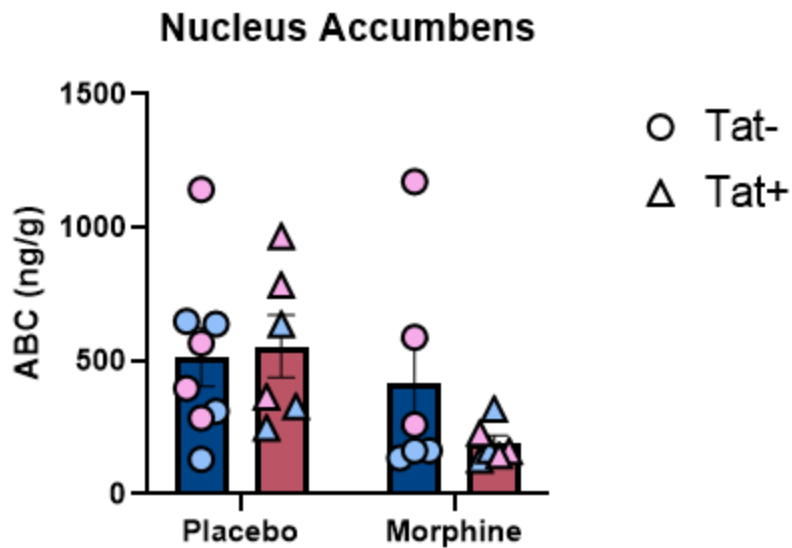


Figure 5: The effects of HIV-1 Tat and morphine on abacavir concentrations in the nucleus accumbens using IR-MALDESI MSI. In the bar graph, Tat(-) mice are depicted by dark blue bars and circles, while Tat(+) mice are depicted by red bars and triangles. The mean abacavir concentrations \pm SEM were sampled from $n = 8$ Tat(-) placebo, $n = 6$ Tat(+) placebo, $n = 6$ Tat(-) morphine, $n = 6$ Tat(+) morphine; both sexes are included in this analysis, where female mice are represented using pink circles or triangles and male mice are represented using light blue circles or triangles.

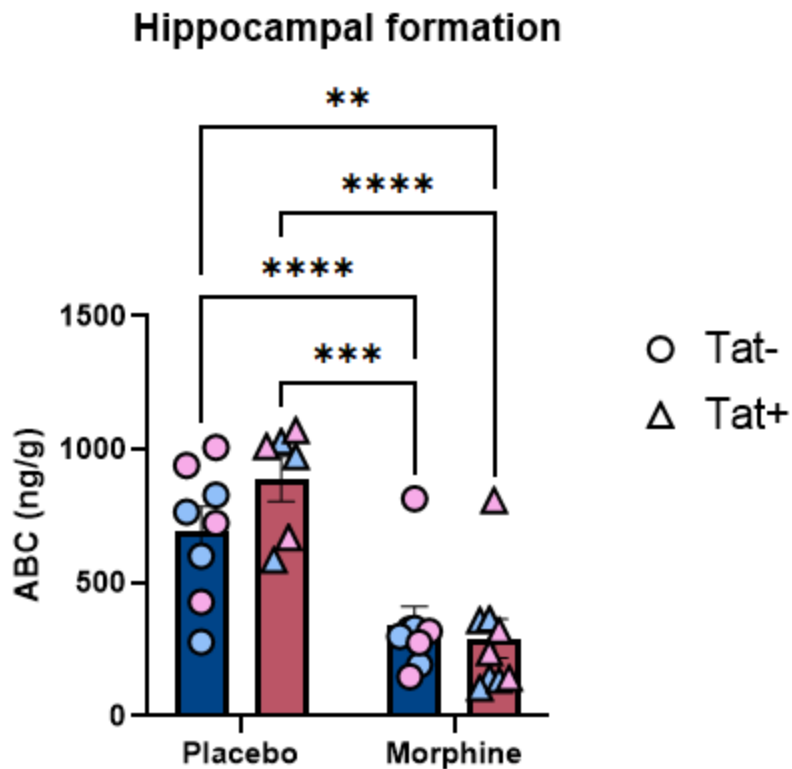


Figure 6: The effects of HIV-1 Tat and morphine on abacavir concentrations in the hippocampal formation using IR-MALDESI MSI. In the bar graph, Tat(-) mice are depicted by dark blue bars and circles, while Tat(+) mice are depicted by red bars and triangles. *Post-hoc* significant differences at $\alpha < 0.05$ are denoted by $**p < 0.0021$, $***p < 0.0002$, and $****p < 0.0001$. The mean abacavir concentrations \pm SEM were sampled from $n = 8$ Tat(-) placebo, $n = 6$ Tat(+) placebo, $n = 8$ Tat(-) morphine, $n = 9$ Tat(+) morphine; both sexes are included in this analysis, where female mice are represented using pink circles or triangles and male mice are represented using light blue circles or triangles.

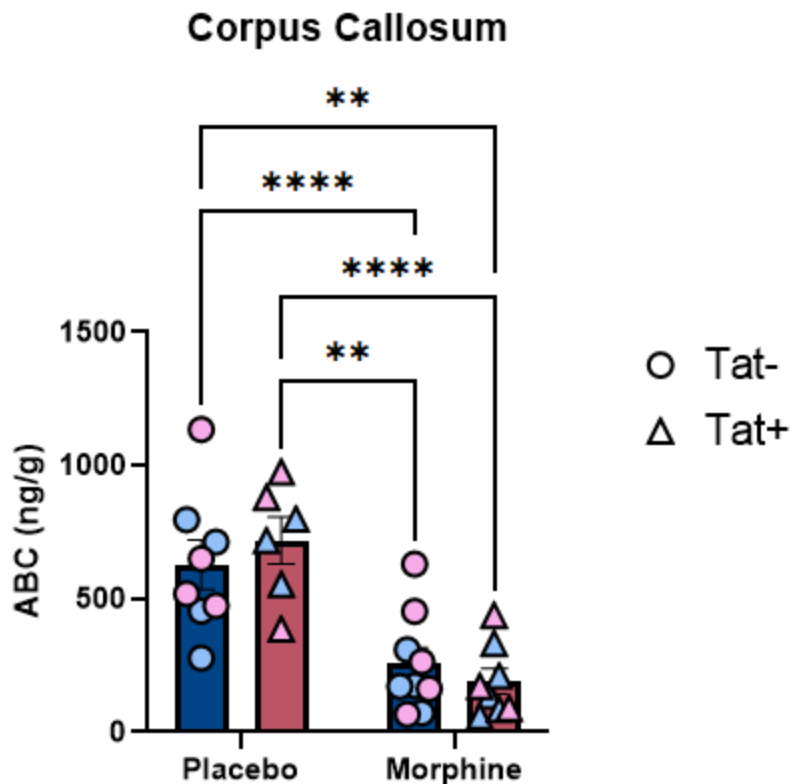


Figure 7: The effects of HIV-1 Tat and morphine on abacavir concentrations in the posterior corpus callosum using IR-MALDESI MSI. In the bar graph, Tat(-) mice are depicted by dark blue bars and circles, while Tat(+) mice are depicted by red bars and triangles. Post-hoc significant differences at $\alpha < 0.05$ are denoted by ** $p < 0.0021$ **** $p < 0.0001$. The mean abacavir concentrations \pm SEM were sampled from $n = 8$ Tat(-) placebo, $n = 6$ Tat(+) placebo, $n = 9$ Tat(-) morphine, $n = 8$ Tat(+) morphine; both sexes are included in this analysis, where female mice are represented using pink circles or triangles and male mice are represented using light blue circles or triangles.

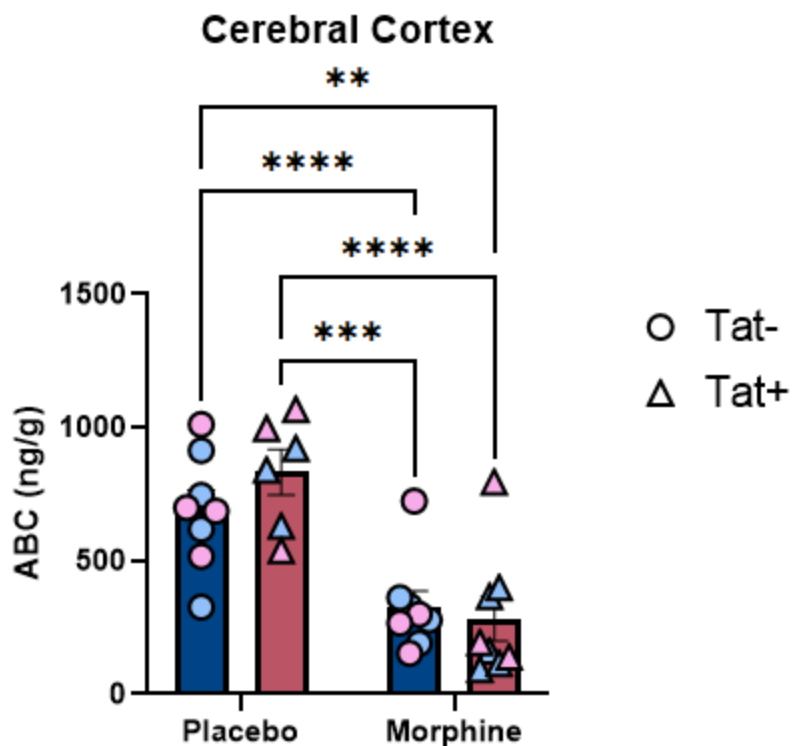


Figure 8: The effects of HIV-1 Tat and morphine on abacavir concentrations in the posterior cerebral cortex using IR-MALDESI MSI. In the bar graph, Tat(-) mice are depicted by dark blue bars and circles, while Tat(+) mice are depicted by red bars and triangles. *Post-hoc* significant differences at $\alpha < 0.05$ are denoted by $**p < 0.0021$, $***p < 0.0002$, and $****p < 0.0001$. The mean abacavir concentrations \pm SEM were sampled from $n = 8$ Tat(-) placebo, $n = 6$ Tat(+) placebo, $n = 8$ Tat(-) morphine, $n = 8$ Tat(+) morphine; both sexes are included in this analysis, where female mice are represented using pink circles or triangles and male mice are represented using light blue circles or triangles.

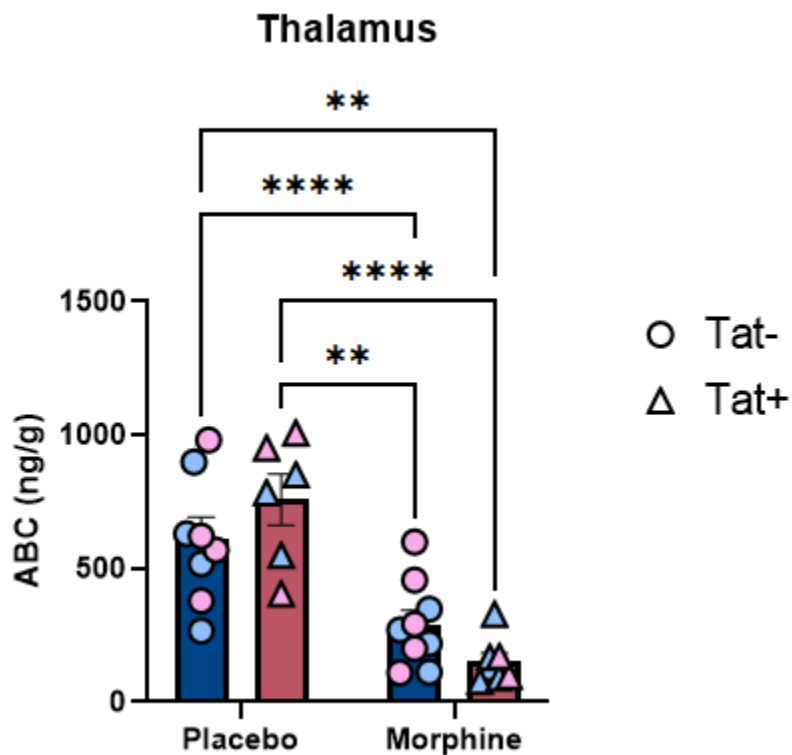


Figure 9: The effects of HIV-1 Tat and morphine on abacavir concentrations in the thalamus using IR-MALDESI MSI. In the bar graph, Tat(-) mice are depicted by dark blue bars and circles, while Tat(+) mice are depicted by red bars and triangles. *Post-hoc* significant differences at $\alpha < 0.05$ are denoted by $**p < 0.0021$ and $****p < 0.0001$. The mean abacavir concentrations \pm SEM were sampled from $n = 8$ Tat(-) placebo, $n = 6$ Tat(+) placebo, $n = 9$ Tat(-) morphine, $n = 7$ Tat(+) morphine; both sexes are included in this analysis, where female mice are represented using pink circles or triangles and male mice are represented using light blue circles or triangles.

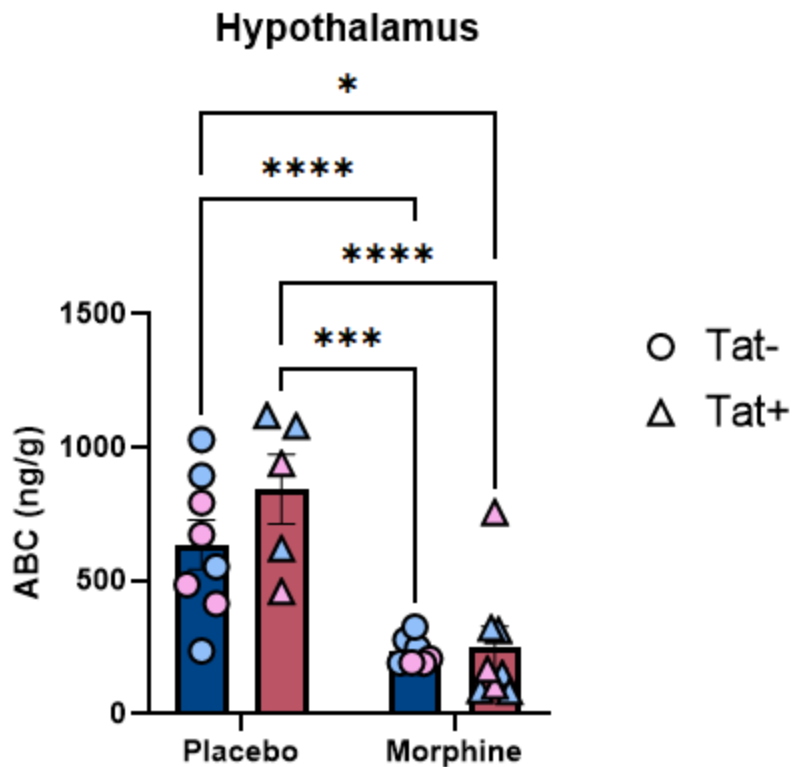


Figure 10: The effects of HIV-1 Tat and morphine on abacavir concentrations in the hypothalamus using IR-MALDESI MSI. In the bar graph, Tat(-) mice are depicted by dark blue bars and circles, while Tat(+) mice are depicted by red bars and triangles. *Post-hoc* significant differences at $\alpha < 0.05$ are denoted by * $p < 0.0032$, *** $p < 0.0002$, and **** $p < 0.0001$. The mean abacavir concentrations \pm SEM were sampled from $n = 8$ Tat(-) placebo, $n = 5$ Tat(+) placebo, $n = 7$ Tat(-) morphine, $n = 8$ Tat(+) morphine; both sexes are included in this analysis, where female mice are represented using pink circles or triangles and male mice are represented using light blue circles or triangles.

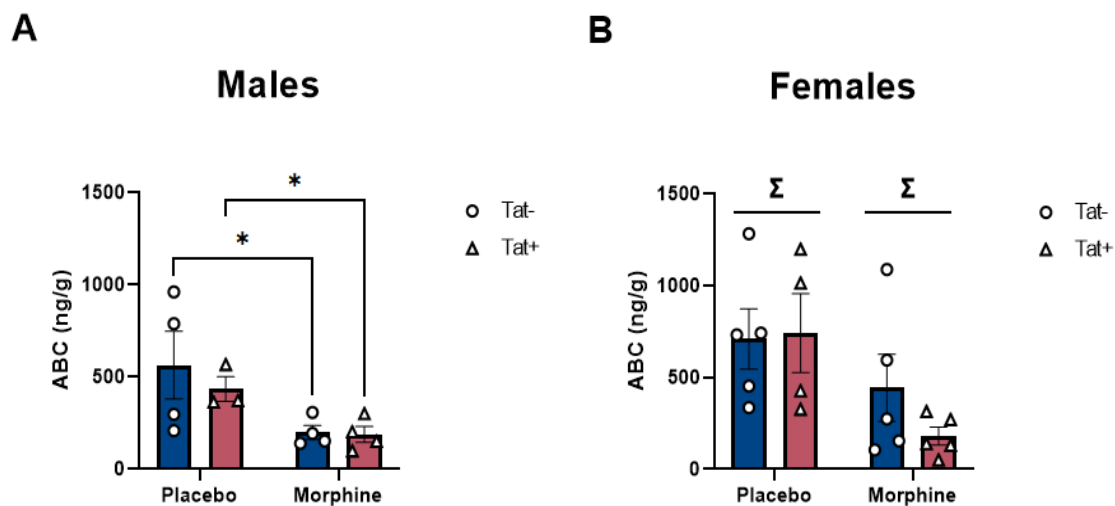


Figure 11: Effects of HIV-1 Tat and morphine on abacavir concentrations in the anterior corpus callosum in males (A) and females (B) using IR-MALDESI MSI. In the bar graph, Tat(-) mice are depicted by dark blue bars and circles, while Tat(+) mice are depicted by red bars and triangles. Main effects from the 2-WAY ANOVA in the anterior corpus callosum are represented by a significant main effect of treatment (Σ) [morphine vs. placebo]. Post-hoc significant differences at $\alpha < 0.05$ are denoted by * $p < 0.0032$. The mean abacavir concentrations \pm SEM were sampled from (A) $n = 4$ Tat(-) placebo, $n = 3$ Tat(+) placebo, $n = 4$ Tat(-) morphine, $n = 4$ Tat(+) morphine; (B) $n = 5$ Tat(-) placebo, $n = 4$ Tat(+) placebo, $n = 5$ Tat(-) morphine, $n = 5$ Tat(+) morphine.

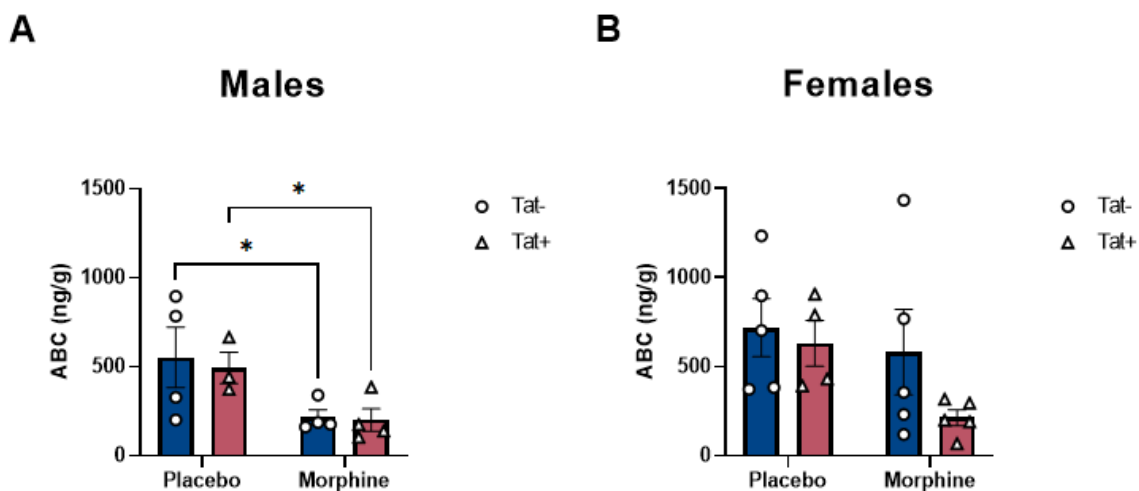


Figure 12: Effects of HIV-1 Tat and morphine on abacavir concentrations in the caudoputamen in males (A) and females (B) using IR-MALDESI MSI. In the bar graph, Tat(-) mice are depicted by dark blue bars and circles, while Tat(+) mice are depicted by red bars and triangles. *Post-hoc* significant differences at $\alpha < 0.05$ are denoted by * $p < 0.0032$. The mean abacavir concentrations \pm SEM were sampled from (A) $n = 4$ Tat(-) placebo, $n = 3$ Tat(+) placebo, $n = 4$ Tat(-) morphine, $n = 4$ Tat(+) morphine; (B) $n = 5$ Tat(-) placebo, $n = 4$ Tat(+) placebo, $n = 5$ Tat(-) morphine, $n = 5$ Tat(+) morphine.

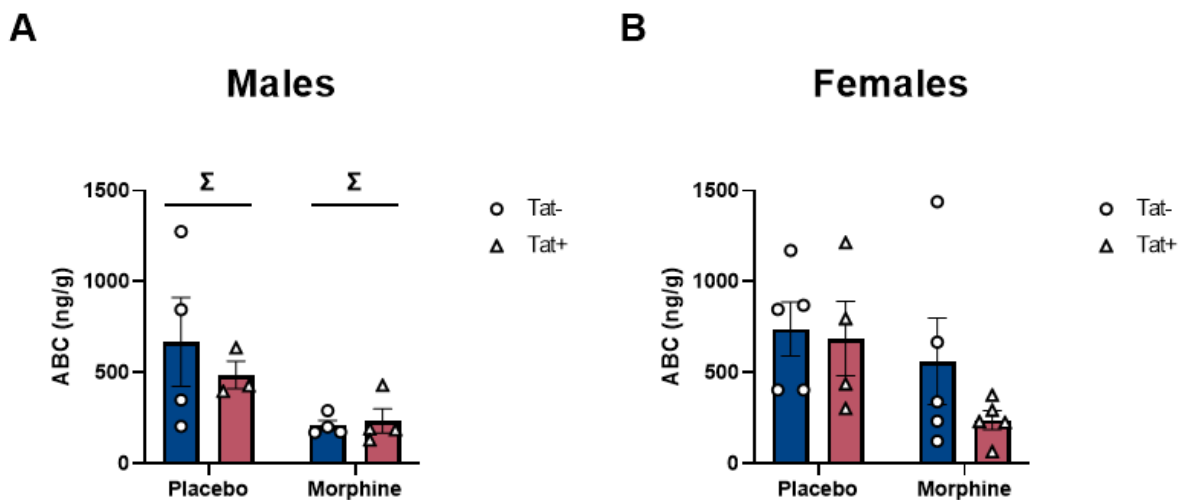


Figure 13: Effects of HIV-1 Tat and morphine on abacavir concentrations in the anterior cerebral cortex in males (A) and females (B) using IR-MALDESI MSI. In the bar graph, Tat(-) mice are depicted by dark blue bars and circles, while Tat(+) mice are depicted by red bars and triangles. Main effects from the 2-WAY ANOVA in the anterior cerebral cortex are represented by a significant main effect of treatment (Σ) [morphine vs. placebo]. The mean abacavir concentrations \pm SEM were sampled from (A) $n = 4$ Tat(-) placebo, $n = 3$ Tat(+) placebo, $n = 4$ Tat(-) morphine, $n = 4$ Tat(+) morphine; (B) $n = 5$ Tat(-) placebo, $n = 4$ Tat(+) placebo, $n = 5$ Tat(-) morphine, $n = 5$ Tat(+) morphine.

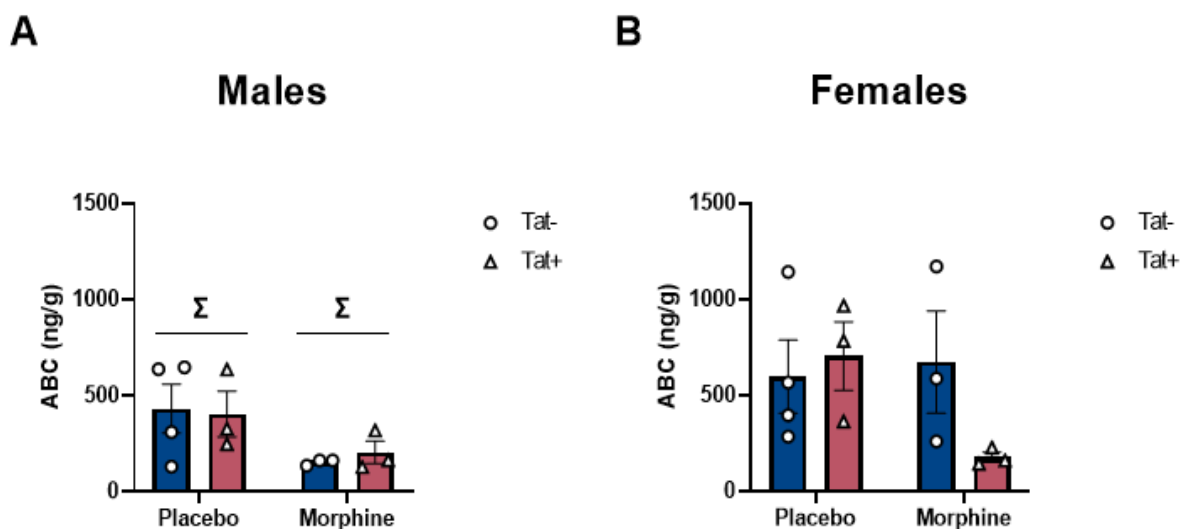


Figure 14: Effects of HIV-1 Tat and morphine on abacavir concentrations in the nucleus accumbens in males (A) and females (B) using IR-MALDESI MSI. In the bar graph, Tat(-) mice are depicted by dark blue bars and circles, while Tat(+) mice are depicted by red bars and triangles. Main effects from the 2-WAY ANOVA in the nucleus accumbens are represented by a significant main effect of treatment (Σ) [morphine vs. placebo]. The mean abacavir concentrations \pm SEM were sampled from (A) $n = 4$ Tat(-) placebo, $n = 3$ Tat(+) placebo, $n = 3$ Tat(-) morphine, $n = 3$ Tat(+) morphine; (B) $n = 4$ Tat(-) placebo, $n = 3$ Tat(+) placebo, $n = 3$ Tat(-) morphine, $n = 3$ Tat(+) morphine.

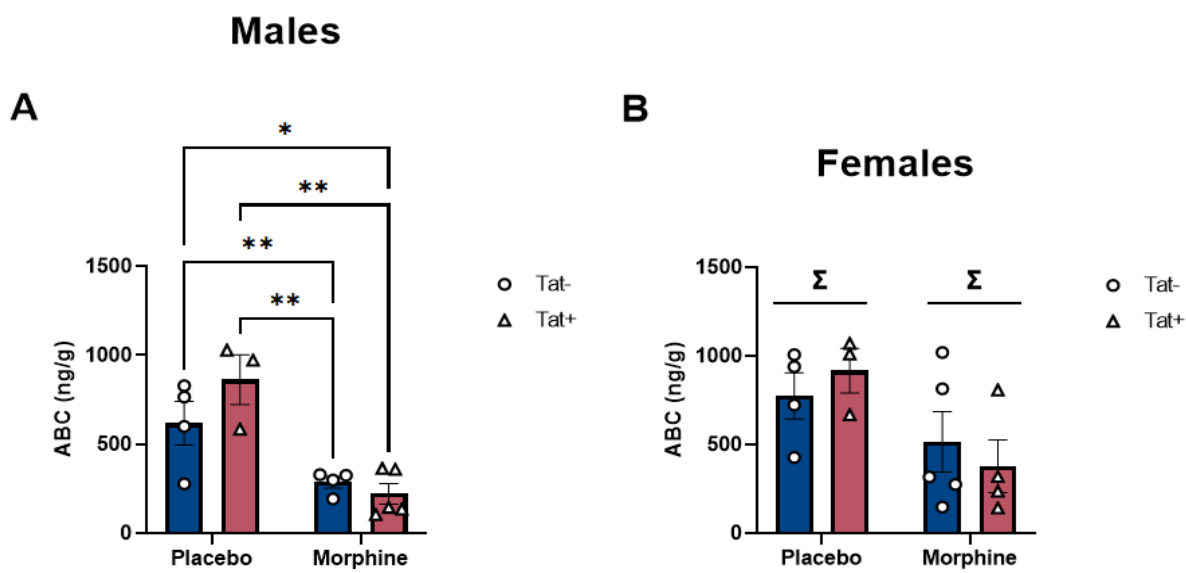
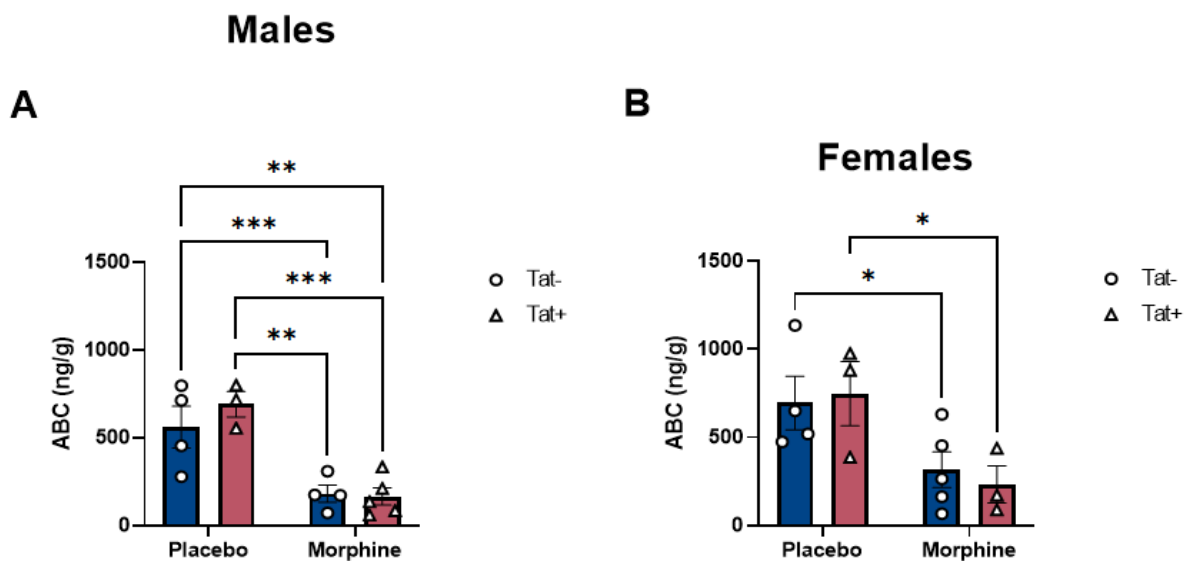


Figure 15: Effects of HIV-1 Tat and morphine on abacavir concentrations in the hippocampal formation in males (**A**) and females (**B**) using IR-MALDESI MSI. In the bar graph, Tat(-) mice are depicted by dark blue bars and circles, while Tat(+) mice are depicted by red bars and triangles. Main effects from the 2-WAY ANOVA in the hippocampal formation are represented by a significant main effect of treatment (Σ) [morphine vs. placebo]. *Post-hoc* significant differences at $\alpha < 0.05$ are denoted by $*p < 0.0032$ and $**p < 0.0021$. The mean abacavir concentrations \pm SEM were sampled from (**A**) $n = 4$ Tat(-) placebo, $n = 3$ Tat(+) placebo, $n = 4$ Tat(-) morphine, $n = 5$ Tat(+) morphine; (**B**) $n = 4$ Tat(-) placebo, $n = 3$ Tat(+) placebo, $n = 5$ Tat(-) morphine, $n = 4$ Tat(+) morphine.



*Figure 16: Effects of HIV-1 Tat and morphine on abacavir concentrations in the posterior corpus callosum in males (A) and females (B) using IR-MALDESI MSI. In the bar graph, Tat(-) mice are depicted by dark blue bars and circles, while Tat(+) mice are depicted by red bars and triangles. Post-hoc significant differences at $\alpha < 0.05$ are denoted by * $p < 0.0032$, ** $p < 0.0021$ and *** $p < 0.0002$. The mean abacavir concentrations \pm SEM were sampled from (A) $n = 4$ Tat(-) placebo, $n = 3$ Tat(+) placebo, $n = 4$ Tat(-) morphine, $n = 5$ Tat(+) morphine; (B) $n = 4$ Tat(-) placebo, $n = 3$ Tat(+) placebo, $n = 5$ Tat(-) morphine, $n = 3$ Tat(+) morphine.*

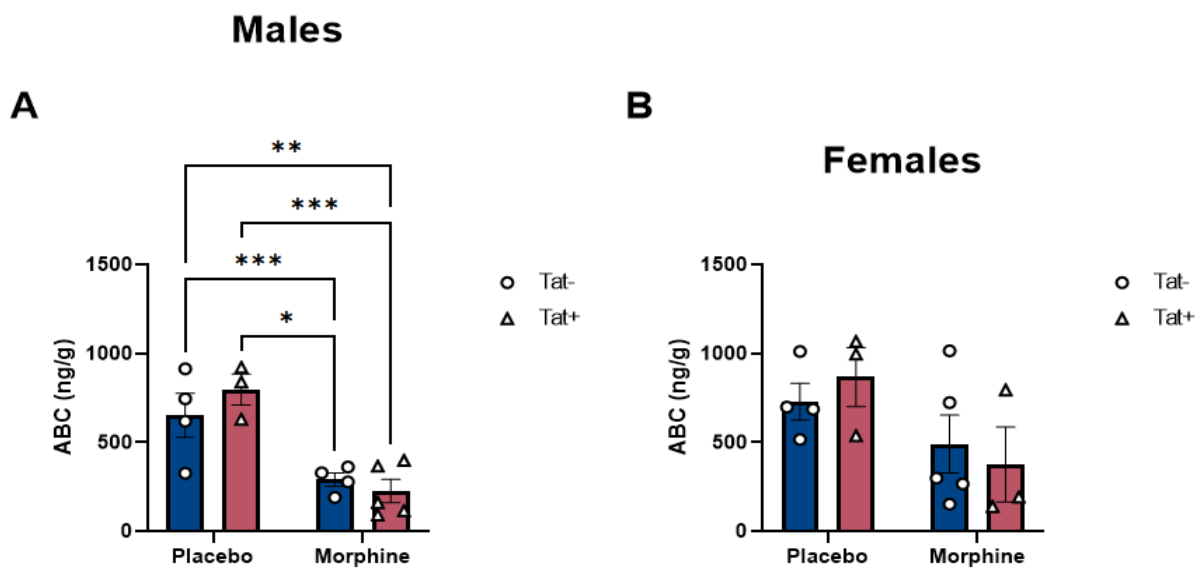


Figure 17: Effects of HIV-1 Tat and morphine on abacavir concentrations in the posterior cerebral cortex in males (A) and females (B) using IR-MALDESI MSI. In the bar graph, Tat(-) mice are depicted by dark blue bars and circles, while Tat(+) mice are depicted by red bars and triangles. *Post-hoc* significant differences at $\alpha < 0.05$ are denoted by * $p < 0.0032$, ** $p < 0.0021$ and *** $p < 0.0002$. The mean abacavir concentrations \pm SEM were sampled from (A) $n = 4$ Tat(-) placebo, $n = 3$ Tat(+) placebo, $n = 4$ Tat(-) morphine, $n = 5$ Tat(+) morphine; (B) $n = 4$ Tat(-) placebo, $n = 3$ Tat(+) placebo, $n = 5$ Tat(-) morphine, $n = 3$ Tat(+) morphine.

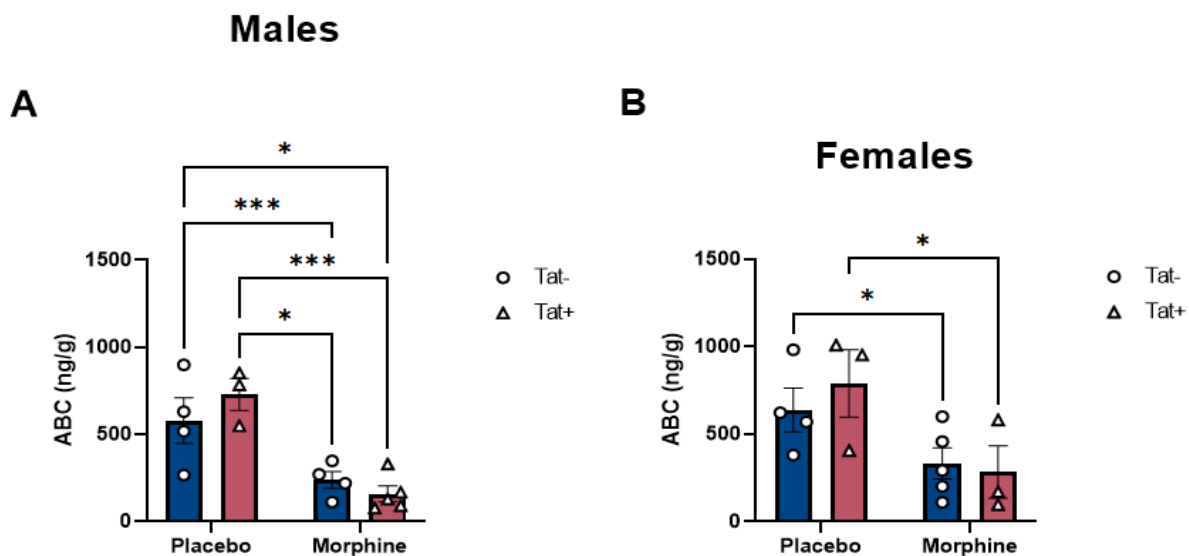


Figure 18: Effects of HIV-1 Tat and morphine on abacavir concentrations in the thalamus in males (A) and females (B) using IR-MALDESI MSI. In the bar graph, Tat(-) mice are depicted by dark blue bars and circles, while Tat(+) mice are depicted by red bars and triangles. . Post-hoc significant differences at $\alpha < 0.05$ are denoted by $*p < 0.0032$ and $***p < 0.0002$. The mean abacavir concentrations \pm SEM were sampled from (A) $n = 4$ Tat(-) placebo, $n = 3$ Tat(+) placebo, $n = 4$ Tat(-) morphine, $n = 5$ Tat(+) morphine; (B) $n = 4$ Tat(-) placebo, $n = 3$ Tat(+) placebo, $n = 5$ Tat(-) morphine, $n = 3$ Tat(+) morphine.

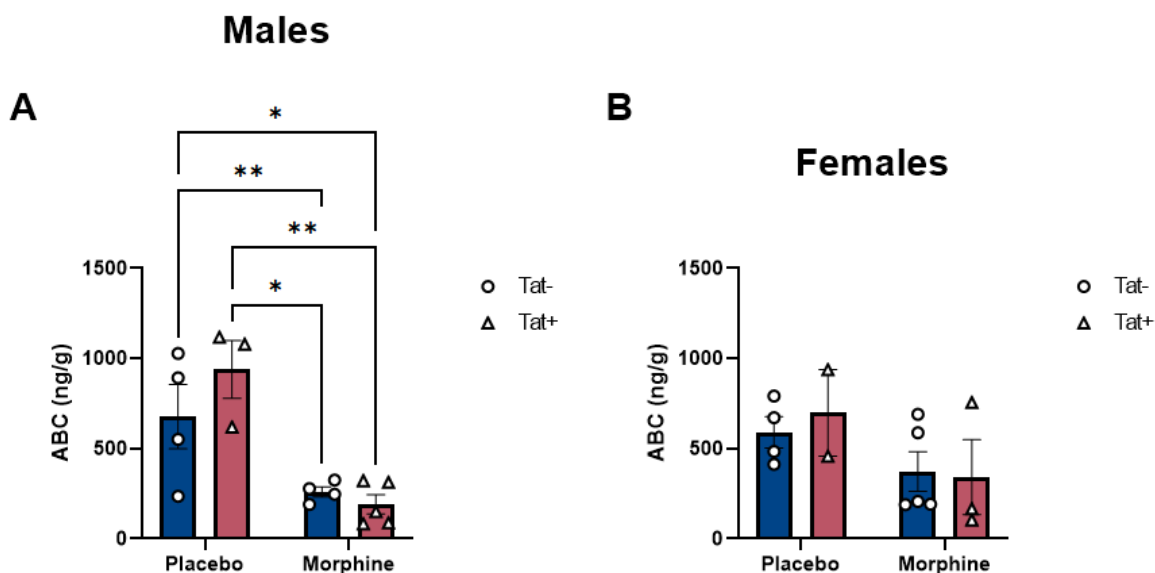


Figure 19: Effects of HIV-1 Tat and morphine on abacavir concentrations in the hypothalamus in males (A) and females (B) using IR-MALDESI MSI. In the bar graph, Tat(-) mice are depicted by dark blue bars and circles, while Tat(+) mice are depicted by red bars and triangles. *Post-hoc* significant differences at $\alpha < 0.05$ are denoted by * $p < 0.0032$ and ** $p < 0.0021$. The mean abacavir concentrations \pm SEM were sampled from (A) $n = 4$ Tat(-) placebo, $n = 3$ Tat(+) placebo, $n = 4$ Tat(-) morphine, $n = 5$ Tat(+) morphine; (B) $n = 4$ Tat(-) placebo, $n = 2$ Tat(+) placebo, $n = 5$ Tat(-) morphine, $n = 3$ Tat(+) morphine.

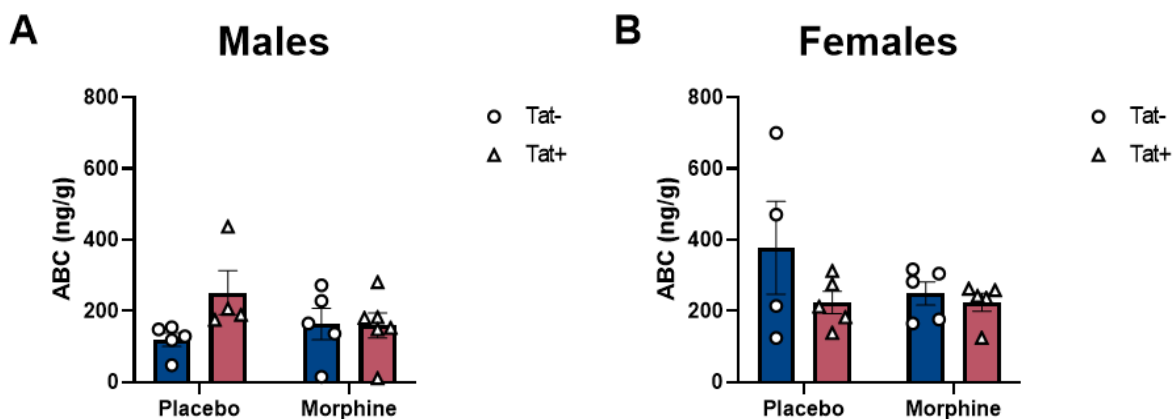


Figure 20: Effects of HIV-1 Tat and morphine on abacavir concentrations in males (A) and females (B) using LC-MS/MS. In the bar graph, Tat(-) mice are depicted by dark blue bars and circles, while Tat(+) mice are depicted by red bars and triangles. The mean abacavir concentrations \pm SEM were sampled from (A) n = 5 Tat(-) placebo, n = 4 Tat(+) placebo, n = 5 Tat(-) morphine, n = 6 Tat(+) morphine; (B) n = 4 Tat(-) placebo, n = 5 Tat(+) placebo, n = 5 Tat(-) morphine, n = 5 Tat(+) morphine.

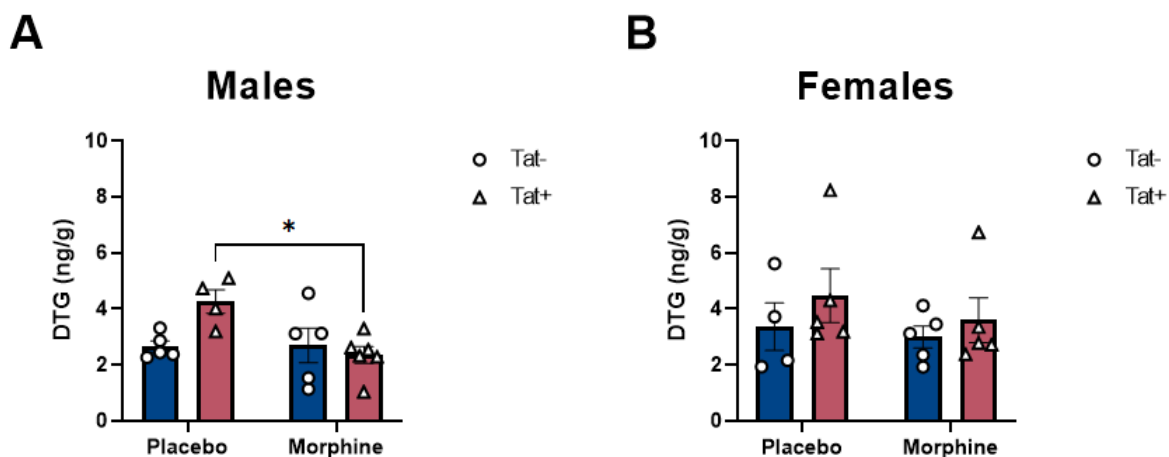


Figure 21: Effects of HIV-1 Tat and morphine on dolutegravir concentrations in males (A) and females (B) using LC-MS/MS. In the bar graph, Tat(-) mice are depicted by dark blue bars and circles, while Tat(+) mice are depicted by red bars and triangles. *Post-hoc* significant differences at $\alpha < 0.05$ are denoted by * $p < 0.0032$. The mean dolutegravir concentrations \pm SEM were sampled from (A) $n = 5$ Tat(-) placebo, $n = 4$ Tat(+) placebo, $n = 5$ Tat(-) morphine, $n = 6$ Tat(+) morphine; (B) $n = 4$ Tat(-) placebo, $n = 5$ Tat(+) placebo, $n = 5$ Tat(-) morphine, $n = 5$ Tat(+) morphine.

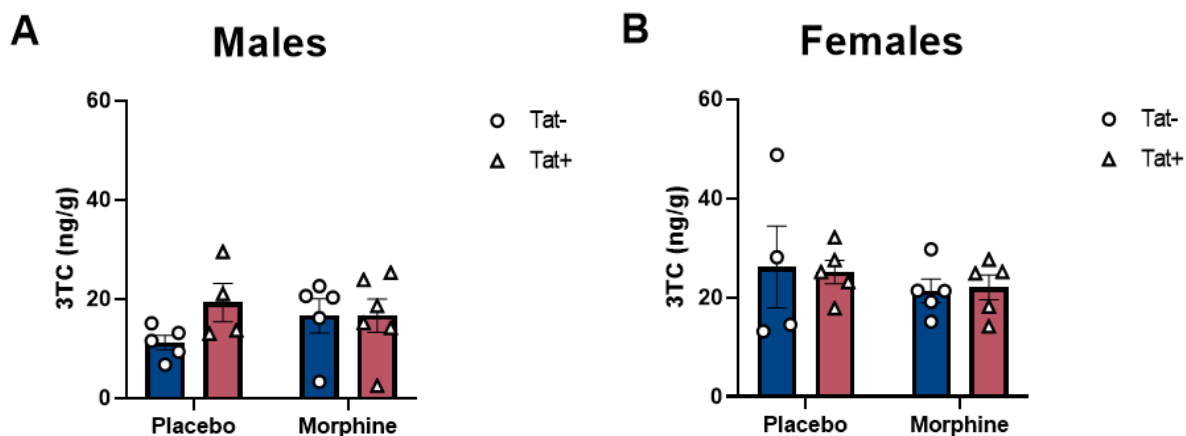


Figure 22: Effects of HIV-1 Tat and morphine on lamivudine concentrations in males (**A**) and females (**B**) using LC-MS/MS. In the bar graph, Tat(-) mice are depicted by dark blue bars and circles, while Tat(+) mice are depicted by red bars and triangles. The mean lamivudine concentrations \pm SEM were sampled from (**A**) $n = 5$ Tat(-) placebo, $n = 4$ Tat(+) placebo, $n = 5$ Tat(-) morphine, $n = 6$ Tat(+) morphine; (**B**) $n = 4$ Tat(-) placebo, $n = 5$ Tat(+) placebo, $n = 5$ Tat(-) morphine, $n = 5$ Tat(+) morphine.

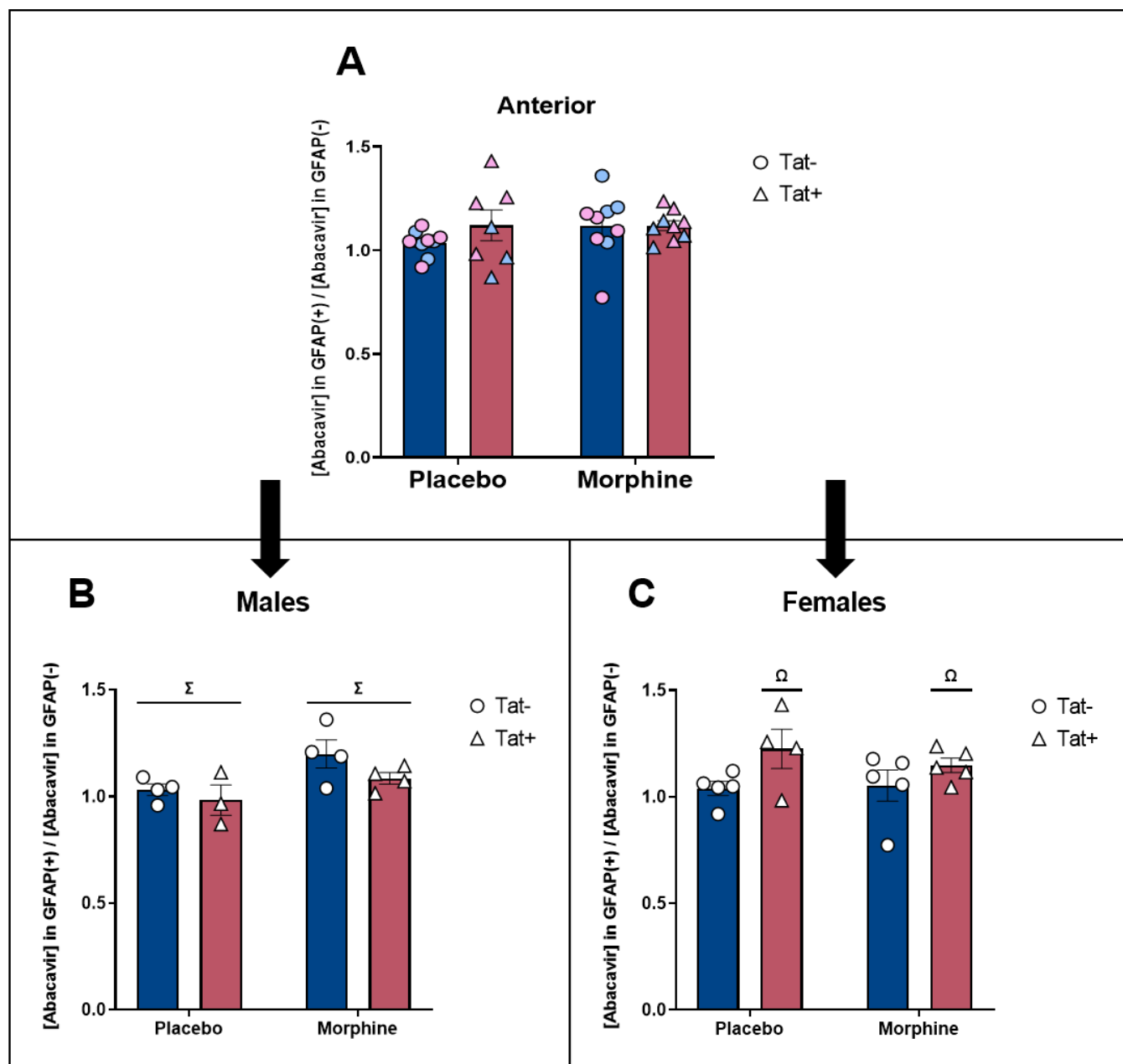


Figure 23: Morphine and HIV-1 Tat-mediated effects on abacavir concentrations evaluated using the ratio of abacavir concentrations with GFAP+ areas to GFAP- areas regardless of sex in the anterior brain section (A) followed by secondary analysis evaluating this response in male (B) and female (C) mice using IR-MALDESI MSI and IHC. In the bar graph, Tat(-) mice are depicted by dark blue bars and circles, while Tat(+) mice are depicted by red bars and triangles. Main effects from the 2-WAY ANOVA are represented by a significant main effect of treatment (Σ) [morphine vs. placebo] and/or main effect of Tat status (Ω). The mean ratio of abacavir concentrations within GFAP+ to GFAP- areas \pm SEM were sampled from (A) $n = 9$ Tat(-) placebo, $n = 7$ Tat(+) placebo, $n = 9$ Tat(-) morphine, $n = 9$ Tat(+) morphine, (B) $n = 4$ Tat(-) placebo, $n = 3$ Tat(+) placebo, $n = 4$ Tat(-) morphine, $n = 4$ Tat(+) morphine and (C) $n = 5$ Tat(-) placebo, $n = 4$ Tat(+) placebo, $n = 5$ Tat(-) morphine, $n = 5$ Tat(+) morphine; Both sexes are included in the primary analysis, where female mice are represented using pink circles or triangles and male mice are represented using light blue circles or triangles.

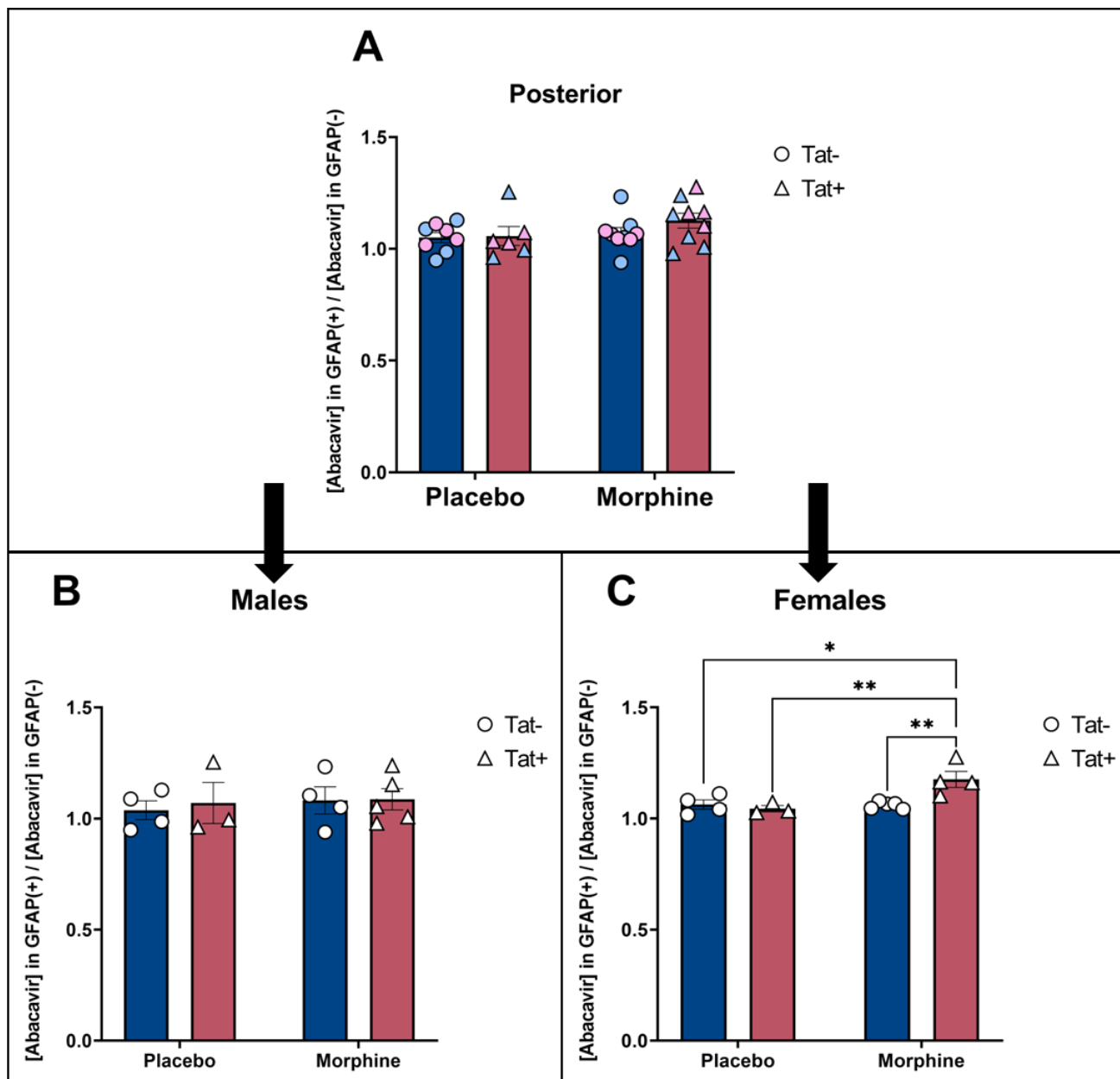


Figure 24: Morphine-mediated effects on abacavir concentrations evaluated using the ratio of abacavir concentrations with GFAP+ areas to GFAP- areas regardless of sex in the posterior brain section (A) followed by secondary analysis evaluating this response in male (B) and female (C) mice using IR-MALDESI MSI and IHC. In the bar graph, Tat(-) mice are depicted by dark blue bars and circles, while Tat(+) mice are depicted by red bars and triangles. Post-hoc significant effects at $\alpha < 0.05$ are denoted by * $p < 0.0032$ and ** $p < 0.0021$. The mean ratio of abacavir concentrations within GFAP+ to GFAP- areas \pm SEM were sampled from (A) $n = 8$ Tat(-) placebo, $n = 6$ Tat(+) placebo, $n = 9$ Tat(-) morphine, $n = 9$ Tat(+) morphine, (B) $n = 4$ Tat(-) placebo, $n = 3$ Tat(+) placebo, $n = 4$ Tat(-) morphine, $n = 5$ Tat(+) morphine and (C) $n = 4$ Tat(-) placebo, $n = 3$ Tat(+) placebo, $n = 5$ Tat(-) morphine, $n = 4$ Tat(+) morphine; Both sexes are included in the primary analysis, where female mice are represented using pink circles or triangles and male mice are represented using light blue circles or triangles.

CHAPTER 4: Evaluate morphine accumulation and distribution in the presence of HIV-1 protein Tat, ARV, and morphine co-exposure.

4A. Introduction

While the global response to HIV has made considerable progress over the past few decades, HIV continues to spread rapidly among people who use illicit drugs in various regions of the world. According to the CDC, in 2018 an estimated 1.2 million people were diagnosed with HIV in the United States, with 186,500 of those reported HIV transmission by injection drug use (*HIV Among People Who Inject Drugs | HIV by Group | HIV/AIDS | CDC, 2022*). Globally, there are approximately 15.6 million injection drug users, with an estimated 3 million of them living with HIV (Mathers et al., 2008). Additionally, a recent study found that of those 15.6 million people, 82.9% (76.6 – 88.9%) mainly injected opioids (Degenhardt et al., 2017). Injection drug use can increase the rates of HIV viral transmission and opioid exposure has been shown to worsen HIV infection, a serious concern for people who inject opioids or are prescribed opioid medications (Dutta & Roy, 2015; El-Hage et al., 2008; Guo et al., 2002; Peterson et al., 1990).

Opioid exposure worsens the neuropathology of HIV in several ways. Studies have demonstrated that exposure to morphine, the prototypical opioid, potentiates neuroHIV through increasing viral replication (Guo et al., 2002; Hauser et al., 2012; Kumar et al., 2006), disrupting calcium homeostasis and glutamate signaling, increasing the release of proinflammatory cytokines and worsening CNS inflammation (D. A. Byrd et al., 2011; Chen et al., 2020; Leibrand et al., 2022; Reddy et al., 2012), which all converges within the CNS to lead to cellular dysfunction and death (Hu et al., 2005;

Murphy et al., 2019; Reddy et al., 2012). Additionally inflammatory mediators serve to recruit infected monocytes across the blood-brain barrier and into the brain. Opioid exposure in the setting of HIV further increases monocyte transmigration across the BBB and into the brain (Dutta & Roy, 2012; Murphy et al., 2019; Strazza et al., 2016). Indeed, exposure to the HIV viral protein Tat, in combination with morphine, also increases the recruitment of inflammatory monocytes within the CNS (Dutta & Roy, 2015; Leibrand et al., 2022; Murphy et al., 2019).

In addition to experiencing neuroHIV and the neurocognitive impairments often associated with HIV infection, people living with HIV experience more chronic pain than uninfected individuals; nearly half of people living with HIV report clinically significant pain (Edelman et al., 2013; Merlin et al., 2012, 2018; R. Parker et al., 2014). As a result, individuals living with HIV are more likely to be prescribed opioids (Edelman et al., 2013; Jeevanjee et al., 2014; Silverberg et al., 2012), and at higher doses, thereby increasing their risk of developing opioid use disorder (Edelman et al., 2013; Silverberg et al., 2012; Tsao et al., 2012). It has been suggested that HIV infection affects opioid efficacy and potency, as the HIV-1 viral protein transactivator of transcription (Tat) expression was shown to increase morphine tolerance and decrease its physical dependence (Fitting et al., 2012, 2016). HIV-1 Tat induction in mice resulted in an increase in morphine tolerance as assessed by the warm water tail-flick assays, where mice exposed to morphine + Tat saw a decrease in percentage of maximal possible effect (Fitting et al., 2016). The authors measured physical dependence to morphine by evaluating the withdrawal effects noted after a 1 mg/kg naloxone injection following chronic morphine administration and discovered that Tat-exposed mice demonstrated

decreased withdrawal effects, suggesting HIV-1 Tat induction decreased the physical dependence to morphine (Fitting et al., 2016). However, the authors did not measure morphine concentrations within the brain of these mice and therefore the effects of Tat expression on morphine brain concentrations are unknown, an effect that may account for the reported behavioral findings.

Our lab previously demonstrated that HIV-1 Tat influences morphine concentrations; however these results were performed using only two brain regions collected among only female mice. Therefore, the purpose of this study was to examine the impact of HIV-1 Tat on morphine levels in the brains of male and female mice across multiple brain regions.

4B. Materials and Methods

4B.1. Subjects and housing

The doxycycline-inducible HIV-1 Tat-1 transgenic mice and their appropriate controls were used for the present studies. Tat transgenic mice are on a C57 background and express HIV-1 Tat₁₋₈₆ controlled by an rtTA-driven, astrocyte-specific GFAP promoter. The tetracycline responsive promoter triggers Tat expression by a specially formulated chow containing 6 mg/g doxycycline. In all experiments using Tat transgenic mice (~4 months of age, ~25 g, males and females), genotype-confirmed Tat(+) and Tat(-) mice were placed on doxycycline chow to induce HIV-1 Tat transcription, if applicable. Tat(+) transgenic mice express both GFAP-rtTA and TRE-tat genes, while control Tat(-) transgenic mice express only the GFAP-rtTA genes. The Tat transgenic model is well characterized and mimics key aspects of the HIV-opioid

interplay (Bruce-Keller et al., 2008; Fitting et al., 2010a; Hauser et al., 2009; Langford et al., 2018; Leibrand et al., 2017). Importantly, recent evidence demonstrated that even in virally suppressed patients on chronic antiretroviral therapy, active Tat viral proteins remain elevated in the CSF of these patients and that there is a significant association between a history of drug abuse and Tat levels (Henderson et al., 2019).

For these studies, Tat(+) and Tat(-) mice were placed on doxycycline chow for 14 days, followed by a 5-day washout (no doxycycline) to minimize potential doxycycline-ARV-morphine drug interactions. Long lasting effects (up to 1 month) of Tat on learning and memory after doxycycline completion has previously been demonstrated (Carey et al., 2012).

4B.2. Drug Administration

Triumeq®, a combination tablet containing abacavir (600 mg), dolutegravir (50 mg), and lamivudine (300 mg), was purchased from the VCU Health Systems Pharmacy. The dosing for mice was calculated based on interspecies allometric scaling from the recommended dose in humans to mice (McArthur et al., 2010; Nair & Jacob, 2016; ViiV Healthcare, 2014), based on an average 25 g mouse and was as follows: abacavir 2.5 mg/day (123.5 mg/kg/day), dolutegravir 0.2 mg/day (10.3 mg/kg/day) and lamivudine 1.2 mg/day (61.7 mg/kg/day). Drugs were administered using osmotic pumps, as previously described (Leibrand et al., 2019). Briefly, the tablets were crushed into a fine powder and resuspended in normal saline. After centrifugation to pellet tablet excipients at 1000 rpm for 5 min, the supernatant was sterile filtered twice using a 0.45 µm followed by a 0.22 µm filter. After filtration, 210 µL was loaded into the ALZET®

osmotic pump (Model 2001, 1 $\mu\text{L/hr}$ delivery). For morphine groups, morphine salt pentahydrate powder was directly diluted into the antiretroviral solution prior to loading the osmotic pump at a concentration sufficient to deliver 2.5 mg/day. Drug preparations were made in batches to minimize dosing variability.

4B.3. Surgical Manipulation

Mice were anesthetized with isoflurane (4% induction, 2% maintenance). A small mid-scapular entry was made in the skin and the osmotic pump (containing both antiretroviral drugs and morphine or placebo) delivering 2.5 mg morphine per day or placebo was subcutaneously implanted. Bupivacaine was applied to all surgical sites immediately post-operation for pain relief. During sample collection, the tissues were minimally handled to maintain tissue morphology. Mice were briefly perfused with cold 1x PBS to flush the blood from within the brain vasculature. All flushing of the tissue was performed for approximately 5 minutes to minimize the leaching of drugs from tissue cells. After perfusions, the mice were decapitated and brain tissue was harvested. The tissue was then carefully transferred to a protective barrier made of foil and placed atop dry ice to freeze. Once frozen (~5 minutes) the samples were placed in a fresh protective barrier made of foil, properly identified, and stored at -80°C until the time of IR-MALDESI MSI analysis.

4B.4. Sample Preparation

Mouse brain samples were placed in a brain matrix (Zivic Instruments, BSMAS001-1) to reproducibly access coronal regions that included the anterior and posterior brain sections. Coronal slices were obtained from the anterior brain at sections

corresponding to the approximate range of images 44 - 53 of the Allen Mouse Brain Atlas, while posterior slices were gathered from images 66 - 85. A clinical cryostat (Leica CM1950, Leica Biosystems, Nussloch, Germany) was used to section tissue from each of these two regions. Serial sections of 10 μm thickness were thaw-mounted onto glass slides and stored at -86°C until analysis by IR-MALDESI MSI and IHC. A diagram of the sectioning plan is found in [Figure 1](#).

4B.5. IR-MALDESI MSI Analysis for Morphine

Conducting MSI analyses using an IR-MALDESI source has been described in detail elsewhere (Bokhart et al., 2015; C. G. Thompson et al., 2015, 2019), and will be briefly summarized. Prepared tissue sections were placed on a thermally controlled stage (a thermoelectric cooler TE Technology, Inc., Traverse City, MI) in the source chamber. Dry nitrogen was introduced to the closed chamber to reduce humidity, after which samples were cooled to -9°C . The source was then opened to ambient environment to increase the relative humidity to $\sim 50\%$ and allow an ice film to form on the surface of the sample, after which the source was closed and a low flow of nitrogen was re-introduced to maintain a relative humidity of $\sim 15\%$ during sample analysis allowing for constant ice thickness. An IR OPO laser (Opotek, Carlsbad, CA) tuned to $2.94\ \mu\text{m}$ was used for sample ablation. The plume of volatilized material from each sampling location was ionized by a perpendicular electrospray. Resulting ions were sampled into the Orbitrap QE Plus mass spectrometer (ThermoFisher Q Exactive Plus, Bremen, Germany), which was triggered to start data acquisition simultaneously with the laser shot and ion injection time was fixed to allow ion transience from the pulsed laser to the Orbitrap. A table of the resulting ions, both identified and unidentified, is

listed in Appendix I. Following acquisition, the sample stage was translated in 100 μm step increments. Laser, stage, and mass spectrometer signaling was controlled by a microcontroller and custom software (Robichaud et al., 2013).

Analysis was conducted in positive mode, with resolving power set to 140,000 at m/z 200. The mass accuracy of better than 1 parts per million (ppm) was confirmed by weekly calibration of the mass spectrometer with the calibration solution recommended by the manufacturer. Antiretrovirals (ARV) were evaluated in a single tissue section using full-scan MS mode, with mass spectra acquired with a mass range m/z 150 – 600, with an electrospray solvent of water and methanol (50:50 v/v) and 0.2% formic acid. A subjacent section was used to measure morphine in MS/MS acquisition, using a m/z 4 isolation window centered at m/z 286.00 and a normalized collision energy NCE=10 with an electrospray solvent of water and acetonitrile (50:50 v/v) and 0.2% formic acid. Automatic gain control (AGC) function was turned off to match trapping conditions required by IR-MALDESI MSI, and ion injection time was fixed at 11 ms.

4B.6. Immunohistochemistry

Immunohistochemistry (IHC) was performed on OCT embedded tissue sections mounted on positively charged slides. This IHC was carried out using the Leica Bond III Autostainer system. Slides were first hydrated in Bond Wash solution (AR9590). Heat induced antigen retrieval was performed at 100°C in Bond-Epitope Retrieval solution 1 pH-6.0 (AR9961) for 20 minutes. The antigen retrieval was followed with a 5 min peroxide blocking step (Biocare, IPB5000L). After pretreatment, slides were incubated with a GFAP primary antibody (Dako, Z0334) at 1:1500 for 60 minutes followed with

Novolink Polymer (Leica, RE7260-CE) secondary. Antibody detection with 3,3'-diaminobenzidine (DAB) and hematoxylin counterstain were performed using the Bond Intense R detection system (Leica, DS9263).

Stained slides were dehydrated and coverslipped with Cytoseal 60 (23-244256, Fisher Scientific). Positive controls were included for this assay. Slides were digitally imaged with the Aperio AT2 (Leica Biosystems) using a 20x objective.

4B.7. Image Analysis

Following immunohistochemistry (IHC), brain regions within the anterior and posterior sections were histologically annotated by hand using the Allen Mouse Brain Atlas for reference. For the anterior sample sections, coronal images 44 - 53 of the Allen Mouse Brain Atlas were used to identify four regions of interest; the corpus callosum, caudoputamen, cerebral cortex, and nucleus accumbens [Appendix IIa]. For the posterior sample sections, coronal images 66 - 85 of the Allen Mouse Brain Atlas were used to identify five regions of interest; the hippocampal formation, corpus callosum, cerebral cortex, thalamus, and hypothalamus [Appendix IIb]. MSConvert (Race et al., 2012) was used to convert raw signal intensity data to .mzXML files, which were then loaded into the mass spectrometry imaging program MSiReader (MATLAB application; Mathworks, Natick, MA) to generate ion distribution maps. MSiReader was used to export pixel intensity matrices for antiretrovirals, morphine, and endogenous ions of interest across the entire tissue slice into Matlab. IHC microscopy data and annotations were downsampled to match the resolution of the IR-MALDESI MSI data (pixel size: 100x100 m) and color thresholded to isolate staining from counterstain.

Using Matlab, several series of coding were performed to co-localize both IR-MALDESI MSI and IHC images to generate region-specific morphine accumulation data [Appendix IV]. Image co-localization was performed by manually selecting a minimum of eight control points between the IR-MALDESI MSI and IHC images [Appendix V]. Once selected the control points were used to align the images atop one another in order to generate regionally-specific ion intensities.

In addition to generating the region-specific morphine abundance data, IR-MALDESI MSI and IHC images were used to determine the proportion of drug that was co-localized with GFAP+ and GFAP- glial cell populations, across the entire slice irrespective of region specificity. Image co-localization was similarly performed by manually selecting at least eight control points between the IR-MALDESI MSI and IHC images and aligning the images based on said points. After image co-registration was performed, morphine drug signal was masked based on the distribution of GFAP, detailing information regarding changes in morphine accumulation within areas of gliosis.

4B.8. Statistical Analysis

Morphine Abundance

The mean morphine abundance in each of the brain regions mentioned above for the anterior and posterior section samples were analyzed using a two-way ANOVA to examine the main effects between brain regions and Tat status for each sex, followed by a Tukey's multiple comparison test.

A significance level of $\alpha = 0.05$ was used for all statistical analyses, and results were considered statistically significant if the p -value was less than α . GraphPad Prism Version 9.4.0 (GraphPad Software, LLC.) was used for all statistical analyses.

Changes in morphine abundance with areas of gliosis

In order to evaluate whether morphine accumulation preferentially localized to regions of gliosis and whether Tat exposure influenced drug accumulation in these areas, morphine abundance within areas of gliosis were analyzed from the IR-MALDESI MSI and IHC generated data. After image colocalization, morphine accumulation was masked onto both areas of positively and negatively-stained GFAP cells. Statistical analyses were performed on the ratio of morphine abundance within GFAP+ to GFAP- areas. An analysis was conducted using whole brain slices from the anterior and posterior brain sections using a two-way analysis of variance (ANOVA) to identify significant main effects and/or interactions between Tat status and sex. A Tukey's post-hoc test was performed after the analysis to assess pairwise comparisons. A significance level of $\alpha = 0.05$ was used for all statistical analyses, and results were considered statistically significant if the p -value was less than α . GraphPad Prism Version 9.4.0 was used for all statistical analyses.

4C. Results

4C.1. The effect of HIV-1 Tat on morphine abundance in distinct brain regions

The effect of HIV-1 Tat on morphine accumulation was qualitatively evaluated using IR-MALDESI MSI. Specifically, morphine abundance was evaluated in several regions within the anterior and posterior brain sections of HIV-1 Tat transgenic mice.

Within the anterior brain section, there was a main effect for Tat status across all regions identified (corpus callosum, caudoputamen, cerebral cortex, and nucleus accumbens) [$F_{(1, 61)} = 14.08, p = 0.0004$] such that Tat(+) mice demonstrated greater morphine abundance compared to Tat(-) mice. Post-hoc analysis revealed that Tat(+) mice had significantly greater levels of morphine abundance than Tat(-) mice for all regions [*Figure 25a*]. Within the posterior brain section, there were no significant main effects for Tat status in any of the brain regions examined (hippocampal formation, corpus callosum, cerebral cortex, thalamus or hypothalamus) [*Figure 25b*]. Additional significant post hoc tests are reported in **Table 1**.

4C.2. Sex differences in morphine abundance in the presence of antiretroviral drugs ± HIV-1 Tat

In an effort to better understand the complexities of morphine accumulation and abundance within the CNS, a secondary analysis was performed to examine potential sex differences. The effects of HIV-1 Tat on morphine abundance within the CNS for males versus females are reported below.

Anterior

For male mice, there were no significant main effects for Tat status across all regions within the anterior section (corpus callosum, caudoputamen, cerebral cortex, or nucleus accumbens) [Figure 26a].

For female mice, there was a significant main effect for Tat status [$F(1, 30) = 21.90$, $p < 0.0001$] such that Tat(+) mice displayed significantly higher morphine abundance in the anterior samples compared to Tat(-) mice. Following a post-hoc analysis, Tat(+) mice demonstrated a significant increase in morphine abundance compared to Tat(-) mice in the corpus callosum, caudoputamen, cerebral cortex, and nucleus accumbens ($p = 0.0013$) [Figure 26b]. Additional significant post hoc tests are reported in **Table 2**.

Posterior

For males, there was a significant main effect for Tat status [$F(1, 38) = 10.55$, $p = 0.0024$] such that Tat(+) mice displayed significantly less morphine abundance across all regions of interest in the posterior section (hippocampal formation, corpus callosum, cerebral cortex, thalamus, and hypothalamus combined) compared to the same combined regions within Tat(-) mice [Figure 27a]. Additional significant post hoc tests are reported in **Table 2**.

For females, there also was a significant main effect for Tat status [$F(1, 35) = 12.78$, $p = 0.0010$]. Tat(+) mice had significantly higher morphine abundance across the different regions of interest compared to Tat(-) mice. Post hoc analyses revealed that Tat(+) mice had significantly greater levels of morphine abundance compared to Tat(-)

mice in the hippocampal formation, corpus callosum, cerebral cortex, thalamus, and hypothalamus ($p = 0.0306$) [*Figure 27b*]. Additional significant post hoc tests are reported in **Table 2**.

4C.3. Sex-based response to HIV-1 Tat on morphine accumulation in the brain

In order to evaluate differences in morphine abundance between males and females in response to Tat induction, an additional secondary analysis was performed. Specifically, morphine accumulation was assessed in Tat(-) and Tat(+) mice between males and females within the anterior and posterior brain.

Anterior

When comparing morphine abundance in Tat(-) males and females, there was a significant main effect for sex [$F(1, 27) = 5.898$, $p = 0.0221$] such that male mice displayed increased morphine abundance across the different regions of interest in the anterior section compared to female mice. No significant differences between the means were revealed following a Tukey post hoc analysis [*Figure 28a*].

When comparing Tat(+) males and females, there was a significant main effect for sex [$F(1, 28) = 11.56$, $p = 0.0020$] such that female mice displayed increased morphine abundance across all regions of interest in the anterior section compared to male mice. A post hoc analysis revealed that Tat(+) female mice had significantly greater levels of morphine abundance compared to Tat(+) male mice in all regions of interest ($p = 0.0372$) [*Figure 28b*]. Additional significant post hoc tests are reported in **Table 3**.

Posterior

When comparing Tat(-) males and females, there was a significant main effect for sex [$F(1, 39) = 23.41, p < 0.0001$] such that male mice displayed increased morphine abundance across the different regions of interest in the posterior brain section compared to female mice. A post hoc analysis revealed that Tat(-) male mice had significantly greater levels of morphine abundance compared to Tat(-) female mice in all regions of interest within the posterior brain section ($p = 0.0008$) [*Figure 28c*]. Additional significant post hoc tests are reported in **Table 3**.

When comparing Tat(+) males and females, there was a significant main effect for sex [$F(1, 28) = 11.56, p = 0.0020$] where female mice displayed increased morphine abundance across the different regions of interest compared to male mice. No significant differences between the means were revealed following a Tukey post hoc analysis [*Figure 28d*].

4C.4. Effects of HIV-1 Tat on morphine abundance in areas of gliosis

In addition to assessing both regional and sex-based differences in morphine-treated mice in the presence of HIV-1 Tat, another secondary analysis was performed to determine the association between morphine abundance and glial activation. Specifically, for males and females and in both the anterior and posterior brain sections, a ratio of morphine abundance within areas of gliosis (GFAP+ areas) to morphine abundance within GFAP- areas was calculated.

In the anterior brain section, a two-way ANOVA revealed that the interaction between sex and Tat status was significant [$F(1,14) = 8.272, p = 0.0122$] where Tat

exposure resulted in decreased changes in morphine levels within areas of gliosis in male mice yet resulted in increased changes in females. No significant differences between the means were revealed following a Tukey post hoc analysis [Figure 29a].

In the posterior brain section, there were no significant main effects or interactions [Figure 29b].

4D. Discussion

This study sought to examine the effects of HIV-1 Tat exposure on morphine accumulation in a region-specific manner and, secondarily, if any sex differences in morphine exposure would be observed. Results from this study demonstrated that morphine accumulation within the anterior section of the brain was increased in the presence of HIV-1 Tat, and secondary analysis revealed that morphine levels were different only in the female mice. The study also revealed that in the posterior brain section, morphine levels in response to Tat exposure were opposite between males and females and that male and female mice differ in response to Tat-mediated changes in morphine accumulation at areas of gliosis within the anterior, but not posterior, brain.

The results from this study are consistent with findings of a previous study by our lab where the distribution of morphine and its major metabolite, morphine-3-glucuronide (M3G), was altered in Tat-exposed mice. Specifically, using the same Tat transgenic mouse model as was used in the present study, Tat(+) female mice had a 2.4-fold increase in morphine concentrations in the plasma. M3G brain concentrations were also increased in Tat(+) compared to Tat(-) mice (Leibrand et al., 2019). Although the present study did not quantify M3G levels, our results in female mice are consistent with

the findings of the prior study because in both studies, Tat expression in female mice resulted in increased morphine accumulation in the brain. The prior study included only females. Other studies have reported physiological outcomes in mouse models that could be associated with changes in morphine or M3G concentration due to Tat-exposure. In Fitting, et al. (2012), where male mice were utilized, it was reported that Tat expression led to increased morphine tolerance (decreased efficacy) and decreased physical dependence to morphine, determined using a warm-water tail-flick and an antagonist-precipitated withdrawal assay, respectively (Fitting et al., 2012, 2016). Although the investigators did not measure opioid concentrations in their study, it is plausible that decreases in brain morphine concentrations could help explain their findings.

There are multiple pharmacokinetic factors that could account for the different responses in morphine abundance to Tat exposure between male and female mice. Females have a lower body weight, a higher proportion of body fat, slower gastrointestinal motility, a higher gastric pH, decreased activity of intestinal enzymes, and a slower rate of glomerular filtration (Fadiran & Zhang, 2015). Differences in transporter expression may also contribute to alterations in morphine accumulation between males and females. For example, it has been reported that expression of the efflux transporter, P-glycoprotein, is threefold higher in males than females (Schuetz et al., 1995). Differences in P-glycoprotein transporter expression between males and females might account for the differences detected in morphine accumulation between male and female mice in the present study, as increased P-glycoprotein expression decreases morphine penetration into the brain. Sex differences have also been reported

in regards to morphine metabolism, where despite a lack of sex differences in morphine concentrations, M3G plasma concentrations were approximately two times higher in females than males (Baker & Ratka, 2002; South et al., 2009). Recent studies investigating the potential sex differences in morphine metabolism and M3G plasma concentrations in rats also report sex differences in the antinociceptive response to morphine, where females with higher M3G plasma concentrations also experience lower levels of antinociception (Baker & Ratka, 2002). While the present study did not investigate sex differences in morphine metabolism or M3G plasma concentrations, other studies report that M3G plasma ratios derived from brain homogenates can be directly associated with morphine concentrations where lower M3G ratios corresponded with lower morphine concentrations in the brain. This further supports the present findings where female mice demonstrated increased morphine accumulation.

Regional differences in morphine accumulation in response to HIV-1 Tat exposure between males and females were also detected in the present study. Specifically, female, but not male, mice demonstrated significant morphine accumulation in response to Tat exposure within the anterior brain. A possible explanation for these findings could be attributable to the nonuniform distribution of glial cells within the brain, as the HIV-1 Tat transgenic mouse model conditionally expresses the Tat gene within astroglia.

Several studies have reported sex differences in humans in response to opioids. Research has shown that women require significantly greater doses of morphine to achieve similar levels of pain relief as men (Burns et al., 1989; Cepeda & Carr, 2003; Sidebotham et al., 1997), although the results from the current study report opposite

directionality, as female mice showed higher concentrations of morphine in the brain, and should theoretically respond better than males to a set dose. Several reasons may account for the conflicting data, including species differences, outcomes measured, and/or experimental design. Research not only demonstrates that women are less susceptible to the analgesic effects of opioids, but also that women are more prone to experiencing adverse reactions to opioid exposure, including gastrointestinal, skin, and nervous system issues and respiratory depression (Dahan et al., 1998; Lopes et al., 2021; Sarton et al., 2000). Although this has not been tested, some of these sex differences in response to opioids could be because of the differential central accumulation of opioids between males and females. Additionally, sex-based differences in neurocognitive impairment associated with HIV have also been described. A clinical study from Nigeria discovered women living with HIV experienced significantly more cognitive impairment when measuring the speed of information processing, verbal fluency, and learning and memory compared to men (Royal et al., 2016). Interestingly, these deficits appeared to be correlated with higher levels of monocytes (Royal et al., 2016). Preclinical studies using HIV-1 transgenic rats demonstrated that the effects of the HIV-1 transgene were more pronounced in females than males when measuring temporal processing, locomotor activity and object recognition (McLaurin et al., 2016, 2018; Rowson et al., 2016). Female mice conditionally expressing HIV-1 Tat demonstrate significantly reduced levels of astrogliosis compared to male counterparts (Hahn et al., 2015). Although behavioral paradigms were not measured in this study, these findings could be the result of sex differences in morphine concentrations in the brain as is observed in our study.

The present study examined morphine accumulation in response to HIV-1 Tat. Morphine accumulation was significantly increased by Tat exposure within the anterior brain, particularly occurring in female mice. Tat-mediated effects on morphine accumulation were also seen in the posterior brain, increasing accumulation in females while decreasing in males. In thinking about how the findings from this study might be translated to humans, special attention needs to be given to individuals living with HIV who use opioids, whether illegally or from prescriptions. Special care should also be provided to women living with HIV using opioids, as HIV infection may increase opioid accumulation in the brain. These results highlight the need for additional studies in both animals and humans, using larger sample sizes, to address the potential sex differences in opioid accumulation and/or response to opioids in the presence of HIV. The current study did not examine the underlying mechanisms responsible for the sex-mediated alterations in morphine accumulation. Future experiments should expand on these findings by investigating other opioids in the setting of HIV infection.

4E. Figures

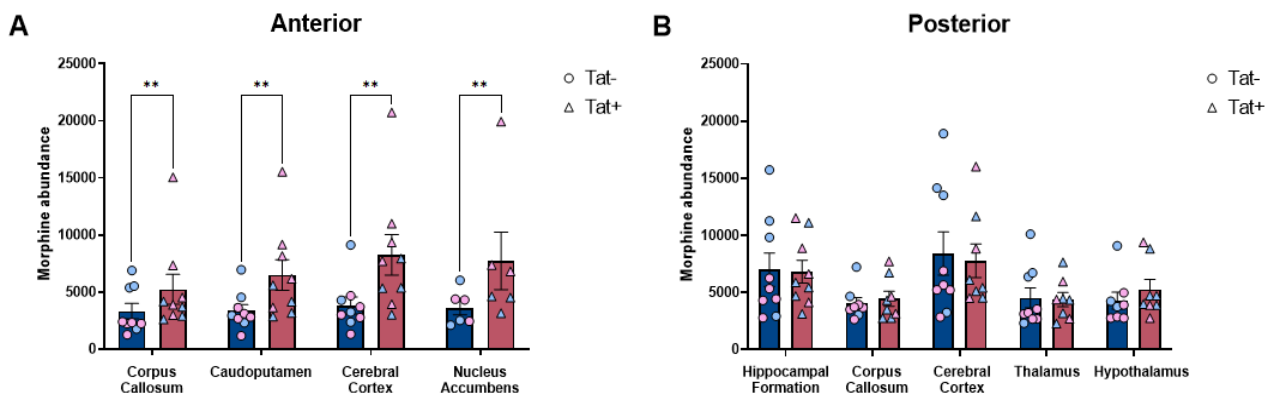


Figure 25: Morphine accumulation and distribution, using both male and female mice, is increased in the presence of HIV-1 Tat within the anterior, but not posterior brain. Tat(-) mice are depicted by dark blue bars and circles, while Tat(+) mice are depicted by red bars and triangles. Post-hoc significant differences at $\alpha < 0.05$ are denoted by $**p < 0.0021$. The mean morphine abundance \pm SEM were sampled from **(A)** $n = 9$ Tat(-) and Tat(+) for corpus callosum, caudoputamen, and cerebral cortex, and $n = 6$ Tat(-) and Tat(+) for nucleus accumbens; **(B)** $n = 9$ Tat(-) and Tat(+) for hippocampal formation, $n = 8$ Tat(-) and Tat(+) corpus callosum, $n = 9$ Tat(-) and 8 Tat(+) cerebral cortex, $n = 9$ Tat(-) and 8 Tat(+) thalamus, and $n = 8$ Tat(-) and Tat(+) hypothalamus. Both sexes are included in this analysis, where female mice are represented using pink circles or triangles and male mice are represented using light blue circles or triangles.

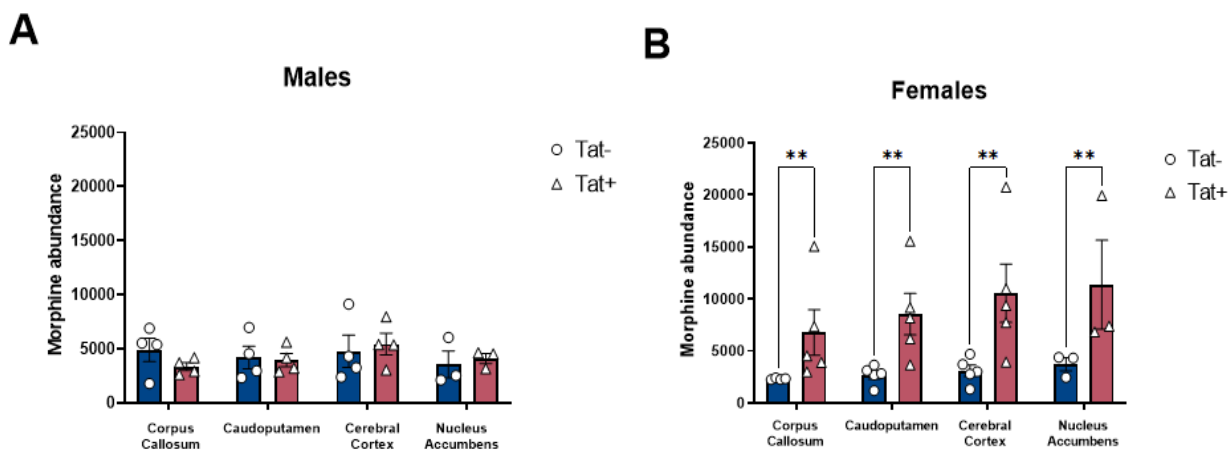
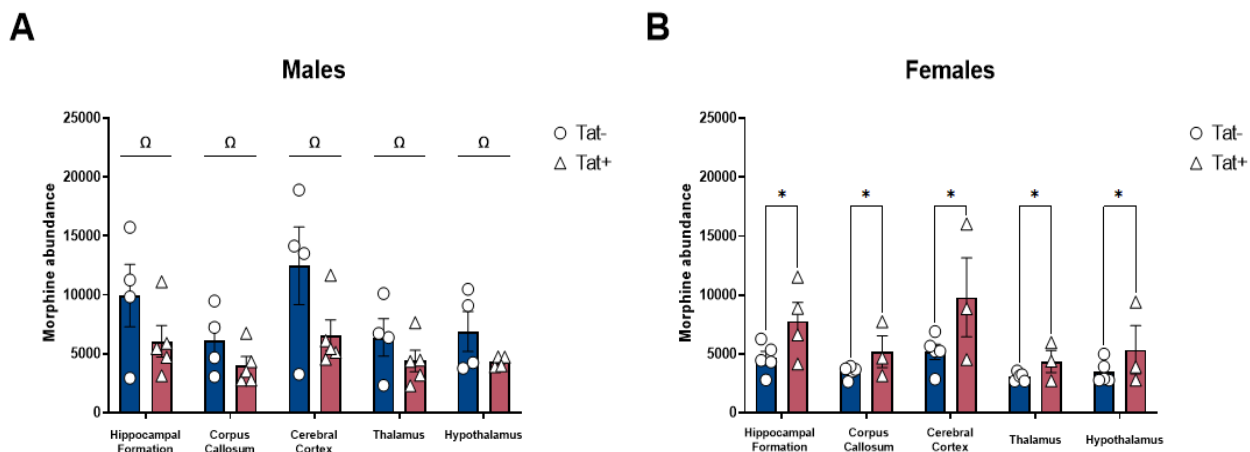
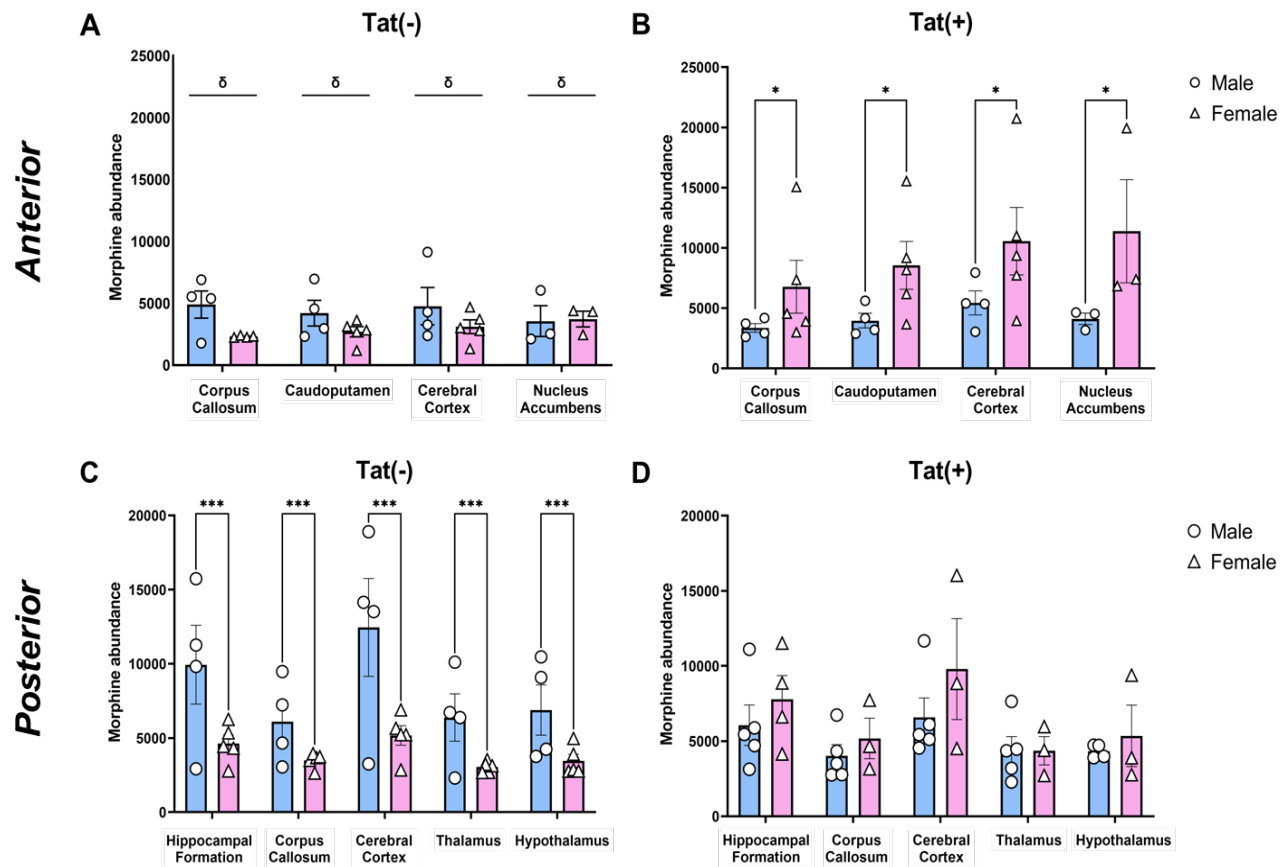


Figure 26: HIV-1 Tat status impacts morphine levels in female, but not male, mice. Tat(-) mice are depicted by dark blue bars and circles, while Tat(+) mice are depicted by red bars and triangles. *Post-hoc* significant differences at $\alpha < 0.05$ are denoted by $**p < 0.0021$. The mean morphine abundance \pm SEM were sampled from **(A)** $n = 4$ Tat(-) and 4 Tat(+) for corpus callosum, caudoputamen, and cerebral cortex, and $n = 3$ Tat(-) and 3 Tat(+) for nucleus accumbens; **(B)** $n = 4$ Tat(-) and 5 Tat(+) mice for corpus callosum, $n = 5$ Tat(-) and $n = 5$ Tat(+) mice for caudoputamen and cerebral cortex, and $n = 3$ Tat(-) and $n = 3$ Tat(+) for nucleus accumbens.



*Figure 27: Effects of HIV-1 Tat on morphine accumulation and distribution within the posterior brain section in males (A) and females (B) across all regions of interest. Male mice (A) demonstrated significantly decreased morphine accumulation in response to Tat exposure. Female mice (B) demonstrated significantly increased morphine accumulation in response to Tat exposure. Tat(-) mice are depicted by dark blue bars and circles, while Tat(+) mice are depicted by red bars and triangles. Main effects from the 2-way ANOVA are represented by a significant main effect of Tat status (Ω). Post-hoc significant differences at $\alpha < 0.05$ are denoted by $*p < 0.0032$. The mean morphine abundance \pm SEM were sampled from (A) $n = 4$ Tat(-) and 5 Tat(+) for hippocampal formation, corpus callosum, cerebral cortex, and thalamus and $n = 4$ Tat(-) and 4 Tat(+) for hypothalamus; (B) $n = 5$ Tat(-) for hippocampal formation, corpus callosum, cerebral cortex, thalamus, and hypothalamus, $n = 4$ Tat(+) for hippocampal formation, and $n = 3$ Tat(+) for corpus callosum, cerebral cortex, thalamus, and hypothalamus.*



*Figure 28: Sex differences in morphine abundance were detected in Tat(-) and Tat(+) mice within the anterior (A,B) and posterior (C,D) brain sections. Male mice are depicted by light blue bars and circles, while female mice are depicted by pink bars and triangles. Main effects from the 2-way ANOVA are represented by a significant main effect of sex (δ). Post-hoc significant differences at $\alpha < 0.05$ are denoted by * $p < 0.0032$ and *** $p < 0.0002$. The mean morphine abundance \pm SEM sampled from (A) $n = 4$ males and 4 females in the corpus callosum, $n = 4$ males and 5 females in the caudoputamen, $n = 4$ males and 3 females in the cerebral cortex, and $n = 3$ males and 3 females in the nucleus accumbens; (B) $n = 4$ males and 5 females in the corpus callosum, caudoputamen, and cerebral cortex, and $n = 3$ males and 3 females in the nucleus accumbens; (C) $n = 4$ males and 5 females in the hippocampal formation, corpus callosum, cerebral cortex, thalamus, and hypothalamus; and (D) $n = 5$ males and 4 females in the hippocampal formation, $n = 5$ males and 3 females in the corpus callosum, cerebral cortex, and thalamus, and $n = 4$ males and 3 females in the hypothalamus.*

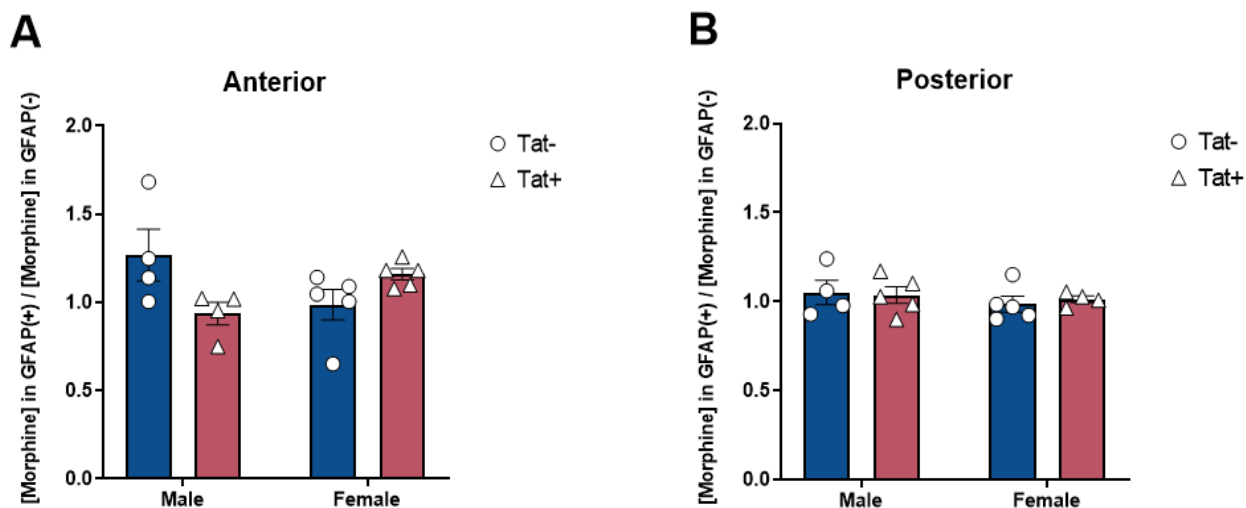


Figure 29: Changes in morphine accumulation demonstrates interactive effects between HIV-1 Tat and sex within areas of gliosis in the anterior (A) but not posterior (B) brain sections. Tat(-) mice are depicted by dark blue bars and circles, while Tat(+) mice are depicted by red bars and triangles. The mean ratio of morphine levels within GFAP+ within GFAP+ areas to morphine levels within areas of GFAP- areas \pm SEM were calculated from (A) $n = 4$ Tat(-) and Tat(+) for males and $n = 5$ Tat(-) and Tat(+) for females; (B) $n = 4$ Tat(-) and 5 Tat(+) for males and $n = 5$ Tat(-) and 4 Tat(+) for females.

Table 1: Significant post hoc tests detected when analyzing morphine abundance \pm HIV-1 Tat.

Comparison	Mean Difference	95% CI of diff.	Adjusted P Value
Anterior			
Corpus Callosum:Tat- vs. Cerebral Cortex:Tat+	-5095	-9787 to -402.3	$p = 0.0242$
Posterior			
Corpus Callosum:Tat- vs. Cerebral Cortex:Tat-	-3862	-7494 to -230.7	$p = 0.028$
Corpus Callosum:Tat+ vs. Cerebral Cortex:Tat+	-3862	-7494 to -230.7	$p = 0.028$
Cerebral Cortex:Tat- vs. Thalamus:Tat-	3655	79.23 to 7230	$p = 0.041$
Cerebral Cortex:Tat+ vs. Thalamus:Tat+	3655	79.23 to 7230	$p = 0.041$

Table 2: Significant post hoc tests analyzing morphine abundance \pm HIV-1 Tat in male and female mice.

Comparison	Mean Difference	95% CI of diff.	Adjusted P Value
Anterior			
[Females] Corpus Callosum:Tat- vs. Cerebral Cortex:Tat+	-8653	-16140 to -1165	$p = 0.0148$
[Females] Corpus Callosum:Tat- vs. Nucleus Accumbens:Tat+	-9376	-17567 to -1185	$p = 0.0162$
[Females] Caudputamen:Tat- vs. Cerebral Cortex:Tat+	-7473	-14688 to -257.9	$p = 0.0382$
[Females] Caudputamen:Tat- vs. Nucleus Accumbens:Tat+	-8196	-16139 to -253.5	$p = 0.0393$
Posterior			
[Males] Corpus Callosum:Tat+ vs. Cerebral Cortex:Tat-	-7537	-13836 to -1238	$p = 0.0089$
[Males] Cerebral Cortex:Tat- vs. Thalamus:Tat+	7210	910.1 to 13509	$p = 0.0144$
[Males] Cerebral Cortex:Tat- vs. Hypothalamus:Tat+	7055	515.9 to 13595	$p = 0.0257$
[Females] Hippocampal Formation:Tat+ vs. Thalamus:Tat-	4865	581.1 to 9150	$p = 0.0159$
[Females] Corpus Callosum:Tat- vs. Cerebral Cortex:Tat+	-5330	-9793 to -867.5	$p = 0.0094$
[Females] Cerebral Cortex:Tat+ vs. Thalamus:Tat-	5915	1452 to 10378	$p = 0.0028$
[Females] Cerebral Cortex:Tat+ vs. Hypothalamus:Tat-	5291	828.2 to 9754	$p = 0.0101$

Table 3: Additional significant post hoc tests detected when analyzing morphine abundance between male and female mice \pm HIV-1 Tat.

Comparison	Mean Difference	95% CI of diff.	Adjusted P Value
Anterior			
[Tat+] Corpus Callosum:Male vs. Cerebral Cortex:Female	-7932	-15847 to -16.81	$p = 0.0492$
Posterior			
[Tat-] Hippocampal Formation:Male vs. Corpus Callosum:Female	6723	1057 to 12390	$p = 0.0097$
[Tat-] Hippocampal Formation:Male vs. Thalamus:Female	6846	1180 to 12513	$p = 0.0079$
[Tat-] Hippocampal Formation:Male vs. Hypothalamus:Female	6396	729.8 to 12063	$p = 0.0165$
[Tat-] Hippocampal Formation:Female vs. Cerebral Cortex:Male	-5812	-11478 to -145.0	$p = 0.0405$
[Tat-] Corpus Callosum:Female vs. Cerebral Cortex:Male	-8144	-13811 to -2477	$p = 0.0008$
[Tat-] Cerebral Cortex:Male vs. Thalamus:Female	8267	2600 to 13933	$p = 0.0007$
[Tat-] Cerebral Cortex:Male vs. Hypothalamus:Female	7817	2150 to 13483	$p = 0.0015$

CHAPTER 5: Conclusions

Overall, the results from the current studies demonstrate the potential harmful and complicated effects of HIV and opioid co-exposure, and also show how sex may alter these effects. Antiretroviral concentrations were decreased in the presence of morphine, and morphine accumulation was increased in the presence of HIV-1 Tat, particularly in females. While our data determined that morphine concentrations were increased in response to Tat, the changes in morphine levels were not large enough to impact abacavir concentrations within the brain, as only morphine exposure was found to significantly alter abacavir levels. Larger studies might be able to further elucidate these interconnecting relationships. Data collected from these studies highlights the importance for monitoring both antiretroviral and opioid levels in the brains of both males and female animal model as regional differences were detected in the current studies. Particularly, morphine's deleterious effects on abacavir concentrations were more prominent in the posterior, rather than anterior, brain. Additionally, morphine levels in male mice were decreased in response to Tat in the posterior brain only, while female mice demonstrated increased morphine levels when exposed to Tat. Further research investigating the regional differences in antiretroviral and opioid brain concentrations is needed to better understand how drug accumulation and distribution relate to the interactions between HIV and opioids, especially between males and females.

These results provide evidence for the need to monitor opioid use/misuse in patients with HIV, as antiretroviral therapy may be less effective in those who use opioids. These results also indicate the need for special care between men and women with HIV who use opioids, as men may be more susceptible to the deleterious effects of

morphine exposure on antiretroviral therapy in the brain, while women living with HIV and use/misuse opioids may show greater opioid levels in their brain. However, results from the current study are conflicting with findings from other studies conducted in humans, where women require significantly higher doses of morphine to achieve similar levels of pain relief as men (Burns et al., 1989; Cepeda & Carr, 2003; Sidebotham et al., 1997). The differences in results between the current study and those conducted in women may be model dependent, as the current study was performed using HIV-1 Tat transgenic mice and did not investigate antinociception. Nevertheless, our findings still warrant the need for future research into the interplay between HIV and opioids.

The decrease in antiretroviral concentrations in the brain resulting from morphine exposure may be related to increased efflux transporter expression and function, such as P-glycoprotein, as shown in prior work from our lab (Leibrand et al., 2019). P-glycoprotein is responsible for expelling substances from the brain back into the blood and several antiretrovirals are substrates from P-glycoprotein, thus providing a potential mechanism whereby morphine decreases antiretroviral concentrations within the brain and possibly antiretroviral efficacy.

HIV, particularly the HIV viral protein Tat, may indirectly impact antiretroviral efficacy, by altering morphine levels within the brain, particularly in women living with HIV who use opioids. Inasmuch as these results can be translated into humans with HIV, women using opioids (whether illicitly or from prescription use) and living with HIV may experience greater opioid levels in the brain, resulting in decreased antiretroviral concentrations in the brain.

The present studies utilize IR-MALDESI MSI as a novel approach for investigating the interplay between HIV and opioid use and provides valuable information in terms of drug accumulation and distribution within the brain of male and female mice. Indeed, by using IR-MALDESI MSI techniques, we are capable of examining both antiretroviral and opioid distribution across multiple brain regions simultaneously. However, these studies are not without limitations. The limit of quantitation was lower for IR-MALDESI MSI compared to traditional LC-MS/MS, and was therefore only able to quantify one of three antiretrovirals used throughout these studies. Morphine levels were also measured qualitatively, and while this may be a limitation of the current studies, future experiments measuring quantitative morphine data might be able to better understand the magnitude of change necessary to impact antiretroviral concentrations. Furthermore, the HIV model used in the present studies was non-infectious, making it difficult to translate these findings into humans.

In order to better understand the interactions between HIV infection, opioids, antiretroviral therapy and sex, future studies should use an infectious HIV rodent model, larger sample sizes, and additional opioids targeting various opioid receptors to see if changes in antiretroviral concentrations are associated with the decreased ability to suppress viral replication and/or specific opioid receptors. Future research may also wish to investigate the neurocognitive impact of opioid and HIV co-exposure.

Appendices

Appendix I: MSI Ions

Appendix II: Anterior and Posterior Regions of Interest

Appendix III: Abacavir Concentration Coding Scripts

Appendix IV: Morphine Abundance Coding Scripts

Appendix V: IR-MALDESI MSI and IHC Image Co-registration

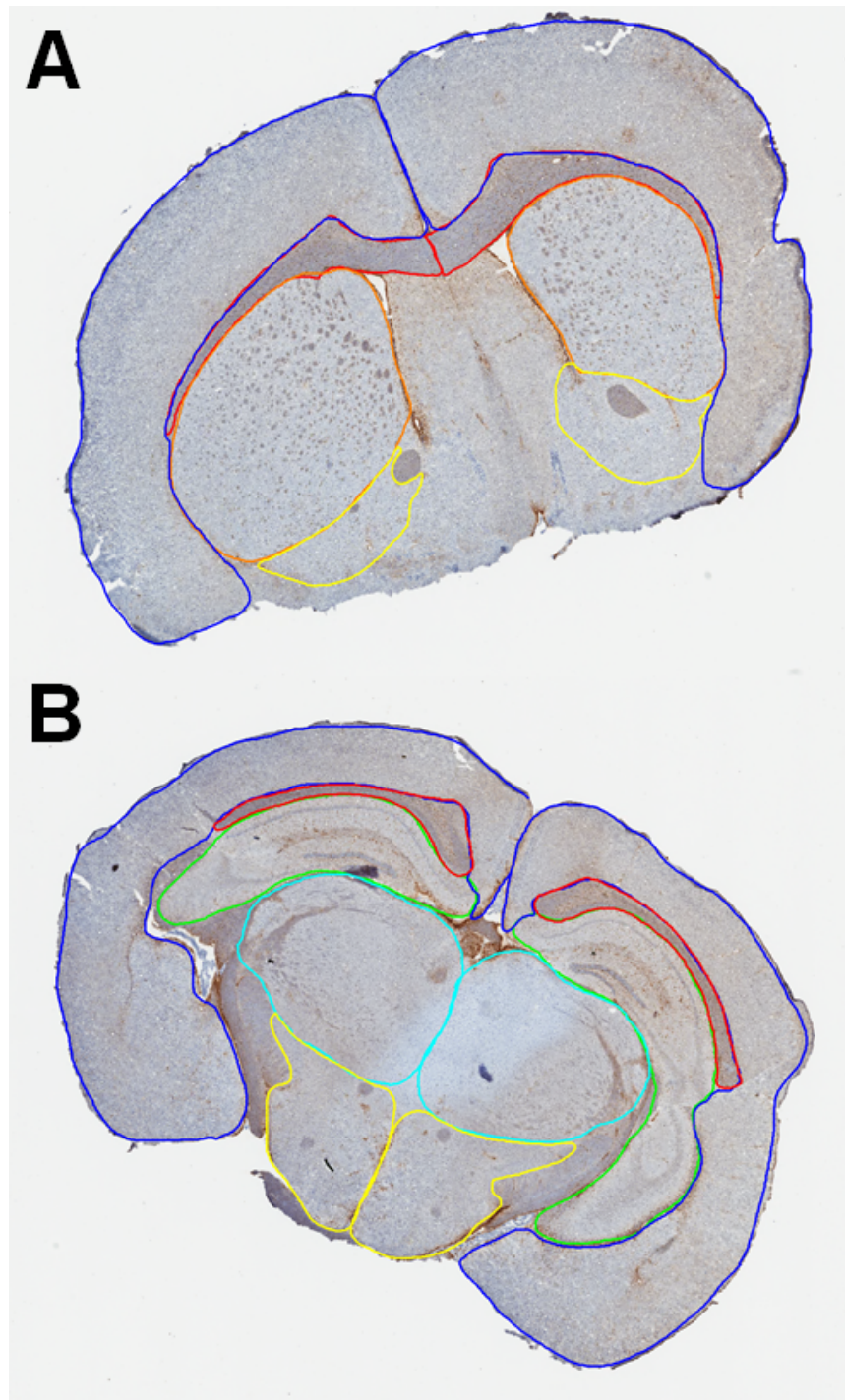
Appendix I: MSI Ions

List of the detected ions during sample analysis

Name	Group	Molecular formula	Ion (m/z)
Dopamine	Endogenous	C ₈ H ₁₁ NO ₂	154.0863
Serotonin	Endogenous	C ₁₀ H ₁₂ N ₂ O	177.1022
Unidentified	Endogenous	-----	203.2230
3TC	ARV	C ₈ H ₁₁ N ₃ O ₃ S	230.0594
Unidentified	Endogenous	-----	268.1040
Morphine	Morphine	C ₁₇ H ₁₉ NO ₃	286.1438
ABC	ARV	C ₁₄ H ₁₈ N ₆ O	287.1615
Unidentified	Endogenous	-----	305.2475
Cholesterol	Endogenous	C ₂₇ H ₄₆ O	369.3516
DTG	ARV	C ₂₀ H ₁₉ F ₂ N ₃ O ₅	420.1366
M3G	Morphine metabolite	C ₂₃ H ₂₇ NO ₉	462.1759
3TCtp	ARV metabolite	C ₈ H ₁₄ N ₃ O ₁₂ P ₃ S	469.9584
ABCtp	ARV metabolite	C ₁₁ H ₁₆ N ₅ O ₁₁ P ₃	488.0132

3TC = lamivudine, ABC = abacavir, DTG = dolutegravir, M3G = Morphine-3-glucuronide, 3TCtp = lamivudine triphosphate, ABCtp = abacavir triphosphate

Appendix II: Anterior and Posterior Regions of Interest



Representation of the regions of interest (ROIs) in two distinct areas of the brain using GFAP-stained IHC images. (A): ROI's within the anterior section; Red=corpus callosum, Orange=caudate putamen, Blue=cerebral cortex, Yellow=nucleus accumbens. (B): ROI's within the posterior section; Red=corpus callosum, Green=hippocampal formation, Blue=cerebral cortex, Light blue=thalamus, Yellow=hypothalamus.

Appendix III: Abacavir Concentration Coding Scripts

A. Image Selection

%SC% Run this code and select the image you want to work with - although it works with different images

%SC% we prefer to select .svs so we can select the layers/page/dimension in the next script.

```
[filename, pathname] = uigetfile( ...
    {'*.tif*;*.png;*.jpg;*.svs;*.scn', 'All Image Files (*.tif*, *.png, *.jpg,
*.svs, *.scn)'};
    '*.tif*', 'TIFF images (*.tif, *.tiff)'; ...
    '*.png', 'PNG images (*.png)'; ...
    '*.jpg', 'JPG images (*.jpg)'; ...
    '*.svs', 'SVS images (*.svs)'; ...
    '*.scn', 'SCN images (*.scn)'; ...
    '*.*', 'All Files (*.*)'}, ...
    'Pick Image');
```

B. Select Layer of Image

%SC% Run this code to select the layers/page - most are the same image in different resolutions,

%SC% but sometimes there are other images as the sticker for the sample.

```
I1info=imfinfo([pathname filename]);
for i=1:numel(I1info),pageinfo1{i}=['Page ' num2str(i) ': '
num2str(I1info(i).Height) ' x ' num2str(I1info(i).Width)]; end
fprintf('done.\n');
fname=[pathname filename];
if numel(I1info)>1,
    [s,v]=listdlg('Name','Choose Level','PromptString','Select a page for Roi
Discovery:','SelectionMode','single','ListSize',[170
120],'ListString',pageinfo1); drawnow;
    if ~v, guidata(hObject, handles); return; end
    fprintf('Reading page %g of image 1... ',s);
    io=imread(fname,s);
    fprintf('done.\n');
else
    fprintf('Image doesnt have any pages!\n');
end
%Dimensions of the IHC TIFF
dims.IHC=size(io);
dims.IHC=dims.IHC(1:2);
nrow=dims.IHC(1);
ncol=dims.IHC(2);
%If importing SVS, this should evaluate the image compression to be applied
%to XML data
hratio=ncol/I1info(1).Width;
wratio=nrow/I1info(1).Height;
```

C. Extract Annotations

```

%SC% is the only code you need to manually change it
    %SC% rename the .svs and .xml file to be the same you want to work with
    %SC% The files don't need to have the same name
[baseName, folder] = uigetfile({'*.xml'}, 'Select annotation data');
xml_file = fullfile(folder, baseName)
xDoc = xmlread(xml_file);
Regions=xDoc.getElementsByTagName('Region'); % get a list of all the region
tags
for regioni = 0:Regions.getLength-1
    Region=Regions.item(regioni); % for each region tag
    %get a list of all the vertexes (which are in order)
    vertices=Region.getElementsByTagName('Vertex');
    xy{1,regioni+1}=zeros(vertices.getLength-1,2); %allocate space for them
    for vertexi = 0:vertices.getLength-1 %iterate through all verticies
        %get the x value of that vertex
        x=str2double(vertices.item(vertexi).getAttribute('X'));

        %get the y value of that vertex
        y=str2double(vertices.item(vertexi).getAttribute('Y'));
        xy{1,regioni+1}(vertexi+1,:)=[x,y]; % finally save them into the array
    end
end

end
stDoc = parseXML(xml_file);
%Some structs from xml extraction need to be cleaned
stDoc.Children = CleanStruct(stDoc.Children, "Annotation");
%Extracting quantity of annotations
NumAnnotations = length(stDoc.Children);
%Cleaning structs again
for i = 1:NumAnnotations
    stDoc.Children(i).Children = CleanStruct(stDoc.Children(i).Children,
"Regions");
end
for i = 1:NumAnnotations
    stDoc.Children(i).Children.Children =
CleanStruct(stDoc.Children(i).Children.Children, "Region");
end
%Extracting quantity of regions
RegionsPerAnnotations = zeros(1,NumAnnotations);
for i = 1:NumAnnotations
    RegionsPerAnnotations(i) = length(stDoc.Children(i).Children.Children);
end

% Extracting Colors
for i = 1:NumAnnotations
    for k = 1:RegionsPerAnnotations(i)

```

```

        xy{2,k+sum(RegionsPerAnnotations(1:i-1))} =
completeRGB(dec2hex(str2double(stDoc.Children(i).Attributes(3).Value)));
    end
end
% Extracting Text boxes of notes from ImageScope
for i = 1:NumAnnotations
    for k = 1:RegionsPerAnnotations(i)
        xy{3,k+sum(RegionsPerAnnotations(1:i-1))} =
stDoc.Children(i).Children.Children(k).Attributes(13).Value;
    end
end
% Extracting Text of Annotation name
for i = 1:NumAnnotations
    for k = 1:RegionsPerAnnotations(i)
        xy{3,k+sum(RegionsPerAnnotations(1:i-1))} =
stDoc.Children(i).Attributes(7).Value;
    end
end
Annotation_Name=strings(NumAnnotations,1);
for i = 1:NumAnnotations
    Annotation_Name(i) = stDoc.Children(i).Attributes(7).Value;
    Annotation_Name(i) = replace(Annotation_Name(i), " ", "_");
    Annotation_Name(i) = replace(Annotation_Name(i), ",", "");
end
% Creating MASK associated with each Annotation Group
for i = 1:NumAnnotations
    mask=zeros(nrow,ncol);
    for k = 1:RegionsPerAnnotations(i)
        smaller_x=xy{1,k+sum(RegionsPerAnnotations(1:i-1))}(:,1)*wratio;
        smaller_y=xy{1,k+sum(RegionsPerAnnotations(1:i-1))}(:,2)*hratio;
        mask=mask+poly2mask(smaller_x,smaller_y,nrow,ncol);
    end

    AnnotationMask.(Annotation_Name(i))=mask;
end
figure('Position', [100 200 dims.IHC(2)*.05 dims.IHC(1)*.05])
imagesc(io)
hold on
for i = 1:NumAnnotations
    mask_plot=imagesc(AnnotationMask.(Annotation_Name(i)));
    set(mask_plot,'AlphaData',0.2)
end

```

D. Isolate GFAP

```

%Defining color thresholds for DAB staining of GFAP
cform = makecform('srgb2lab', 'AdaptedWhitePoint', whitepoint('D65'));
% Define thresholds for channel 1 based on histogram settings
channell1Min = 35.125;
channell1Max = 55.509;

```

```

% Define thresholds for channel 2 based on histogram settings
channel2Min = -2.513;
channel2Max = 7.547;
% Define thresholds for channel 3 based on histogram settings
channel3Min = -0.436;
channel3Max = 35.898;
% Isolating GFAP stain based on color threshold
IHC=im2double(io);
LABspace=applycform(IHC,cform);
GFAPmask=(LABspace(:,:,1) >= channel1Min ) & (LABspace(:,:,1) <= channel1Max)
& ...
    (LABspace(:,:,2) >= channel2Min ) & (LABspace(:,:,2) <= channel2Max) & ...
    (LABspace(:,:,3) >= channel3Min ) & (LABspace(:,:,3) <= channel3Max);
GFAP=IHC;
GFAP(repmat(~GFAPmask,[1 1 3])) = 0;
GFAP=rgb2gray(GFAP);
slice=rgb2gray(IHC);
slice=imcomplement(slice);
slice=slice.*(slice>0.1);
clear LABspace IHC;
%Show images of the GFAP and section as a check to make sure thresholding
%worked
figure('Position', [1 500 dims.IHC(2)*.035 dims.IHC(1)*.035])
imagesc(GFAP)
figure('Position', [1 500 dims.IHC(2)*.035 dims.IHC(1)*.035])
imagesc(slice)
GFAP_red=GFAP(:,:,1);
GFAP_red=GFAP_red.*GFAPmask;

GFAP_single=min(GFAP(GFAP>0));
GFAP_stats(1)=GFAP_single;
GFAP_total=sum(GFAP(:));
GFAP_stats(2)=GFAP_total;
GFAP_count=GFAP_total/GFAP_single;
GFAP_stats(3)=GFAP_count;
GFAP_area=nnz(GFAP);
GFAP_stats(4)=GFAP_area;
slice_area=nnz(slice);
GFAP_stats(5)=slice_area;
GFAP_fraction=GFAP_area/slice_area;
GFAP_stats(6)=GFAP_fraction;
GFAP_stats=transpose(GFAP_stats);
nonGFAPmask=imcomplement(GFAP_red);

```

E. MSI Data Import

```

%Read MSI data from Excel file
[baseName, folder] = uigetfile({'*.xlsx'; '*.xls'}, 'Select MSI data');
MSIFileName = fullfile(folder, baseName)
ProjectName = strsplit(baseName, '.')

```

```

[RawMSI.Data]=xlsread(MSiFileName,-1)%Select ion data
[RawMSI.Label]=xlsread(MSiFileName,-1)%Select ion label
%Prompt user for ROI
ROI=inputdlg({'Number of lines','Scans per line','Voxel size X', 'Voxel size
Y'},'Define ROI',1,{'','','0.1','0.1'})
dims.MSI=[str2num(ROI{1}) str2num(ROI{2})]
dims.SpotSpacing=[str2num(ROI{3}) str2num(ROI{4})]
dims.boundsx=[0 dims.MSI(2)*dims.SpotSpacing(1)]
dims.boundsy=[0 dims.MSI(1)*dims.SpotSpacing(2)]
multiplier = 5;
clear ROI;
%Parse imported data and generate ion images
num_ions=size(RawMSI.Label)
label='mz'
rawlabel='MSI_Raw'
mkdir(folder,rawlabel)
scaledlabel='MSI_Scaled'
mkdir(folder,scaledlabel)
for i=1:num_ions(2)
    ionstring=num2str(RawMSI.Label(i),3)
    ion=strcat(label,ionstring)
    ion_names{i}=ion

    %Save images of raw MSI data
    ARV.raw.(ion)=RawMSI.Data(:,i)
    ARV.reshape.(ion)=reshape(ARV.raw.(ion),[dims.MSI(2),dims.MSI(1)])
    ARV.reshape.(ion)=transpose(ARV.reshape.(ion))
    ARV.scaled.(ion)=imadjust(mat2gray(ARV.reshape.(ion)));
    a=figure('name',ion,'Colormap',hot,'Position',[1 1 dims.MSI(2)*multiplier
dims.MSI(1)*multiplier])
    imagesc(dims.boundsx,dims.boundsy,ARV.reshape.(ion))
    set(gcf,'Color','w');
    imagename=strcat(folder,'\ ',rawlabel,'\ ', 'Raw_',ion)
    c=colorbar

    a.Position(3)=(dims.MSI(2)+c.Position(3)/dims.SpotSpacing(1)*1.5*multiplier)*
multiplier
    export_fig(imagename,'-jpg')
    close(gcf)
end
%Mask any off-tissue response based on Cholesterol ion map and scale image
ARVmask=double(ARV.scaled.mz369>0.05)
ARVmask=imfill(ARVmask);
figure,imagesc(ARVmask)
ARVmask_boundary=bwperim(ARVmask);
chol_flip=flipud(ARV.scaled.mz369);
for i=1:num_ions(2)
    ionstring=num2str(RawMSI.Label(i),3)
    ion=strcat(label,ionstring)

```

```

ion_names{i}=ion

ARV.mask.(ion)=ARVmask.*ARV.reshape.(ion);
%Tabulate stats on ion
Raw_stats{i}=sum(ARV.mask.(ion)(:));
%Scale intensities of MSI data for comparison to IHC and save images of
scaled MSI data
ARV.scaled.(ion)=imadjust(mat2gray(ARV.mask.(ion)));
figure('name',ion,'Colormap',hot,'Position',[1 1 dims.MSI(2)*multiplier
dims.MSI(1)*multiplier])
imagesc(dims.boundsx,dims.boundsy,ARV.scaled.(ion))
set(gcf,'Color','w');
imagename=strcat(folder,scaledlabel,'\','Scaled_',ion)
export_fig(imagename,'-jpg')
close(gcf)

overlay=figure('Colormap',hot,'Position',[1 1 dims.MSI(2)*multiplier
dims.MSI(1)*multiplier])
arv_axes=axes('Parent',overlay)
chol_axes=axes('Parent',overlay)
colormap(arv_axes,hot)
colormap(chol_axes,parula)
set(arv_axes,'Visible','off')
set(chol_axes,'Visible','off')
linkaxes([arv_axes,chol_axes])

arv_plot=imagesc(dims.boundsx,dims.boundsy,ARV.scaled.(ion),'Parent',arv_axes
)
hold on
chol_plot=imagesc(dims.boundsx,dims.boundsy,chol_flip,'Parent',chol_axes)
set(chol_plot,'AlphaData',0.2)
hold off
imagename=strcat(folder,scaledlabel,'\','Overlay_Scaled_',ion)
export_fig(imagename,'-png')
close(gcf)
end
ARVnames=fieldnames(ARV.scaled)

```

F. Image Co-Registration

```

%Downsample IHC data and annotation masks
dims.resize=max(dims.MSI./dims.IHC);
length = num2str(dims.resize);
length = strsplit(length, '.');
zero_find=strfind(char(length(2)), '0');
numzeros=size(zero_find,2);
n=2;
for i= 1 : numzeros
    if i==1
        n=n+1;
    end
end

```

```

elseif i>1
    increment = zero_find(i)-zero_find(i-1);
    if increment==1
        n=n+1;
    end
end
end

end

dims.resize_scale=ceil(dims.resize*10^n)/10^n;
DS_IHC.GFAP_resize=imresize(GFAP,dims.resize_scale,'box');
DS_IHC.slice_resize=imresize(slice,dims.resize_scale);
%Crop downsampled IHC data to match dimensions of MSI data
figure('Position', [1 1 dims.MSI(2)*multiplier dims.MSI(1)*multiplier])
imagesc(DS_IHC.slice_resize)
h = imrect(gca, [1 1 dims.MSI(2) dims.MSI(1)]); % create rectangle on the
image
message = sprintf('Drag, set position of the rectangle cropping box and
double click on the rectangle box');
uiwait(msgbox(message));
position = wait(h); % get position
DS_IHC.GFAP_cropped = imcrop(DS_IHC.GFAP_resize,position);
DS_IHC.slice_cropped = imcrop(DS_IHC.slice_resize,position);
% Perform the same downsampling and cropping for each Annotation Group
for i = 1:NumAnnotations

AnnotationMask_DS.(Annotation_Name(i))=imresize(AnnotationMask.(Annotation_Na
me(i)),dims.resize_scale,'nearest');

AnnotationMask_DS.(Annotation_Name(i))=imcrop(AnnotationMask_DS.(Annotation_N
ame(i)),position);

AnnotationMask_DS.(Annotation_Name(i))=AnnotationMask_DS.(Annotation_Name(i))
end
dims.slice_cropped=size(DS_IHC.slice_cropped);
dims.GFAP_cropped=size(DS_IHC.GFAP_cropped);
% Verify whether cropped dimensions match MSI
cropcheck_slice=dims.slice_cropped-dims.MSI;
cropcheck_GFAP=dims.GFAP_cropped-dims.MSI;
    if cropcheck_slice(1)>0
        start=cropcheck_slice(1)+1;
        DS_IHC.slice_cropped =
DS_IHC.slice_cropped(start:dims.slice_cropped(1),:);
        DS_IHC.GFAP_cropped =
DS_IHC.GFAP_cropped(start:dims.GFAP_cropped(1),:);
        for i = 1:NumAnnotations

AnnotationMask_DS.(Annotation_Name(i))=AnnotationMask_DS.(Annotation_Name(i))
(start:dims.GFAP_cropped(1),:);
        end

```

```

end
if cropcheck_slice(1)<0
    start=1;
    limit=dims.slice_cropped(1)-cropcheck_slice(1);
    DS_IHC.slice_cropped = DS_IHC.slice_cropped(start:limit,:);
    DS_IHC.GFAP_cropped = DS_IHC.GFAP_cropped(start:limit,:);
    for i = 1:NumAnnotations

AnnotationMask_DS.(Annotation_Name(i))=AnnotationMask_DS.(Annotation_Name(i))
(start:limit,:);
        end
    end
    if cropcheck_slice(2)>0
        start=cropcheck_slice(2)+1;
        DS_IHC.slice_cropped =
DS_IHC.slice_cropped(:,start:dims.slice_cropped(2))
        DS_IHC.GFAP_cropped =
DS_IHC.GFAP_cropped(:,start:dims.GFAP_cropped(2))
        for i = 1:NumAnnotations

AnnotationMask_DS.(Annotation_Name(i))=AnnotationMask_DS.(Annotation_Name(i))
(:,start:dims.GFAP_cropped(2));
            end
        end
        if cropcheck_slice(2)<0
            start=1;
            limit=dims.slice_cropped(2)-cropcheck_slice(2);
            DS_IHC.slice_cropped = DS_IHC.slice_cropped(:,start:limit);
            DS_IHC.GFAP_cropped = DS_IHC.GFAP_cropped(:,start:limit);
            for i = 1:NumAnnotations

AnnotationMask_DS.(Annotation_Name(i))=AnnotationMask_DS.(Annotation_Name(i))
(:,start:limit);
                end
            end
            dims.IHCcropped_slice=size(DS_IHC.slice_cropped);
            dims.IHCcropped_GFAP=size(DS_IHC.GFAP_cropped);
            % Creating images to check rescale
            DS_IHC.GFAP_scaled = imadjust(DS_IHC.GFAP_cropped);
            DS_IHC.slice_scaled = imadjust(DS_IHC.slice_cropped);
            DS_IHC.GFAP_scaledmask=DS_IHC.GFAP_scaled>0.15;
            DS_IHC.GFAP_invertmask=imcomplement(DS_IHC.GFAP_scaledmask);
            GFAP_area_DS=nnz(DS_IHC.GFAP_scaledmask);
            figure, imagesc(DS_IHC.GFAP_scaledmask);
            figure, imagesc(DS_IHC.GFAP_invertmask);
            %Register MSI data to IHC data
            [Endog_selection,ok]=listdlg('PromptString', 'Select endogenous ions
representing tissue morphology:', 'ListString', ARVnames)
            num_endog=max(size(Endog_selection));

```

```

composite_endog=zeros(dims.MSI(1),dims.MSI(2));
for i = 1:num_endog
    ionstring=num2str(RawMSI.Label(Endog_selection(i)),3)
    ion=strcat(label,ionstring)
    composite_endog=composite_endog+ARV.scaled.(ion);
end
figure('Position', [1 1 dims.MSI(2)*multiplier dims.MSI(1)*multiplier])
imagesc(composite_endog)
%control point registration, translating MSI to IHC
cpselect(composite_endog,DS_IHC.slice_scaled) %select control points
J_tform=fitgeotrans(movingPoints,fixedPoints,'affine') %create transformation
matrix
Rfixed=imref2d(dims.MSI)
xformlabel='MSI_Xform'
mkdir(folder,xformlabel)
for i=1:num_ions(2) %transform all MSI data
    ion=char(ARVnames(i))
    ARV.xform.(ion)=imwarp(ARV.scaled.(ion),J_tform,'OutputView',Rfixed,
'interp', 'nearest')
    ARV.xform_raw.(ion)=imwarp(ARV.mask.(ion),J_tform,'OutputView',Rfixed,
'interp', 'nearest')
    figure('name',ion,'Colormap',hot,'Position', [1 1 dims.MSI(2)*multiplier
dims.MSI(1)*multiplier])
    imagesc(dims.boundsx,dims.boundsy,ARV.xform.(ion))
    set(gcf, 'Color', 'w');
    imagename=strcat(folder,xformlabel,'\','Xform_',ion)
    export_fig(imagename,'-jpg')
    close(gcf)
end
slice_flip=flipud(DS_IHC.slice_scaled);
for i=1:num_ions(2)
    ionstring=num2str(RawMSI.Label(i),3)
    ion=strcat(label,ionstring)
    ion_names{i}=ion

    overlay=figure('Colormap',hot,'Position', [1 1 dims.MSI(2)*multiplier
dims.MSI(1)*multiplier])
    arv_axes=axes('Parent',overlay)
    chol_axes=axes('Parent',overlay)
    colormap(arv_axes,hot)
    colormap(chol_axes,bone)
    set(arv_axes,'Visible','off')
    set(chol_axes,'Visible','off')
    linkaxes([arv_axes,chol_axes])

arv_plot=imagesc(dims.boundsx,dims.boundsy,ARV.xform.(ion),'Parent',arv_axes)
hold on
chol_plot=imagesc(dims.boundsx,dims.boundsy,slice_flip,'Parent',chol_axes)

```

```

set(chol_plot, 'AlphaData', 0.4)
hold off
imagenamename=strcat(folder, xformlabel, '\', 'Overlay_TissueSlice_', ion)
export_fig(imagenamename, '-png')
close(gcf)
end
%Check registration
multiplier=5;
fuse_overlay_IHC=imfuse(DS_IHC.GFAP_scaled, DS_IHC.slice_scaled,
'falsecolor', 'ColorChannels', [1 2 0]);
figure('Position', [1 1 dims.MSI(2)*multiplier dims.MSI(1)*multiplier])
imagesc(dims.boundsx, dims.boundsy, fuse_overlay_IHC)
imagenamename=strcat(folder, 'Fuse_IHC_GFAPandSlice')
export_fig(imagenamename, '-jpg')
close(gcf)
fuse_overlay_prexfrom=imfuse(DS_IHC.slice_scaled, ARV.scaled.mz369,
'falsecolor', 'ColorChannels', [1 2 0]);
figure('Position', [1 1 dims.MSI(2)*multiplier dims.MSI(1)*multiplier])
image(fuse_overlay_prexfrom)
imagenamename=strcat(folder, 'Fuse_SliceandMSI_prexform')
hold on
plot(movingPoints(:,1), movingPoints(:,2), 'xw')
plot(fixedPoints(:,1), fixedPoints(:,2), 'ow')
export_fig(imagenamename, '-jpg')
close(gcf)
movingPoints_xform=transformPointsForward(J_tform, movingPoints)
fuse_overlay=imfuse(DS_IHC.GFAP_scaled, ARV.xform.mz369,
'falsecolor', 'ColorChannels', [1 2 0]);
figure('Position', [1 1 dims.MSI(2)*multiplier dims.MSI(1)*multiplier])
image(fuse_overlay)
hold on
plot(movingPoints_xform(:,1), movingPoints_xform(:,2), 'xw')
plot(fixedPoints(:,1), fixedPoints(:,2), 'ow')
imagenamename=strcat(folder, 'Fuse_GFAPandMSI')
export_fig(imagenamename, '-jpg')
close(gcf)
fuse_overlay_Caudoputamen=imfuse(AnnotationMask_DS.Caudoputamen,
ARV.xform.mz154, 'falsecolor', 'ColorChannels', [1 2 0]);
figure('Position', [1 1 dims.MSI(2)*multiplier dims.MSI(1)*multiplier])
imagesc(dims.boundsx, dims.boundsy, fuse_overlay_Caudoputamen)
imagenamename=strcat(folder, 'Fuse_GFAPandMSI_CerebralCortex')
export_fig(imagenamename, '-jpg')
close(gcf)
fuse_overlay_slice=imfuse(DS_IHC.slice_scaled, ARV.xform.mz369,
'falsecolor', 'ColorChannels', [1 2 0]);
figure('Position', [1 1 dims.MSI(2)*multiplier dims.MSI(1)*multiplier])
image(fuse_overlay_slice)
hold on
plot(movingPoints_xform(:,1), movingPoints_xform(:,2), 'xw')

```

```

plot(fixedPoints(:,1),fixedPoints(:,2),'ow')
imagenam= strcat(folder,'Fuse_SliceandMSI')
export_fig(imagenam,'-jpg')
close(gcf)

```

G. Co-Registration Check

```

J_tform=fitgeotrans(movingPoints,fixedPoints,'affine') %create transformation
matrix
Rfixed=imref2d(dims.MSI)
xformlabel='MSI_Xform'
mkdir(folder,xformlabel)
for i=1:num_ions(2) %transform all MSI data
    ion=char(ARVnames(i))
    ARV.xform.(ion)=imwarp(ARV.scaled.(ion),J_tform,'OutputView',Rfixed,
'interp','nearest')
    ARV.xform_raw.(ion)=imwarp(ARV.mask.(ion),J_tform,'OutputView',Rfixed,
'interp','nearest')
    figure('name',ion,'Colormap',hot,'Position',[1 1 dims.MSI(2)*multiplier
dims.MSI(1)*multiplier])
    imagesc(dims.boundsx,dims.boundsy,ARV.xform.(ion))
    set(gcf,'Color','w');
    imagenam= strcat(folder,xformlabel,'\','Xform_',ion)
    export_fig(imagenam,'-jpg')
    close(gcf)
end
slice_flip=flipud(DS_IHC.slice_scaled);
for i=1:num_ions(2)
    ionstring=num2str(RawMSI.Label(i),3)
    ion= strcat(label,ionstring)
    ion_names{i}=ion

    overlay=figure('Colormap',hot,'Position',[1 1 dims.MSI(2)*multiplier
dims.MSI(1)*multiplier])
    arv_axes=axes('Parent',overlay)
    chol_axes=axes('Parent',overlay)
    colormap(arv_axes,hot)
    colormap(chol_axes,bone)
    set(arv_axes,'Visible','off')
    set(chol_axes,'Visible','off')
    linkaxes([arv_axes,chol_axes])

arv_plot=imagesc(dims.boundsx,dims.boundsy,ARV.xform.(ion),'Parent',arv_axes)
hold on
chol_plot=imagesc(dims.boundsx,dims.boundsy,slice_flip,'Parent',chol_axes)
set(chol_plot,'AlphaData',0.4)
hold off
imagenam= strcat(folder,xformlabel,'\','Overlay_TissueSlice_',ion)

```

```

    export_fig(imagename, '-png')
    close(gcf)
end
%Check registration
multiplier=5;
fuse_overlay_IHC=imfuse(DS_IHC.GFAP_scaled, DS_IHC.slice_scaled,
'falsecolor', 'ColorChannels', [1 2 0]);
figure('Position', [1 1 dims.MSI(2)*multiplier dims.MSI(1)*multiplier])
imagesc(dims.boundsx, dims.boundsy, fuse_overlay_IHC)
imagename=strcat(folder, 'Fuse_IHC_GFAPandSlice')
export_fig(imagename, '-jpg')
close(gcf)
fuse_overlay_prexfrom=imfuse(DS_IHC.slice_scaled, ARV.scaled.mz369,
'falsecolor', 'ColorChannels', [1 2 0]);
figure('Position', [1 1 dims.MSI(2)*multiplier dims.MSI(1)*multiplier])
image(fuse_overlay_prexfrom)
imagename=strcat(folder, 'Fuse_SliceandMSI_prexform')
hold on
plot(movingPoints(:,1), movingPoints(:,2), 'xw')
plot(fixedPoints(:,1), fixedPoints(:,2), 'ow')
export_fig(imagename, '-jpg')
close(gcf)
movingPoints_xform=transformPointsForward(J_tform, movingPoints)
fuse_overlay=imfuse(DS_IHC.GFAP_scaled, ARV.xform.mz369,
'falsecolor', 'ColorChannels', [1 2 0]);
figure('Position', [1 1 dims.MSI(2)*multiplier dims.MSI(1)*multiplier])
image(fuse_overlay)
hold on
plot(movingPoints_xform(:,1), movingPoints_xform(:,2), 'xw')
plot(fixedPoints(:,1), fixedPoints(:,2), 'ow')
imagename=strcat(folder, 'Fuse_GFAPandMSI')
export_fig(imagename, '-jpg')
close(gcf)
fuse_overlay_Corpus_callosum=imfuse(AnnotationMask_DS.Corpus_callosum,
ARV.xform.mz154, 'falsecolor', 'ColorChannels', [1 2 0]);
figure('Position', [1 1 dims.MSI(2)*multiplier dims.MSI(1)*multiplier])
imagesc(dims.boundsx, dims.boundsy, fuse_overlay_Corpus_callosum)
imagename=strcat(folder, 'Fuse_GFAPandMSI_CerebralCortex')
export_fig(imagename, '-jpg')
close(gcf)
fuse_overlay_slice=imfuse(DS_IHC.slice_scaled, ARV.xform.mz369,
'falsecolor', 'ColorChannels', [1 2 0]);
figure('Position', [1 1 dims.MSI(2)*multiplier dims.MSI(1)*multiplier])
image(fuse_overlay_slice)
hold on
plot(movingPoints_xform(:,1), movingPoints_xform(:,2), 'xw')
plot(fixedPoints(:,1), fixedPoints(:,2), 'ow')
imagename=strcat(folder, 'Fuse_SliceandMSI')
export_fig(imagename, '-jpg')

```

```
close(gcf)
```

H. Quantify ARVs with Inverted GFAP Mask

```
% Get user input about ABC concentration from section as quantified by MSI
ABC_input=inputdlg({'Enter TOTAL abacavir concentration (ng)'},'Quantifying
ABC',1,{''});
ABC_total_ng=str2num(ABC_input{1});
clear ABC_input;
% QUANTITATIVE ASSESSMENT OF ABACAVIR
% Proportional scaling of total drug across all voxels, and scaling by
% tissue mass to get units of (ng/g)
ABC_ng.Whole_Section=ARV.xform_raw.mz287.*ABC_total_ng./sum(ARV.xform_raw.mz2
87(:));
ABC_total_ng_check=sum(ABC_ng.Whole_Section(:));
voxel_area=0.1^2; %mm^2
voxel_thickness=0.01; %mm
tissue_density=1.06/1000; %g/mm^3
ABC_ng_g.Whole_Section=ABC_ng.Whole_Section/voxel_area/voxel_thickness/tissue
_density;
ABC_ng.GFAP=DS_IHC.GFAP_scaledmask.*ABC_ng.Whole_Section;
ABC_ng_g.GFAP=DS_IHC.GFAP_scaledmask.*ABC_ng_g.Whole_Section;
ABC_ng.nonGFAP=DS_IHC.GFAP_invertmask.*ABC_ng.Whole_Section;
ABC_ng_g.nonGFAP=DS_IHC.GFAP_invertmask.*ABC_ng_g.Whole_Section;
for i = 1:NumAnnotations
    region=Annotation_Name(i);
    ABC_ng.(region)=AnnotationMask_DS.(region).*ABC_ng.Whole_Section;
    ABC_ng_g.(region)=AnnotationMask_DS.(region).*ABC_ng_g.Whole_Section;
end
Summary_names=fieldnames(ABC_ng_g);
%Evaluate descriptive statistics on selected MSI data
section_area=nnz(ARVmask)*voxel_area
for j=1:max(size(Summary_names))
    Summary_field=char(Summary_names(j));
    loopnum=j;
    if j==1
        area=nnz(ARVmask);
    elseif j==2
        area=nnz(DS_IHC.GFAP_scaledmask);
    elseif j==3
        area=nnz(DS_IHC.GFAP_invertmask);
    else
        region=Annotation_Name(j-3);
        area=nnz(AnnotationMask_DS.(region));
    end
    vals_ng=nonzeros(ABC_ng.(Summary_field));
    vals_ng_g=nonzeros(ABC_ng_g.(Summary_field));

ARV_stats(1,j)=sum(vals_ng)/(area*voxel_area)/voxel_thickness/tissue_density;
ARV_stats(2,j)=min(vals_ng_g);
```

```

ARV_stats(3,j)=max(vals_ng_g);
ARV_stats(4,j)=mean(vals_ng_g);
ARV_stats(5,j)=median(vals_ng_g);
ARV_stats(6,j)=mode(vals_ng_g);
ARV_stats(7,j)=std(vals_ng_g);
ARV_stats(8,j)=var(vals_ng_g);
ARV_stats(9,j)=nnz(ABC_ng_g.(Summary_field));
ARV_stats(10,j)=ARV_stats(9,j)/area;
end

```

I. Saving ARV Data Output

```

%Writing Summary File for Abacavir
Statfile=strcat(folder,ProjectName(1),'_ARVstats_updated.xlsx');
Statfile=char(Statfile(1));
Rowstats=['Region';'Min    '; 'Max    '; 'Mean  '; 'Median'; 'Mode  '; 'Std   '; 'Var
'; 'Area  '; 'FrcTIS'];
Rowstats=cellstr(Rowstats);
Rownames=Rowstats;
ARV_stat_table_updated=array2table(ARV_stats,'VariableNames',Summary_names,'R
owNames',Rownames);
writetable(ARV_stat_table_updated, Statfile, 'Sheet',
'Abacavir_Summary','WriteRowNames',true);
Workspacefile=strcat(folder,ProjectName(1));
Workspacefile=char(Workspacefile);
save(Workspacefile);

```

Appendix IV: Morphine Abundance Coding Scripts

A. Image Selection

%SC% Run this code and select the image you want to work with - although it works with different images

%SC% we prefer to select .svs so we can select the layers/page/dimension in the next script.

```
[filename, pathname] = uigetfile( ...
    {'*.tif*;*.png;*.jpg;*.svs;*.scn', 'All Image Files (*.tif*, *.png, *.jpg,
*.svs, *.scn)'};
    '*.tif*', 'TIFF images (*.tif, *.tiff)'; ...
    '*.png', 'PNG images (*.png)'; ...
    '*.jpg', 'JPG images (*.jpg)'; ...
    '*.svs', 'SVS images (*.svs)'; ...
    '*.scn', 'SCN images (*.scn)'; ...
    '*.*', 'All Files (*.*)'}, ...
    'Pick Image');
```

B. Select Layer of Image

%SC% Run this code to select the layers/page - most are the same image in different resolutions,

%SC% but sometimes there are other images as the sticker for the sample.

```
I1info=imfinfo([pathname filename]);
for i=1:numel(I1info),pageinfo1{i}=['Page ' num2str(i) ': '
num2str(I1info(i).Height) ' x ' num2str(I1info(i).Width)]; end
fprintf('done.\n');
fname=[pathname filename];
if numel(I1info)>1,
    [s,v]=listdlg('Name','Choose Level','PromptString','Select a page for Roi
Discovery:','SelectionMode','single','ListSize',[170
120],'ListString',pageinfo1); drawnow;
    if ~v, guidata(hObject, handles); return; end
    fprintf('Reading page %g of image 1... ',s);
    io=imread(fname,s);
    fprintf('done.\n');
else
    fprintf('Image doesnt have any pages!\n');
end
%Dimensions of the IHC TIFF
dims.IHC=size(io);
dims.IHC=dims.IHC(1:2);
nrow=dims.IHC(1);
ncol=dims.IHC(2);
%If importing SVS, this should evaluate the image compression to be applied
%to XML data
hratio=ncol/I1info(1).Width;
wratio=nrow/I1info(1).Height;
```

C. Extract Annotations

```

%SC% is the only code you need to manually change it
    %SC% rename the .svs and .xml file to be the same you want to work with
    %SC% The files don't need to have the same name
[baseName, folder] = uigetfile({'*.xml'}, 'Select annotation data');
xml_file = fullfile(folder, baseName)
xDoc = xmlread(xml_file);
Regions=xDoc.getElementsByTagName('Region'); % get a list of all the region
tags
for regioni = 0:Regions.getLength-1
    Region=Regions.item(regioni); % for each region tag
    %get a list of all the vertexes (which are in order)
    vertices=Region.getElementsByTagName('Vertex');
    xy{1,regioni+1}=zeros(vertices.getLength-1,2); %allocate space for them
    for vertexi = 0:vertices.getLength-1 %iterate through all verticies
        %get the x value of that vertex
        x=str2double(vertices.item(vertexi).getAttribute('X'));

        %get the y value of that vertex
        y=str2double(vertices.item(vertexi).getAttribute('Y'));
        xy{1,regioni+1}(vertexi+1,:)=[x,y]; % finally save them into the array
    end
end

end
stDoc = parseXML(xml_file);
%Some structs from xml extraction need to be cleaned
stDoc.Children = CleanStruct(stDoc.Children, "Annotation");
%Extracting quantity of annotations
NumAnnotations = length(stDoc.Children);
%Cleaning structs again
for i = 1:NumAnnotations
    stDoc.Children(i).Children = CleanStruct(stDoc.Children(i).Children,
"Regions");
end
for i = 1:NumAnnotations
    stDoc.Children(i).Children.Children =
CleanStruct(stDoc.Children(i).Children.Children, "Region");
end
%Extracting quantity of regions
RegionsPerAnnotations = zeros(1,NumAnnotations);
for i = 1:NumAnnotations
    RegionsPerAnnotations(i) = length(stDoc.Children(i).Children.Children);
end

% Extracting Colors
for i = 1:NumAnnotations
    for k = 1:RegionsPerAnnotations(i)

```

```

        xy{2,k+sum(RegionsPerAnnotations(1:i-1))} =
completeRGB(dec2hex(str2double(stDoc.Children(i).Attributes(3).Value)));
    end
end
% Extracting Text boxes of notes from ImageScope
for i = 1:NumAnnotations
    for k = 1:RegionsPerAnnotations(i)
        xy{3,k+sum(RegionsPerAnnotations(1:i-1))} =
stDoc.Children(i).Children.Children(k).Attributes(13).Value;
    end
end
% Extracting Text of Annotation name
for i = 1:NumAnnotations
    for k = 1:RegionsPerAnnotations(i)
        xy{3,k+sum(RegionsPerAnnotations(1:i-1))} =
stDoc.Children(i).Attributes(7).Value;
    end
end
Annotation_Name=strings(NumAnnotations,1);
for i = 1:NumAnnotations
    Annotation_Name(i) = stDoc.Children(i).Attributes(7).Value;
    Annotation_Name(i) = replace(Annotation_Name(i), " ", "_");
    Annotation_Name(i) = replace(Annotation_Name(i), ",", "");
end
% Creating MASK associated with each Annotation Group
for i = 1:NumAnnotations
    mask=zeros(nrow,ncol);
    for k = 1:RegionsPerAnnotations(i)
        smaller_x=xy{1,k+sum(RegionsPerAnnotations(1:i-1))}(:,1)*wratio;
        smaller_y=xy{1,k+sum(RegionsPerAnnotations(1:i-1))}(:,2)*hratio;
        mask=mask+poly2mask(smaller_x,smaller_y,nrow,ncol);
    end

    AnnotationMask.(Annotation_Name(i))=mask;
end
figure('Position', [100 200 dims.IHC(2)*.05 dims.IHC(1)*.05])
imagesc(io)
hold on
for i = 1:NumAnnotations
    mask_plot=imagesc(AnnotationMask.(Annotation_Name(i)));
    set(mask_plot,'AlphaData',0.2)
end

```

D. Isolate GFAP

```

%Defining color thresholds for DAB staining of GFAP
cform = makecform('srgb2lab', 'AdaptedWhitePoint', whitepoint('D65'));
% Define thresholds for channel 1 based on histogram settings
channell1Min = 35.125;
channell1Max = 55.509;

```

```

% Define thresholds for channel 2 based on histogram settings
channel2Min = -2.513;
channel2Max = 7.547;
% Define thresholds for channel 3 based on histogram settings
channel3Min = -0.436;
channel3Max = 35.898;
% Isolating GFAP stain based on color threshold
IHC=im2double(io);
LABspace=applycform(IHC,cform);
GFAPmask=(LABspace(:,:,1) >= channel1Min ) & (LABspace(:,:,1) <= channel1Max)
& ...
    (LABspace(:,:,2) >= channel2Min ) & (LABspace(:,:,2) <= channel2Max) & ...
    (LABspace(:,:,3) >= channel3Min ) & (LABspace(:,:,3) <= channel3Max);
GFAP=IHC;
GFAP(repmat(~GFAPmask,[1 1 3])) = 0;
GFAP=rgb2gray(GFAP);
slice=rgb2gray(IHC);
slice=imcomplement(slice);
slice=slice.*(slice>0.1);
clear LABspace IHC;
% Show images of the GFAP and section as a check to make sure thresholding
% worked
figure('Position', [1 500 dims.IHC(2)*.035 dims.IHC(1)*.035])
imagesc(GFAP)
figure('Position', [1 500 dims.IHC(2)*.035 dims.IHC(1)*.035])
imagesc(slice)
GFAP_red=GFAP(:,:,1);
GFAP_red=GFAP_red.*GFAPmask;

GFAP_single=min(GFAP(GFAP>0));
GFAP_stats(1)=GFAP_single;
GFAP_total=sum(GFAP(:));
GFAP_stats(2)=GFAP_total;
GFAP_count=GFAP_total/GFAP_single;
GFAP_stats(3)=GFAP_count;
GFAP_area=nnz(GFAP);
GFAP_stats(4)=GFAP_area;
slice_area=nnz(slice);
GFAP_stats(5)=slice_area;
GFAP_fraction=GFAP_area/slice_area;
GFAP_stats(6)=GFAP_fraction;
GFAP_stats=transpose(GFAP_stats);
nonGFAPmask=imcomplement(GFAP_red);

```

E. MSI Morphine Data Import

```

% Read MSI data from Excel file
[baseName_morphine, folder_morphine] = uigetfile({'*.xlsx'; '*.xls'}, 'Select
morphine data');

```

```

MSiFileName_morphine = fullfile(folder_morphine, baseName_morphine)
ProjectName_morphine = strsplit(baseName_morphine, '.')
[RawMSI_morphine.Data]=xlsread(MSiFileName_morphine,-1)%Select ion data
[RawMSI_morphine.Label]=xlsread(MSiFileName_morphine,-1)%Select ion label
%Prompt user for ROI
ROI_morphine=inputdlg({'Number of lines','Scans per line','Voxel size X',
'Voxel size Y'},'Define ROI',1,{'','','0.1','0.1'})
dims.MSI_morphine=[str2num(ROI_morphine{1}) str2num(ROI_morphine{2})]
dims.SpotSpacing_morphine=[str2num(ROI_morphine{3}) str2num(ROI_morphine{4})]
dims.boundsx_morphine=[0 dims.MSI_morphine(2)*dims.SpotSpacing_morphine(1)]
dims.boundsy_morphine=[0 dims.MSI_morphine(1)*dims.SpotSpacing_morphine(2)]
multiplier = 5;
clear ROI_morphine;
%Parse imported data and generate ion images
num_ions_morphine=size(RawMSI_morphine.Label)
label='mz'
rawlabel='MSI_Raw_morphine'
mkdir(folder_morphine,rawlabel)
scaledlabel='MSI_Scaled_morphine'
mkdir(folder_morphine,scaledlabel)
for i=1:num_ions_morphine(2)
    ionstring=num2str(RawMSI_morphine.Label(i),7)
    ionstring=regexprep(ionstring,'\.','_')
    ion=strcat(label,ionstring)
    ion_names{i}=ion

    %Save images of raw MSI data
    Morphine.raw.(ion)=RawMSI_morphine.Data(:,i)

Morphine.reshape.(ion)=reshape(Morphine.raw.(ion),[dims.MSI_morphine(2),dims.
MSI_morphine(1)])
Morphine.reshape.(ion)=transpose(Morphine.reshape.(ion))
Morphine.scaled.(ion)=imadjust(mat2gray(Morphine.reshape.(ion)));
a=figure('name',ion,'Colormap',hot,'Position',[1 1
dims.MSI_morphine(2)*multiplier dims.MSI_morphine(1)*multiplier])

imagesc(dims.boundsx_morphine,dims.boundsy_morphine,Morphine.reshape.(ion))
set(gcf, 'Color', 'w');
imagename=strcat(folder_morphine,'\','rawlabel','\','Raw_',ion)
c=colorbar

a.Position(3)=(dims.MSI_morphine(2)+c.Position(3)/dims.SpotSpacing_morphine(1)
)*1.5*multiplier)*multiplier
export_fig(imagename,'-jpg')
close(gcf)
end
%Mask any off-tissue response based on Cholesterol ion map and scale image
Morphinemask=double(Morphine.scaled.mz287_2728>0.12);
Morphinemask=imfill(Morphinemask);

```

```

figure, imagesc (Morphinemask)
Morphinemask_boundary=bwperim (Morphinemask);
chol_flip=flipud (Morphine.scaled.mz287_2728);
for i=1:num_ions_morphine (2)
    ionstring=num2str (RawMSI_morphine.Label (i), 7)
    ionstring=regexprep (ionstring, '\\.', '_')
    ion=strcat (label, ionstring)
    ion_names{i}=ion

    Morphine.mask. (ion)=Morphinemask.*Morphine.reshape. (ion);
    %Tabulate stats on ion
    Raw_stats{i}=sum (Morphine.mask. (ion) (:));
    %Scale intensities of MSI data for comparison to IHC and save images of
scaled MSI data
    Morphine.scaled. (ion)=imadjust (mat2gray (Morphine.mask. (ion)));
    figure ('name', ion, 'Colormap', hot, 'Position', [1 1
dims.MSI_morphine (2)*multiplier dims.MSI_morphine (1)*multiplier])
    imagesc (dims.boundsx_morphine, dims.boundsy_morphine, Morphine.scaled. (ion))
    set (gcf, 'Color', 'w');
    imagename=strcat (folder_morphine, scaledlabel, '\\', 'Scaled_', ion)
    export_fig (imagename, '-jpg')
    close (gcf)

    overlay=figure ('Colormap', hot, 'Position', [1 1
dims.MSI_morphine (2)*multiplier dims.MSI_morphine (1)*multiplier])
    Morphine_axes=axes ('Parent', overlay)
    chol_axes=axes ('Parent', overlay)
    colormap (Morphine_axes, hot)
    colormap (chol_axes, parula)
    set (Morphine_axes, 'Visible', 'off')
    set (chol_axes, 'Visible', 'off')
    linkaxes ([Morphine_axes, chol_axes])

Morphine_plot=imagesc (dims.boundsx_morphine, dims.boundsy_morphine, Morphine.sc
aled. (ion), 'Parent', Morphine_axes)
    hold on

chol_plot=imagesc (dims.boundsx_morphine, dims.boundsy_morphine, chol_flip, 'Pare
nt', chol_axes)
    set (chol_plot, 'AlphaData', 0.2)
    hold off
    imagename=strcat (folder_morphine, scaledlabel, '\\', 'Overlay_Scaled_', ion)
    export_fig (imagename, '-png')
    close (gcf)
end
Morphinenames=fieldnames (Morphine.scaled)

```

F. Image Co-Registration - Morphine

```

%Select ion from morphine analysis for control point selection
composite_endog_xform=imwarp(composite_endog,J_tform,'OutputView',Rfixed,
'interp','nearest')
[Morphine_endog_selection,ok]=listdlg('PromptString','Select endogenous ions
representing tissue morphology for the MORPHINE
section:','ListString',Morphinenames)
num_morphine_endog=max(size(Morphine_endog_selection));
morphine_composite_endog=zeros(dims.MSI_morphine(1),dims.MSI_morphine(2));
for i = 1:num_morphine_endog
    ionstring=num2str(RawMSI_morphine.Label(Morphine_endog_selection(i)),7)
    ionstring=regexprep(ionstring,'\.','_')
    ion=strcat(label,ionstring)
    morphine_composite_endog=morphine_composite_endog+Morphine.scaled.(ion);
end
figure('Position',[1 1 dims.MSI_morphine(2)*multiplier
dims.MSI_morphine(1)*multiplier])
imagesc(morphine_composite_endog)
%control point registration, translating MSI to IHC
cpselect(morphine_composite_endog,composite_endog_xform) %select control
points

```

G. Co-Registration Check - Morphine

```

J_tform_morphine=fitgeotrans(movingPoints2,fixedPoints2,'affine') %create
transformation matrix
Rfixed=imref2d(dims.MSI)
xformlabel='MSI_Xform_morphine'
mkdir(folder_morphine,xformlabel)
for i=1:num_ions_morphine(2) %transform all MSI data
    ion=char(Morphinenames(i))

Morphine.xform.(ion)=imwarp(Morphine.scaled.(ion),J_tform_morphine,'OutputVie
w',Rfixed,'interp','nearest')

Morphine.xform_raw.(ion)=imwarp(Morphine.mask.(ion),J_tform_morphine,'OutputV
iew',Rfixed,'interp','nearest')
    figure('name',ion,'Colormap',hot,'Position',[1 1 dims.MSI(2)*multiplier
dims.MSI(1)*multiplier])
    imagesc(dims.boundsx,dims.boundsy,Morphine.xform.(ion))
    set(gcf,'Color','w');
    imagename=strcat(folder_morphine,xformlabel,'\','Xform_',ion)
    export_fig(imagename,'-jpg')
    close(gcf)
end
% slice_flip=flipud(DS_IHC.slice_scaled);
for i=1:num_ions_morphine(2)
    ionstring=num2str(RawMSI_morphine.Label(i),7)
    ionstring=regexprep(ionstring,'\.','_')
    ion=strcat(label,ionstring)
    ion_names{i}=ion

```

```

    overlay=figure('Colormap',hot,'Position',[1 1 dims.MSI(2)*multiplier
dims.MSI(1)*multiplier])
    arv_axes=axes('Parent',overlay)
    chol_axes=axes('Parent',overlay)
    colormap(arv_axes,hot)
    colormap(chol_axes,bone)
    set(arv_axes,'Visible','off')
    set(chol_axes,'Visible','off')
    linkaxes([arv_axes,chol_axes])

arv_plot=imagesc(dims.boundsx,dims.boundsy,Morphine.xform.(ion),'Parent',arv_
axes)
    hold on
    chol_plot=imagesc(dims.boundsx,dims.boundsy,slice_flip,'Parent',chol_axes)
    set(chol_plot,'AlphaData',0.4)
    hold off
    imagename=strcat(folder,xformlabel,'\','Overlay_TissueSlice_',ion)
    export_fig(imagename,'-png')
    close(gcf)
end

```

H. Qualitatively Assess Morphine with Inverted GFAP Mask

```

% Get user input about which drugs to assess
Morphine.segmented.GFAP=DS_IHC.GFAP_scaledmask.*Morphine.xform_raw.mz286_1438
;
Morphine.segmented.nonGFAP=DS_IHC.GFAP_invertmask.*Morphine.xform_raw.mz286_1
438;
for i = 1:NumAnnotations
    region=Annotation_Name(i);

Morphine.segmented.(region)=AnnotationMask_DS.(region).*Morphine.xform_raw.mz
286_1438;
end
Summary_names=fieldnames(Morphine.segmented);
%Evaluate descriptive statistics on selected MSI data
section_area=nnz(Morphinemask)
for j=1:max(size(Summary_names))
    Summary_field=char(Summary_names(j));
    if j==1
        area=section_area;
    elseif j==2
        area=nnz(DS_IHC.GFAP_scaledmask);
    elseif j==3
        area=nnz(DS_IHC.GFAP_invertmask);
    else
        region=Annotation_Name(j-3);
        area=nnz(AnnotationMask_DS.(region));
    end
end

```

```

vals=nonzeros(Morphine.segmented.(Summary_field));
Morphine_stats(1,j)=sum(vals);
Morphine_stats(2,j)=min(vals);
Morphine_stats(3,j)=max(vals);
Morphine_stats(4,j)=mean(vals);
Morphine_stats(5,j)=median(vals);
Morphine_stats(6,j)=mode(vals);
Morphine_stats(7,j)=std(vals);
Morphine_stats(8,j)=var(vals);
Morphine_stats(9,j)=nnz(vals);
Morphine_stats(10,j)=Morphine_stats(9,j)/area;
end

```

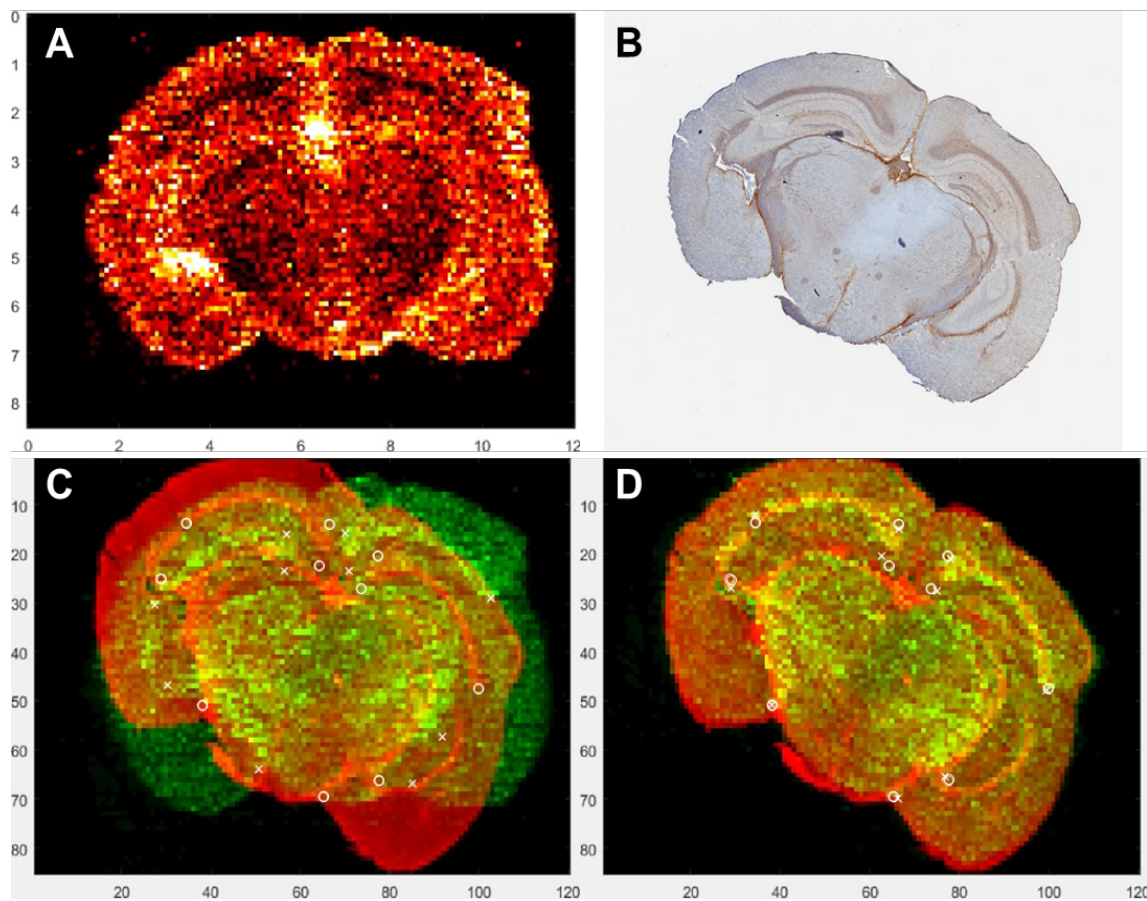
I. Saving Morphine Data Output

```

%Writing Summary File for Abacavir
Statfile=strcat(folder,ProjectName(1),'_ARVstats_updated.xlsx');
Statfile=char(Statfile(1));
Rowstats=['Region';'Min   '; 'Max   '; 'Mean  '; 'Median'; 'Mode  '; 'Std   '; 'Var
'; 'Area  '; 'FrcTIS'];
Rowstats=cellstr(Rowstats);
Rownames=Rowstats;
Morphine_stat_table_updated=array2table(Morphine_stats,'VariableNames',Summary_names,'RowNames',Rownames);
writetable(Morphine_stat_table_updated, Statfile, 'Sheet', 'Morphine_Summary', 'WriteRowNames', true);
Workspacefile=strcat(folder,ProjectName(1));
Workspacefile=char(Workspacefile);
save(Workspacefile);

```

Appendix V: IR-MALDESI MSI and IHC Image Co-registration



Visual representation of the image co-registration process between the MSI and IHC images. (A): MSI data image. (B): GFAP-stained IHC image. (C): Overlay of the MSI (green) and IHC (red) images before co-localization. Corresponding control points were manually selected based on relative geographical positioning of the MSI (X's) and IHC (O's) images. (D): Overlay of the MSI and IHC images after co-localization.

References

- Abbott, N. J. (2013). Blood–brain barrier structure and function and the challenges for CNS drug delivery. *Journal of Inherited Metabolic Disease*, *36*(3), 437–449.
<https://doi.org/10.1007/s10545-013-9608-0>
- Abbott, N. J., & Friedman, A. (2012). Overview and introduction: The blood–brain barrier in health and disease. *Epilepsia*, *53*(0 6), 1–6. <https://doi.org/10.1111/j.1528-1167.2012.03696.x>
- Abbott, N. J., Patabendige, A. A. K., Dolman, D. E. M., Yusof, S. R., & Begley, D. J. (2010). Structure and function of the blood–brain barrier. *Neurobiology of Disease*, *37*(1), 13–25.
<https://doi.org/10.1016/j.nbd.2009.07.030>
- Abbott, N. J., Rönnbäck, L., & Hansson, E. (2006). Astrocyte–endothelial interactions at the blood–brain barrier. *Nature Reviews Neuroscience*, *7*(1), Article 1.
<https://doi.org/10.1038/nrn1824>
- About HIV/AIDS | HIV Basics | HIV/AIDS | CDC.* (2022, June 30).
<https://www.cdc.gov/hiv/basics/whatishiv.html>
- Acaz-Fonseca, E., Avila-Rodriguez, M., Garcia-Segura, L. M., & Barreto, G. E. (2016). Regulation of astroglia by gonadal steroid hormones under physiological and pathological conditions. *Progress in Neurobiology*, *144*, 5–26.
<https://doi.org/10.1016/j.pneurobio.2016.06.002>
- Adler, M. W. (2001). Development of the epidemic. *BMJ : British Medical Journal*, *322*(7296), 1226–1229.
- Agarwal, S., Hartz, A. M. S., Elmquist, W. F., & Bauer, B. (2011). Breast Cancer Resistance Protein and P-glycoprotein in Brain Cancer: Two Gatekeepers Team Up. *Current Pharmaceutical Design*, *17*(26), 2793–2802.
- Ajasin, D., & Eugenin, E. A. (2020). HIV-1 Tat: Role in Bystander Toxicity. *Frontiers in Cellular and Infection Microbiology*, *10*. <https://www.frontiersin.org/articles/10.3389/fcimb.2020.00061>
- Alfahad, T. B., & Nath, A. (2013). Update on HIV-associated Neurocognitive Disorders. *Current Neurology and Neuroscience Reports*, *13*(10), 387. <https://doi.org/10.1007/s11910-013-0387-7>
- Alford, K., Banerjee, S., Nixon, E., O'Brien, C., Pounds, O., Butler, A., Elphick, C., Henshaw, P., Anderson, S., & Vera, J. H. (2019). Assessment and Management of HIV-Associated Cognitive Impairment: Experience from a Multidisciplinary Memory Service for People Living with HIV. *Brain Sciences*, *9*(2), Article 2. <https://doi.org/10.3390/brainsci9020037>
- Alford, K., Daley, S., Banerjee, S., & Vera, J. H. (2021). Quality of life in people living with HIV-associated neurocognitive disorder: A scoping review study. *PLOS ONE*, *16*(5), e0251944.
<https://doi.org/10.1371/journal.pone.0251944>
- Amateau, S. K., & McCarthy, M. M. (2002). Sexual Differentiation of Astrocyte Morphology in the Developing Rat Preoptic Area. *Journal of Neuroendocrinology*, *14*(11), 904–910.
<https://doi.org/10.1046/j.1365-2826.2002.00858.x>

Anand, K. S., & Dhikav, V. (2012). Hippocampus in health and disease: An overview. *Annals of Indian Academy of Neurology*, 15(4), 239–246. <https://doi.org/10.4103/0972-2327.104323>

Anderson, P. L., Kakuda, T. N., Kawle, S., & Fletcher, C. V. (2003). Antiviral dynamics and sex differences of zidovudine and lamivudine triphosphate concentrations in HIV-infected individuals. *AIDS*, 17(15), 2159.

Anthony, I. C., Arango, J.-C., Stephens, B., Simmonds, P., & Bell, J. E. (2008). The effects of illicit drugs on the HIV infected brain. *Frontiers in Bioscience: A Journal and Virtual Library*, 13, 1294–1307. <https://doi.org/10.2741/2762>

Antinori, A., Arendt, G., Becker, J. T., Brew, B. J., Byrd, D. A., Cherner, M., Clifford, D. B., Cinque, P., Epstein, L. G., Goodkin, K., Gisslen, M., Grant, I., Heaton, R. K., Joseph, J., Marder, K., Marra, C. M., McArthur, J. C., Nunn, M., Price, R. W., ... Wojna, V. E. (2007). Updated research nosology for HIV-associated neurocognitive disorders. *Neurology*, 69(18), 1789–1799. <https://doi.org/10.1212/01.WNL.0000287431.88658.8b>

Arentoft, A., Troxell, K., Alvarez, K., Aghvinian, M., Rivera Mindt, M., Cherner, M., Van Dyk, K., Razani, J., Roxas, M., & Gavilanes, M. (2022). HIV Antiretroviral Medication Neuropenetration and Neurocognitive Outcomes in HIV+ Adults: A Review of the Literature Examining the Central Nervous System Penetration Effectiveness Score. *Viruses*, 14(6), 1151. <https://doi.org/10.3390/v14061151>

Arias, C., Zepeda, A., Hernández-Ortega, K., Leal-Galicia, P., Lojero, C., & Camacho-Arroyo, I. (2009). Sex and estrous cycle-dependent differences in glial fibrillary acidic protein immunoreactivity in the adult rat hippocampus. *Hormones and Behavior*, 55(1), 257–263. <https://doi.org/10.1016/j.yhbeh.2008.10.016>

Avdoshina, V., Caragher, S. P., Wenzel, E. D., Taraballi, F., Mocchetti, I., & Harry, G. J. (2017). The viral protein gp120 decreases the acetylation of neuronal tubulin: Potential mechanism of neurotoxicity. *Journal of Neurochemistry*, 141(4), 606–613. <https://doi.org/10.1111/jnc.14015>

Aylward, E. H., Henderer, J. D., McArthur, J. C., Brettschneider, P. D., Harris, G. J., Barta, P. E., & Pearlson, G. D. (1993). Reduced basal ganglia volume in HIV-1-associated dementia: Results from quantitative neuroimaging. *Neurology*, 43(10), 2099–2104. <https://doi.org/10.1212/wnl.43.10.2099>

Bachis, A., Forcelli, P., Masliah, E., Campbell, L., & Mocchetti, I. (2016). Expression of gp120 in mice evokes anxiety behavior: Co-occurrence with increased dendritic spines and brain-derived neurotrophic factor in the amygdala. *Brain, Behavior, and Immunity*, 54, 170–177. <https://doi.org/10.1016/j.bbi.2016.01.020>

Baker, L., & Ratka, A. (2002). Sex-specific differences in levels of morphine, morphine-3-glucuronide, and morphine antinociception in rats. *Pain*, 95(1), 65–74. [https://doi.org/10.1016/S0304-3959\(01\)00376-1](https://doi.org/10.1016/S0304-3959(01)00376-1)

Ballester, L. Y., Capó-Vélez, C. M., García-Beltrán, W. F., Ramos, F. M., Vázquez-Rosa, E., Ríos, R., Mercado, J. R., Meléndez, R. I., & Lasalde-Dominicci, J. A. (2012). Up-regulation of the Neuronal Nicotinic Receptor $\alpha 7$ by HIV Glycoprotein 120. *The Journal of Biological Chemistry*, 287(5), 3079–3086. <https://doi.org/10.1074/jbc.M111.262543>

Bandera, A., Taramasso, L., Bozzi, G., Muscatello, A., Robinson, J. A., Burdo, T. H., & Gori, A. (2019). HIV-Associated Neurocognitive Impairment in the Modern ART Era: Are We Close to Discovering Reliable Biomarkers in the Setting of Virological Suppression? *Frontiers in Aging Neuroscience*, *11*. <https://www.frontiersin.org/articles/10.3389/fnagi.2019.00187>

Banks, W. A. (2009). Characteristics of compounds that cross the blood-brain barrier. *BMC Neurology*, *9*(1), S3. <https://doi.org/10.1186/1471-2377-9-S1-S3>

Bansal, A. K., Mactutus, C. F., Nath, A., Maragos, W., Hauser, K. F., & Booze, R. M. (2000). Neurotoxicity of HIV-1 proteins gp120 and Tat in the rat striatum. *Brain Research*, *879*(1), 42–49. [https://doi.org/10.1016/S0006-8993\(00\)02725-6](https://doi.org/10.1016/S0006-8993(00)02725-6)

Barry, J. A., Robichaud, G., Bokhart, M. T., Thompson, C., Sykes, C., Kashuba, A. D. M., & Muddiman, D. C. (2014). Mapping antiretroviral drugs in tissue by IR-MALDESI MSI coupled to the Q Exactive and comparison with LC-MS/MS SRM Assay. *Journal of the American Society for Mass Spectrometry*, *25*(12), 2038–2047. <https://doi.org/10.1007/s13361-014-0884-1>

Bartels, K., & Meissner, K. (2017). Morphine and the blood-brain barrier: Diffusion, uptake, or efflux? *Canadian Journal of Anaesthesia = Journal Canadien d'anesthésie*, *64*(10), 997–1001. <https://doi.org/10.1007/s12630-017-0932-y>

Bazzoni, G., Martinez-Estrada, O. M., Orsenigo, F., Cordenonsi, M., Citi, S., & Dejana, E. (2000). Interaction of junctional adhesion molecule with the tight junction components ZO-1, cingulin, and occludin. *The Journal of Biological Chemistry*, *275*(27), 20520–20526. <https://doi.org/10.1074/jbc.M905251199>

Bell, J. E., Arango, J.-C., & Anthony, I. C. (2006). Neurobiology of multiple insults: HIV-1-associated brain disorders in those who use illicit drugs. *Journal of Neuroimmune Pharmacology: The Official Journal of the Society on Neuroimmune Pharmacology*, *1*(2), 182–191. <https://doi.org/10.1007/s11481-006-9018-2>

Bell, J. E., Brettell, R. P., Chiswick, A., & Simmonds, P. (1998). HIV encephalitis, proviral load and dementia in drug users and homosexuals with AIDS. Effect of neocortical involvement. *Brain: A Journal of Neurology*, *121* (Pt 11), 2043–2052. <https://doi.org/10.1093/brain/121.11.2043>

Bell, R. D., Winkler, E. A., Sagare, A. P., Singh, I., LaRue, B., Deane, R., & Zlokovic, B. V. (2010). Pericytes Control Key Neurovascular Functions and Neuronal Phenotype in the Adult Brain and during Brain Aging. *Neuron*, *68*(3), 409–427. <https://doi.org/10.1016/j.neuron.2010.09.043>

Berger, E. A., Murphy, P. M., & Farber, J. M. (1999). CHEMOKINE RECEPTORS AS HIV-1 CORECEPTORS: Roles in Viral Entry, Tropism, and Disease. *Annual Review of Immunology*, *17*(1), 657–700. <https://doi.org/10.1146/annurev.immunol.17.1.657>

Beyer, C., Epp, B., Fassberg, J., Reiser, I., & Pilgrim, C. (1990). Region- and sex-related differences in maturation of astrocytes in dissociated cell cultures of embryonic rat brain. *Glia*, *3*(1), 55–64. <https://doi.org/10.1002/glia.440030108>

Bokhari, S. M., Hegde, R., Callen, S., Yao, H., Adany, I., Li, Q., Li, Z., Pinson, D., Yeh, H.-W., Cheney, P. D., & Buch, S. (2011). Morphine potentiates neuropathogenesis of SIV infection in

rhesus macaques. *Journal of Neuroimmune Pharmacology*, 6(4), 626–639. <https://doi.org/10.1007/s11481-011-9272-9>

Bokhart, M. T., Rosen, E., Thompson, C., Sykes, C., Kashuba, A. D. M., & Muddiman, D. C. (2015). Quantitative mass spectrometry imaging of emtricitabine in cervical tissue model using infrared matrix-assisted laser desorption electrospray ionization. *Analytical and Bioanalytical Chemistry*, 407(8), 2073–2084. <https://doi.org/10.1007/s00216-014-8220-y>

Bors, L. A., & Erdő, F. (2019). Overcoming the Blood–Brain Barrier. Challenges and Tricks for CNS Drug Delivery. *Scientia Pharmaceutica*, 87(1), Article 1. <https://doi.org/10.3390/scipharm87010006>

Bougea, A., Spantideas, N., Galanis, P., Gkekas, G., & Thomaidis, T. (2019). Optimal treatment of HIV-associated neurocognitive disorders: Myths and reality. A critical review. *Therapeutic Advances in Infectious Disease*, 6, 2049936119838228. <https://doi.org/10.1177/2049936119838228>

Bozzelli, P. L., Yin, T., Avdoshina, V., Mocchetti, I., Conant, K. E., & Maguire-Zeiss, K. A. (2019). HIV-1 Tat promotes astrocytic release of CCL2 through MMP/PAR-1 signaling. *Glia*, 67(9), 1719–1729. <https://doi.org/10.1002/glia.23642>

Brahmachari, S., Fung, Y. K., & Pahan, K. (2006). Induction of Glial Fibrillary Acidic Protein Expression in Astrocytes by Nitric Oxide. *The Journal of Neuroscience*, 26(18), 4930–4939. <https://doi.org/10.1523/JNEUROSCI.5480-05.2006>

Brailoiu, E., Brailoiu, G. C., Mamelii, G., Dolei, A., Sawaya, B. E., & Dun, N. J. (2006). Acute exposure to ethanol potentiates human immunodeficiency virus type 1 Tat-induced Ca(2+) overload and neuronal death in cultured rat cortical neurons. *Journal of Neurovirology*, 12(1), 17–24. <https://doi.org/10.1080/13550280500516427>

Broz, D., Carnes, N., Chapin-Bardales, J., Jarlais, D. C. D., Handanagic, S., Jones, C. M., McClung, R. P., & Asher, A. K. (2021). Syringe Services Programs' Role in Ending the HIV Epidemic in the U.S.: Why We Cannot Do It Without Them. *American Journal of Preventive Medicine*, 61(5), S118–S129. <https://doi.org/10.1016/j.amepre.2021.05.044>

Bruce, B. B. (2014). State-of-the-Art Review: Non-invasive assessment of cerebrospinal fluid pressure. *Journal of Neuro-Ophthalmology: The Official Journal of the North American Neuro-Ophthalmology Society*, 34(3), 288–294. <https://doi.org/10.1097/WNO.000000000000153>

Bruce-Keller, A. J., Turchan-Cholewo, J., Smart, E. J., Geurin, T., Chauhan, A., Reid, R., Xu, R., Nath, A., Knapp, P. E., & Hauser, K. F. (2008). Morphine Causes Rapid Increases in Glial Activation and Neuronal Injury in the Striatum of Inducible HIV-1 Tat Transgenic Mice. *Glia*, 56(13), 1414–1427. <https://doi.org/10.1002/glia.20708>

Burns, J. W., Hodsman, N. B. A., McLINTOCK, T. T. C., Gillies, G. W. A., Kenny, G. N. C., & McARDLE, C. S. (1989). The influence of patient characteristics on the requirements for postoperative analgesia. *Anaesthesia*, 44(1), 2–6. <https://doi.org/10.1111/j.1365-2044.1989.tb11086.x>

Butzbach, D. M. (2010). The influence of putrefaction and sample storage on post-mortem toxicology results. *Forensic Science, Medicine, and Pathology*, 6(1), 35–45. <https://doi.org/10.1007/s12024-009-9130-8>

Byrd, D. A., Fellows, R. P., Morgello, S., Franklin, D., Heaton, R. K., Deutsch, R., Atkinson, J. H., Clifford, D. B., Collier, A. C., Marra, C. M., Gelman, B., McCutchan, J. A., Duarte, N. A., Simpson, D. M., McArthur, J., & Grant, I. (2011). Neurocognitive Impact of Substance Use in HIV Infection. *Journal of Acquired Immune Deficiency Syndromes (1999)*, 58(2), 154–162. <https://doi.org/10.1097/QAI.0b013e318229ba41>

Byrd, D., Murray, J., Safdieh, G., & Morgello, S. (2012). Impact of opiate addiction on neuroinflammation in HIV. *Journal of NeuroVirology*, 18(5), 364–373. <https://doi.org/10.1007/s13365-012-0118-x>

Calcagno, A., Alberione, M. C., Romito, A., Imperiale, D., Ghisetti, V., Audagnotto, S., Lipani, F., Raviolo, S., Di Perri, G., & Bonora, S. (2014). Prevalence and predictors of blood-brain barrier damage in the HAART era. *Journal of NeuroVirology*, 20(5), 521–525. <https://doi.org/10.1007/s13365-014-0266-2>

Caligaris, G., Trunfio, M., Ghisetti, V., Cusato, J., Nigra, M., Atzori, C., Imperiale, D., Bonora, S., Di Perri, G., & Calcagno, A. (2021). Blood–Brain Barrier Impairment in Patients Living with HIV: Predictors and Associated Biomarkers. *Diagnostics*, 11(5), Article 5. <https://doi.org/10.3390/diagnostics11050867>

Caporello, E., Nath, A., Slevin, J., Galey, D., Hamilton, G., Williams, L., Steiner, J. P., & Haughey, N. J. (2006). The immunophilin ligand GPI1046 protects neurons from the lethal effects of the HIV-1 proteins gp120 and Tat by modulating endoplasmic reticulum calcium load. *Journal of Neurochemistry*, 98(1), 146–155. <https://doi.org/10.1111/j.1471-4159.2006.03863.x>

Caprioli, R. M., Farmer, T. B., & Gile, J. (1997). Molecular Imaging of Biological Samples: Localization of Peptides and Proteins Using MALDI-TOF MS. *Analytical Chemistry*, 69(23), 4751–4760. <https://doi.org/10.1021/ac970888i>

Carey, A. N., Sypek, E. I., Singh, H. D., Kaufman, M. J., & McLaughlin, J. P. (2012). Expression of HIV-Tat protein is associated with learning and memory deficits in the mouse. *Behavioural Brain Research*, 229(1), 48–56. <https://doi.org/10.1016/j.bbr.2011.12.019>

Castro-Gonzalez, S., Colomer-Lluch, M., & Serra-Moreno, R. (2018). Barriers for HIV Cure: The Latent Reservoir. *AIDS Research and Human Retroviruses*, 34(9), 739–759. <https://doi.org/10.1089/aid.2018.0118>

Cepeda, M. S., & Carr, D. B. (2003). Women Experience More Pain and Require More Morphine Than Men to Achieve a Similar Degree of Analgesia. *Anesthesia & Analgesia*, 97(5), 1464. <https://doi.org/10.1213/01.ANE.0000080153.36643.83>

Cernasev, A., Veve, M. P., Cory, T. J., Summers, N. A., Miller, M., Kodidela, S., & Kumar, S. (2020). Opioid Use Disorders in People Living with HIV/AIDS: A Review of Implications for Patient Outcomes, Drug Interactions, and Neurocognitive Disorders. *Pharmacy*, 8(3), 168. <https://doi.org/10.3390/pharmacy8030168>

- Chaganti, J., MARRIPUDI, K., Staub, L. P., Rae, C. D., Gates, T. M., Moffat, K. J., & Brew, B. J. (2019). Imaging correlates of the blood–brain barrier disruption in HIV-associated neurocognitive disorder and therapeutic implications. *AIDS*, *33*(12), 1843. <https://doi.org/10.1097/QAD.0000000000002300>
- Chen, K., Phan, T., Lin, A., Sardo, L., Mele, A. R., Nonnemacher, M. R., & Klase, Z. (2020). Morphine exposure exacerbates HIV-1 Tat driven changes to neuroinflammatory factors in cultured astrocytes. *PLoS ONE*, *15*(3). <https://doi.org/10.1371/journal.pone.0230563>
- Chowen, J. A., Busiguina, S., & García-Segura, L. M. (1995). Sexual dimorphism and sex steroid modulation of glial fibrillary acidic protein messenger RNA and immunoreactivity levels in the rat hypothalamus. *Neuroscience*, *69*(2), 519–532. [https://doi.org/10.1016/0306-4522\(95\)00250-M](https://doi.org/10.1016/0306-4522(95)00250-M)
- Chowen, J. A., & Garcia-Segura, L. M. (2021). Role of glial cells in the generation of sex differences in neurodegenerative diseases and brain aging. *Mechanisms of Ageing and Development*, *196*, 111473. <https://doi.org/10.1016/j.mad.2021.111473>
- Cicero, T. J., Ellis, M. S., Surratt, H. L., & Kurtz, S. P. (2014). The Changing Face of Heroin Use in the United States: A Retrospective Analysis of the Past 50 Years. *JAMA Psychiatry*, *71*(7), 821–826. <https://doi.org/10.1001/jamapsychiatry.2014.366>
- Clifford, D. B., & Ances, B. M. (2013). HIV-Associated Neurocognitive Disorder (HAND). *The Lancet Infectious Diseases*, *13*(11), 976–986. [https://doi.org/10.1016/S1473-3099\(13\)70269-X](https://doi.org/10.1016/S1473-3099(13)70269-X)
- Crespo-Castrillo, A., Garcia-Segura, L.-M., & Arevalo, M.-A. (2020). The synthetic steroid tibolone exerts sex-specific regulation of astrocyte phagocytosis under basal conditions and after an inflammatory challenge. *Journal of Neuroinflammation*, *17*(1), 37. <https://doi.org/10.1186/s12974-020-1719-6>
- Dahan, A. M., Sarton, E., Teppema, L., & Olievier, C. (1998). Sex-related Differences in the Influence of Morphine on Ventilatory Control in Humans. *Anesthesiology*, *88*(4), 903–913. <https://doi.org/10.1097/0000542-199804000-00009>
- Danta, C. C., & Piplani, P. (2020). Investigation of Molecular Properties of Antiretroviral Agents to Enhance CNS Penetration Abilities for the Treatment of Cognitive Impairment in HIV-Associated Neurocognitive Disorder. *ACS Chemical Neuroscience*, *11*(14), 2034–2038. <https://doi.org/10.1021/acscchemneuro.0c00329>
- Davis, L. E., Hjelle, B. L., Miller, V. E., Palmer, D. L., Llewellyn, A. L., Merlin, T. L., Young, S. A., Mills, R. G., Wachsman, W., & Wiley, C. A. (1992). Early viral brain invasion in iatrogenic human immunodeficiency virus infection. *Neurology*, *42*(9), 1736–1739. <https://doi.org/10.1212/wnl.42.9.1736>
- Dawson, T. M., & Dawson, V. L. (1994). Gp120 neurotoxicity in primary cortical cultures. *Advances in Neuroimmunology*, *4*(3), 167–173. [https://doi.org/10.1016/S0960-5428\(06\)80253-6](https://doi.org/10.1016/S0960-5428(06)80253-6)
- Degenhardt, L., Peacock, A., Colledge, S., Leung, J., Grebely, J., Vickerman, P., Stone, J., Cunningham, E. B., Trickey, A., Dumchev, K., Lynskey, M., Griffiths, P., Mattick, R. P., Hickman, M., & Larney, S. (2017). Global prevalence of injecting drug use and sociodemographic characteristics and prevalence of HIV, HBV, and HCV in people who inject

drugs: A multistage systematic review. *The Lancet Global Health*, 5(12), e1192–e1207. [https://doi.org/10.1016/S2214-109X\(17\)30375-3](https://doi.org/10.1016/S2214-109X(17)30375-3)

Denis, C. M., Morales, K. H., Wu, Q., Metzger, D. S., & Cheattle, M. D. (2019). Association Between Diagnoses of Chronic Noncancer Pain, Substance Use Disorder, and HIV-Related Outcomes in People Living With HIV. *Journal of Acquired Immune Deficiency Syndromes (1999)*, 82(2), S142–S147. <https://doi.org/10.1097/QAI.0000000000002179>

DePaula-Silva, A. B., Gorbea, C., Doty, D. J., Libbey, J. E., Sanchez, J. M. S., Hanak, T. J., Cazalla, D., & Fujinami, R. S. (2019). Differential transcriptional profiles identify microglial- and macrophage-specific gene markers expressed during virus-induced neuroinflammation. *Journal of Neuroinflammation*, 16(1), 152. <https://doi.org/10.1186/s12974-019-1545-x>

Des Jarlais, D. C., KERR, T., CARRIERI, P., FEELEMYER, J., & ARASTEH, K. (2016). HIV Infection among Persons who inject Drugs: Ending Old Epidemics and Addressing New Outbreaks. *AIDS (London, England)*, 30(6), 815–826. <https://doi.org/10.1097/QAD.0000000000001039>

Doyle, H. H., Eidson, L. N., Sinkiewicz, D. M., & Murphy, A. Z. (2017). Sex Differences in Microglia Activity within the Periaqueductal Gray of the Rat: A Potential Mechanism Driving the Dimorphic Effects of Morphine. *The Journal of Neuroscience*, 37(12), 3202–3214. <https://doi.org/10.1523/JNEUROSCI.2906-16.2017>

Dutta, R., & Roy, S. (2012). Mechanism(s) involved in Opioid drug abuse modulation of HAND. *Current HIV Research*, 10(5), 469–477.

Dutta, R., & Roy, S. (2015). Chronic morphine and HIV-1 Tat promote differential central nervous system trafficking of CD3+ and Ly6C+ immune cells in a murine Streptococcus pneumoniae infection model. *Journal of Neuroinflammation*, 12. <https://doi.org/10.1186/s12974-015-0341-5>

Edelman, E. J., Gordon, K., Becker, W. C., Goulet, J. L., Skanderson, M., Gaither, J. R., Brennan Braden, J., Gordon, A. J., Kerns, R. D., Justice, A. C., & Fiellin, D. A. (2013). Receipt of Opioid Analgesics by HIV-Infected and Uninfected Patients. *Journal of General Internal Medicine*, 28(1), 82–90. <https://doi.org/10.1007/s11606-012-2189-z>

El-Hage, N., Bruce-Keller, A. J., Yakovleva, T., Bazov, I., Bakalkin, G., Knapp, P. E., & Hauser, K. F. (2008). Morphine Exacerbates HIV-1 Tat-Induced Cytokine Production in Astrocytes through Convergent Effects on [Ca²⁺]_i, NF-κB Trafficking and Transcription. *PLoS ONE*, 3(12). <https://doi.org/10.1371/journal.pone.0004093>

El-Hage, N., Gurwell, J. A., Singh, I. N., Knapp, P. E., Nath, A., & Hauser, K. F. (2005). Synergistic increases in intracellular Ca²⁺, and the release of MCP-1, RANTES, and IL-6 by astrocytes treated with opiates and HIV-1 Tat. *Glia*, 50(2), 91–106. <https://doi.org/10.1002/glia.20148>

El-Hage, N., Wu, G., Wang, J., Ambati, J., Knapp, P. E., Reed, J. L., Bruce-Keller, A. J., & Hauser, K. F. (2006). HIV Tat1-72 and Opiate-induced changes in astrocytes promote chemotaxis of microglia through the expression of MCP-1 and alternative chemokines. *Glia*, 53(2), 132–146. <https://doi.org/10.1002/glia.20262>

- Ellis, R. J., Deutsch, R., Heaton, R. K., Marcotte, T. D., McCutchan, J. A., Nelson, J. A., Abramson, I., Thal, L. J., Atkinson, J. H., Wallace, M. R., & Grant, I. (1997). Neurocognitive Impairment Is an Independent Risk Factor for Death in HIV Infection. *Archives of Neurology*, *54*(4), 416–424. <https://doi.org/10.1001/archneur.1997.00550160054016>
- Elmeliegy, M. A., Carcaboso, A. M., Tagen, M., Bai, F., & Stewart, C. F. (2011). Role of ATP-Binding Cassette and Solute Carrier Transporters in Erlotinib CNS Penetration and Intracellular Accumulation. *Clinical Cancer Research*, *17*(1), 89–99. <https://doi.org/10.1158/1078-0432.CCR-10-1934>
- Ene, L. (2018). Human Immunodeficiency Virus in the Brain—Culprit or Facilitator? *Infectious Diseases: Research and Treatment*, *11*, 117863371775268. <https://doi.org/10.1177/1178633717752687>
- Ene, L., Duiculescu, D., & Ruta, S. M. (2011). How much do antiretroviral drugs penetrate into the central nervous system? *Journal of Medicine and Life*, *4*(4), 432–439.
- Eng, L. F., & Ghirnikar, R. S. (1994). GFAP and astrogliosis. *Brain Pathology (Zurich, Switzerland)*, *4*(3), 229–237. <https://doi.org/10.1111/j.1750-3639.1994.tb00838.x>
- Esser, S., Gelbrich, G., Brockmeyer, N., Goehler, A., Schadendorf, D., Erbel, R., Neumann, T., & Reinsch, N. (2013). Prevalence of cardiovascular diseases in HIV-infected outpatients: Results from a prospective, multicenter cohort study. *Clinical Research in Cardiology*, *102*(3), 203–213. <https://doi.org/10.1007/s00392-012-0519-0>
- Etherton, M. R., Lyons, J. L., & Ard, K. L. (2015). HIV-associated Neurocognitive Disorders and Antiretroviral Therapy: Current Concepts and Controversies. *Current Infectious Disease Reports*, *17*(6), 485. <https://doi.org/10.1007/s11908-015-0485-6>
- Eugenin, E. A., & Berman, J. W. (2007). Gap Junctions Mediate Human Immunodeficiency Virus-Bystander Killing in Astrocytes. *The Journal of Neuroscience*, *27*(47), 12844–12850. <https://doi.org/10.1523/JNEUROSCI.4154-07.2007>
- Eugenin, E. A., Clements, J. E., Zink, M. C., & Berman, J. W. (2011). Human Immunodeficiency Virus Infection of Human Astrocytes Disrupts Blood–Brain Barrier Integrity by a Gap Junction-Dependent Mechanism. *The Journal of Neuroscience*, *31*(26), 9456–9465. <https://doi.org/10.1523/JNEUROSCI.1460-11.2011>
- Eugenin, E. A., Dyer, G., Calderon, T. M., & Berman, J. W. (2005). HIV-1 tat Protein Induces a Migratory Phenotype in Human Fetal Microglia by a CCL2 (MCP-1)-Dependent Mechanism: Possible Role in NeuroAIDS. *Glia*, *49*(4), 501–510. <https://doi.org/10.1002/glia.20137>
- Fadiran, E. O., & Zhang, L. (2015). Effects of Sex Differences in the Pharmacokinetics of Drugs and Their Impact on the Safety of Medicines in Women. In M. Harrison-Woolrych (Ed.), *Medicines For Women* (pp. 41–68). Springer International Publishing. https://doi.org/10.1007/978-3-319-12406-3_2
- Fattakhov, N., Torices, S., Stangis, M., Park, M., & Toborek, M. (2021). Synergistic Impairment of the Neurovascular Unit by HIV-1 Infection and Methamphetamine Use: Implications for HIV-1-Associated Neurocognitive Disorders. *Viruses*, *13*(9), 1883. <https://doi.org/10.3390/v13091883>

Fauci, A. S., & Marston, H. D. (2015). Ending the HIV–AIDS Pandemic—Follow the Science. *New England Journal of Medicine*, *373*(23), 2197–2199. <https://doi.org/10.1056/NEJMp1502020>

Ferbinteanu, J. (2020). The Hippocampus and Dorsolateral Striatum Integrate Distinct Types of Memories through Time and Space, Respectively. *Journal of Neuroscience*, *40*(47), 9055–9065. <https://doi.org/10.1523/JNEUROSCI.1084-20.2020>

Ferner, R. E. (2008). Post-mortem clinical pharmacology. *British Journal of Clinical Pharmacology*, *66*(4), 430–443. <https://doi.org/10.1111/j.1365-2125.2008.03231.x>

Ferrara, M., Bumpus, N. N., Ma, Q., Ellis, R. J., Soontornniyomkij, V., Fields, J. A., Bharti, A., Achim, C. L., Moore, D. J., & Letendre, S. L. (2020). Antiretroviral drug concentrations in brain tissue of adult decedents. *AIDS*, *34*(13), 1907. <https://doi.org/10.1097/QAD.0000000000002628>

Ferrer, I., Martinez, A., Boluda, S., Parchi, P., & Barrachina, M. (2008). Brain banks: Benefits, limitations and cautions concerning the use of post-mortem brain tissue for molecular studies. *Cell and Tissue Banking*, *9*(3), 181–194. <https://doi.org/10.1007/s10561-008-9077-0>

Fischer-Smith, T., Croul, S., Sverstiuk, A. E., Capini, C., L'Heureux, D., Régulier, E. G., Richardson, M. W., Amini, S., Morgello, S., Khalili, K., & Rappaport, J. (2001). CNS invasion by CD14+/CD16+ peripheral blood-derived monocytes in HIV dementia: Perivascular accumulation and reservoir of HIV infection. *Journal of NeuroVirology*, *7*(6), 528–541. <https://doi.org/10.1080/135502801753248114>

Fitting, S., McRae, M., & Hauser, K. F. (2020). Opioid and neuroHIV Comorbidity – Current and Future Perspectives. *Journal of Neuroimmune Pharmacology*, *15*(4), 584–627. <https://doi.org/10.1007/s11481-020-09941-8>

Fitting, S., Scoggins, K. L., Xu, R., Dever, S. M., Knapp, P. E., Dewey, W. L., & Hauser, K. F. (2012). Morphine efficacy is altered in conditional HIV-1 Tat transgenic mice. *European Journal of Pharmacology*, *689*(1–3), 96–103. <https://doi.org/10.1016/j.ejphar.2012.05.029>

Fitting, S., Stevens, D. L., Khan, F. A., Scoggins, K. L., Enga, R. M., Beardsley, P. M., Knapp, P. E., Dewey, W. L., & Hauser, K. F. (2016). Morphine Tolerance and Physical Dependence Are Altered in Conditional HIV-1 Tat Transgenic Mice. *The Journal of Pharmacology and Experimental Therapeutics*, *356*(1), 96–105. <https://doi.org/10.1124/jpet.115.226407>

Fitting, S., Xu, R., Bull, C., Buch, S. K., El-Hage, N., Nath, A., Knapp, P. E., & Hauser, K. F. (2010). Interactive Comorbidity between Opioid Drug Abuse and HIV-1 Tat. *The American Journal of Pathology*, *177*(3), 1397–1410. <https://doi.org/10.2353/ajpath.2010.090945>

Fridén, M., Winiwarter, S., Jerndal, G., Bengtsson, O., Wan, H., Bredberg, U., Hammarlund-Udenaes, M., & Antonsson, M. (2009). Structure–Brain Exposure Relationships in Rat and Human Using a Novel Data Set of Unbound Drug Concentrations in Brain Interstitial and Cerebrospinal Fluids. *Journal of Medicinal Chemistry*, *52*(20), 6233–6243. <https://doi.org/10.1021/jm901036q>

Gallant, J., Hsue, P. Y., Shreay, S., & Meyer, N. (2017). Comorbidities Among US Patients With Prevalent HIV Infection—A Trend Analysis. *The Journal of Infectious Diseases*, *216*(12), 1525–1533. <https://doi.org/10.1093/infdis/jix518>

Gandhi, M., Aweeka, F., Greenblatt, R. M., & Blaschke, T. F. (2004). Sex Differences in Pharmacokinetics and Pharmacodynamics. *Annual Review of Pharmacology and Toxicology*, 44(1), 499–523. <https://doi.org/10.1146/annurev.pharmtox.44.101802.121453>

Gandhi, R. T., Spritzler, J., Chan, E., Asmuth, D. M., Rodriguez, B., Merigan, T. C., Hirsch, M. S., Shafer, R. W., Robbins, G. K., Pollard, R. B., & ACTG 384 Team. (2006). Effect of baseline- and treatment-related factors on immunologic recovery after initiation of antiretroviral therapy in HIV-1-positive subjects: Results from ACTG 384. *Journal of Acquired Immune Deficiency Syndromes (1999)*, 42(4), 426–434. <https://doi.org/10.1097/01.qai.0000226789.51992.3f>

Gannon, P., Khan, M. Z., & Kolson, D. L. (2011). Current understanding of HIV-associated neurocognitive disorders pathogenesis. *Current Opinion in Neurology*, 24(3), 275–283. <https://doi.org/10.1097/WCO.0b013e32834695fb>

Ghosh, A. K., Sarkar, A., & Mitsuya, H. (2017). HIV-Associated Neurocognitive Disorder (HAND) and the Prospect of Brain-Penetrating Protease Inhibitors for Antiretroviral Treatment. *Medical Research Archives*, 5(4), 1113.

Global HIV & AIDS statistics—Fact sheet. (n.d.). Retrieved May 16, 2022, from <https://www.unaids.org/en/resources/fact-sheet>

Grassivaro, F., Menon, R., Acquaviva, M., Ottoboni, L., Ruffini, F., Bergamaschi, A., Muzio, L., Farina, C., & Martino, G. (2020). Convergence between Microglia and Peripheral Macrophages Phenotype during Development and Neuroinflammation. *Journal of Neuroscience*, 40(4), 784–795. <https://doi.org/10.1523/JNEUROSCI.1523-19.2019>

Griesbeck, M., Scully, E., & Altfeld, M. (2016). Sex and gender differences in HIV-1 infection. *Clinical Science (London, England: 1979)*, 130(16), 1435–1451. <https://doi.org/10.1042/CS20160112>

Gu, C.-J., Borjabad, A., Hadas, E., Kelschenbach, J., Kim, B.-H., Chao, W., Arancio, O., Suh, J., Polsky, B., McMillan, J., Edagwa, B., Gendelman, H. E., Potash, M. J., & Volsky, D. J. (2018). EcoHIV infection of mice establishes latent viral reservoirs in T cells and active viral reservoirs in macrophages that are sufficient for induction of neurocognitive impairment. *PLoS Pathogens*, 14(6). <https://doi.org/10.1371/journal.ppat.1007061>

Guaraldi, G., Prakash, M., Moecklinghoff, C., & Stellbrink, H.-J. (2014). Morbidity in older HIV-infected patients: Impact of long-term antiretroviral use. *AIDS Reviews*, 16(2), 75–89.

Guo, C.-J., Li, Y., Tian, S., Wang, X., Douglas, S. D., & Ho, W.-Z. (2002). Morphine Enhances HIV Infection of Human Blood Mononuclear Phagocytes through Modulation of β -Chemokines and CCR5 Receptor. *Journal of Investigative Medicine*, 50(6), 435–442. <https://doi.org/10.1136/jim-50-06-03>

Gurwell, J. A., Nath, A., Sun, Q., Zhang, J., Martin, K. M., Chen, Y., & Hauser, K. F. (2001). Synergistic Neurotoxicity of Opioids and Human Immunodeficiency Virus-1 Tat Protein in Striatal Neurons In Vitro. *Neuroscience*, 102(3), 555–563.

Hahn, Y. K., Podhaizer, E. M., Farris, S. P., Miles, M. F., Hauser, K. F., & Knapp, P. E. (2015). Effects of chronic HIV-1 Tat exposure in the CNS: Heightened vulnerability of males versus

- females to changes in cell numbers, synaptic integrity, and behavior. *Brain Structure & Function*, 220(2), 605–623. <https://doi.org/10.1007/s00429-013-0676-6>
- Harris, M., Back, D., Kewn, S., Jutha, S., Marina, R., & Montaner, J. S. G. (2002). Intracellular carbovir triphosphate levels in patients taking abacavir once a day. *AIDS*, 16(8), 1196.
- Hart, T. K., Kirsh, R., Ellens, H., Sweet, R. W., Lambert, D. M., Petteway, S. R., Leary, J., & Bugelski, P. J. (1991). Binding of soluble CD4 proteins to human immunodeficiency virus type 1 and infected cells induces release of envelope glycoprotein gp120. *Proceedings of the National Academy of Sciences*, 88(6), 2189–2193. <https://doi.org/10.1073/pnas.88.6.2189>
- Haughey, N. J., & Mattson, M. P. (2002). Calcium Dysregulation and Neuronal Apoptosis by the HIV-1 Proteins Tat and gp120. *JAIDS Journal of Acquired Immune Deficiency Syndromes*, 31, S55.
- Hauser, K. F., El-Hage, N., Buch, S., Berger, J. R., Tyor, W. R., Nath, A., Bruce-Keller, A. J., & Knapp, P. E. (2005). Molecular targets of opiate drug abuse in neuroAIDS. *Neurotoxicity Research*, 8(1–2), 63–80. <https://doi.org/10.1007/BF03033820>
- Hauser, K. F., El-Hage, N., Stiene-Martin, A., Maragos, W. F., Nath, A., Persidsky, Y., Volsky, D. J., & Knapp, P. E. (2007). HIV-1 neuropathogenesis: Glial mechanisms revealed through substance abuse. *Journal of Neurochemistry*, 100(3), 567–586. <https://doi.org/10.1111/j.1471-4159.2006.04227.x>
- Hauser, K. F., Fitting, S., Dever, S. M., Podhaizer, E. M., & Knapp, P. E. (2012). Opiate Drug Use and the Pathophysiology of NeuroAIDS. *Current HIV Research*, 10(5), 435–452. <https://doi.org/10.2174/157016212802138779>
- Hauser, K. F., Hahn, Y. K., Adjan, V. V., Zou, S., Buch, S. K., Nath, A., Bruce-Keller, A. J., & Knapp, P. E. (2009). HIV-1 Tat and Morphine Have Interactive Effects on Oligodendrocyte Survival and Morphology. *Glia*, 57(2), 194–206. <https://doi.org/10.1002/glia.20746>
- Hauser, K. F., & Knapp, P. E. (2014). Interactions of HIV and drugs of abuse: The importance of glia, neural progenitors, and host genetic factors. *International Review of Neurobiology*, 118, 231–313. <https://doi.org/10.1016/B978-0-12-801284-0.00009-9>
- Hazleton, J. E., Berman, J. W., & Eugenin, E. A. (2010). Novel mechanisms of central nervous system damage in HIV infection. *HIV/AIDS (Auckland, N.Z.)*, 2, 39–49.
- He, H., Sharer, L. R., Chao, W., Gu, C.-J., Borjabad, A., Hadas, E., Kelschenbach, J., Ichiyama, K., Do, M., Potash, M. J., & Volsky, D. J. (2014). Enhanced Human Immunodeficiency Virus Type 1 Expression and Neuropathogenesis in Knockout Mice Lacking Type I Interferon Responses. *Journal of Neuropathology and Experimental Neurology*, 73(1), 59–71. <https://doi.org/10.1097/NEN.000000000000026>
- Heaton, R. K., Clifford, D. B., Franklin, D. R., Woods, S. P., Ake, C., Vaida, F., Ellis, R. J., Letendre, S. L., Marcotte, T. D., Atkinson, J. H., Rivera-Mindt, M., Vigil, O. R., Taylor, M. J., Collier, A. C., Marra, C. M., Gelman, B. B., McArthur, J. C., Morgello, S., Simpson, D. M., ... Grant, I. (2010). HIV-associated neurocognitive disorders persist in the era of potent antiretroviral therapy. *Neurology*, 75(23), 2087–2096. <https://doi.org/10.1212/WNL.0b013e318200d727>

Heaton, R. K., Franklin, D. R., Ellis, R. J., McCutchan, J. A., Letendre, S. L., LeBlanc, S., Corkran, S. H., Duarte, N. A., Clifford, D. B., Woods, S. P., Collier, A. C., Marra, C. M., Morgello, S., Mindt, M. R., Taylor, M. J., Marcotte, T. D., Atkinson, J. H., Wolfson, T., Gelman, B. B., ... Grant, I. (2011). HIV-associated neurocognitive disorders before and during the era of combination antiretroviral therapy: Differences in rates, nature, and predictors. *Journal of Neurovirology*, *17*(1), 3–16. <https://doi.org/10.1007/s13365-010-0006-1>

Heaton, R. K., Marcotte, T. D., Mindt, M. R., Sadek, J., Moore, D. J., Bentley, H., McCutchan, J. A., Reicks, C., Grant, I., & HNRC Group. (2004). The impact of HIV-associated neuropsychological impairment on everyday functioning. *Journal of the International Neuropsychological Society: JINS*, *10*(3), 317–331. <https://doi.org/10.1017/S1355617704102130>

Heinemann, U., & Schuetz, A. (2019). Structural Features of Tight-Junction Proteins. *International Journal of Molecular Sciences*, *20*(23), 6020. <https://doi.org/10.3390/ijms20236020>

Henderson, L. J., Johnson, T. P., Smith, B. R., Reoma, L. B., Santamaria, U. A., Bachani, M., Demarino, C., Barclay, R. A., Snow, J., Sacktor, N., Mearthur, J., Letendre, S., Steiner, J., Kashanchi, F., & Nath, A. (2019). Presence of Tat and transactivation response element in spinal fluid despite antiretroviral therapy. *AIDS*, *33*, S145. <https://doi.org/10.1097/QAD.0000000000002268>

High-Impact HIV Prevention: CDC's Approach to Reducing HIV Infections in the United States. (n.d.). *HIV Among People Who Inject Drugs | HIV by Group | HIV/AIDS | CDC.* (2022, June 28). <https://www.cdc.gov/hiv/group/hiv-idu.html>

HIV Infection and Cancer Risk—NCI (nciglobal.ncicenterprise). (2017, October 5). [CgvArticle]. <https://www.cancer.gov/about-cancer/causes-prevention/risk/infectious-agents/hiv-fact-sheet>

Hoefler, M. M., Sanchez, A. B., Maung, R., de Rozieres, C. M., Catalan, I. C., Dowling, C. C., Thaney, V. E., Piña-Crespo, J., Zhang, D., Roberts, A. J., & Kaul, M. (2015). Combination of Methamphetamine and HIV-1 gp120 causes distinct long-term alterations of behavior, gene expression, and injury in the central nervous system. *Experimental Neurology*, *263*, 221–234. <https://doi.org/10.1016/j.expneurol.2014.09.010>

Hong, S., & Banks, W. A. (2015). Role of the Immune System in HIV-associated Neuroinflammation and Neurocognitive Implications. *Brain, Behavior, and Immunity*, *0*, 1–12. <https://doi.org/10.1016/j.bbi.2014.10.008>

Hu, S., Sheng, W. S., Lokensgard, J. R., & Peterson, P. K. (2005). Morphine Potentiates HIV-1 gp120-Induced Neuronal Apoptosis. *The Journal of Infectious Diseases*, *191*(6), 886–889. <https://doi.org/10.1086/427830>

Huang, X., Hussain, B., & Chang, J. (2021). Peripheral inflammation and blood–brain barrier disruption: Effects and mechanisms. *CNS Neuroscience & Therapeutics*, *27*(1), 36–47. <https://doi.org/10.1111/cns.13569>

Hutchinson, M. R., Shavit, Y., Grace, P. M., Rice, K. C., Maier, S. F., & Watkins, L. R. (2011). Exploring the Neuroimmunopharmacology of Opioids: An Integrative Review of Mechanisms of

- Central Immune Signaling and Their Implications for Opioid Analgesia. *Pharmacological Reviews*, 63(3), 772–810. <https://doi.org/10.1124/pr.110.004135>
- Ivey, N. S., MacLean, A. G., & Lackner, A. A. (2009). AIDS and the blood-brain barrier. *Journal of Neurovirology*, 15(2), 111–122. <https://doi.org/10.1080/13550280902769764>
- Jaeger, L. B., & Nath, A. (2012). Modeling HIV-associated neurocognitive disorders in mice: New approaches in the changing face of HIV neuropathogenesis. *Disease Models & Mechanisms*, 5(3), 313–322. <https://doi.org/10.1242/dmm.008763>
- Jantzie, L. L., Rauw, G. A., & Todd, K. G. (2006). The effects of doxycycline administration on amino acid neurotransmitters in an animal model of neonatal hypoxia-ischemia. *Neurochemistry International*, 49(8), 717–728. <https://doi.org/10.1016/j.neuint.2006.06.010>
- Jeevanjee, S., Penko, J., Guzman, D., Miaskowski, C., Bangsberg, D. R., & Kushel, M. B. (2014). Opioid analgesic misuse is associated with incomplete antiretroviral adherence in a cohort of HIV-infected indigent adults in San Francisco. *AIDS and Behavior*, 18(7), 1352–1358. <https://doi.org/10.1007/s10461-013-0619-5>
- Jones, C. M. (2013). Heroin use and heroin use risk behaviors among nonmedical users of prescription opioid pain relievers – United States, 2002–2004 and 2008–2010. *Drug and Alcohol Dependence*, 132(1), 95–100. <https://doi.org/10.1016/j.drugalcdep.2013.01.007>
- Jones, L. D., Jackson, J. W., & Maggirwar, S. B. (2016). Modeling HIV-1 Induced Neuroinflammation in Mice: Role of Platelets in Mediating Blood-Brain Barrier Dysfunction. *PLoS ONE*, 11(3). <https://doi.org/10.1371/journal.pone.0151702>
- Joshi, C. R., Stacy, S., Sumien, N., Ghorpade, A., & Borgmann, K. (2020). Astrocyte HIV-1 Tat Differentially Modulates Behavior and Brain MMP/TIMP Balance During Short and Prolonged Induction in Transgenic Mice. *Frontiers in Neurology*, 11, 593188. <https://doi.org/10.3389/fneur.2020.593188>
- Kadry, H., Noorani, B., & Cucullo, L. (2020). A blood–brain barrier overview on structure, function, impairment, and biomarkers of integrity. *Fluids and Barriers of the CNS*, 17(1), 69. <https://doi.org/10.1186/s12987-020-00230-3>
- Kaul, M. (2008). HIV's double strike at the brain. *Frontiers in Bioscience : A Journal and Virtual Library*, 13, 2484–2494.
- Kaul, M., & Lipton, S. A. (1999). Chemokines and activated macrophages in HIV gp120-induced neuronal apoptosis. *Proceedings of the National Academy of Sciences of the United States of America*, 96(14), 8212–8216.
- Kelschenbach, J., He, H., Kim, B.-H., Borjabad, A., Gu, C.-J., Chao, W., Do, M., Sharer, L. R., Zhang, H., Arancio, O., Potash, M. J., & Volsky, D. J. (2019). Efficient Expression of HIV in Immunocompetent Mouse Brain Reveals a Novel Nonneurotoxic Viral Function in Hippocampal Synaptodendritic Injury and Memory Impairment. *MBio*, 10(4). <https://doi.org/10.1128/mBio.00591-19>
- Kelschenbach, J. L., Saini, M., Hadas, E., Gu, C., Chao, W., Bentsman, G., Hong, J. P., Hanke, T., Sharer, L. R., Potash, M. J., & Volsky, D. J. (2012). Mice Chronically Infected with Chimeric

- HIV Resist Peripheral and Brain Superinfection: A Model of Protective Immunity to HIV. *Journal of Neuroimmune Pharmacology*, 7(2), 380–387. <https://doi.org/10.1007/s11481-011-9316-1>
- Kennedy, C. A., & Zerbo, E. (2014). HIV-Related Neurocognitive Disorders and Drugs of Abuse: Mired in Confound, Surrounded by Risk. *Current Addiction Reports*, 1(3), 229–236. <https://doi.org/10.1007/s40429-014-0028-5>
- Kerr, T., Marshall, B. D. L., Milloy, M.-J., Zhang, R., Guillemi, S., Montaner, J. S. G., & Wood, E. (2012). Patterns of heroin and cocaine injection and plasma HIV-1 RNA suppression among a long-term cohort of injection drug users. *Drug and Alcohol Dependence*, 124(1–2), 108–112. <https://doi.org/10.1016/j.drugalcdep.2011.12.019>
- Kim, B. O., Liu, Y., Ruan, Y., Xu, Z. C., Schantz, L., & He, J. J. (2003). Neuropathologies in Transgenic Mice Expressing Human Immunodeficiency Virus Type 1 Tat Protein under the Regulation of the Astrocyte-Specific Glial Fibrillary Acidic Protein Promoter and Doxycycline. *The American Journal of Pathology*, 162(5), 1693–1707.
- Kim, B.-H., Kelschenbach, J., Borjabad, A., Hadas, E., He, H., Potash, M. J., Nedelcovych, M. T., Rais, R., Haughey, N. J., McArthur, J. C., Slusher, B. S., & Volsky, D. J. (2019). Intranasal insulin therapy reverses hippocampal dendritic injury and cognitive impairment in a model of HIV-associated neurocognitive disorders in EcoHIV-infected mice. *AIDS (London, England)*, 33(6), 973–984. <https://doi.org/10.1097/QAD.0000000000002150>
- Kim, J., Lesko, C. R., Fojo, A. T., Keruly, J. C., Moore, R. D., Chander, G., & Lau, B. (2021). The Effect of Buprenorphine on Human Immunodeficiency Virus Viral Suppression. *Clinical Infectious Diseases: An Official Publication of the Infectious Diseases Society of America*, 73(11), 1951–1956. <https://doi.org/10.1093/cid/ciab578>
- King, J. E., Eugenin, E. A., Buckner, C. M., & Berman, J. W. (2006). HIV tat and neurotoxicity. *Microbes and Infection*, 8(5), 1347–1357. <https://doi.org/10.1016/j.micinf.2005.11.014>
- Kodaira, H., Kusuhara, H., Fujita, T., Ushiki, J., Fuse, E., & Sugiyama, Y. (2011). Quantitative evaluation of the impact of active efflux by p-glycoprotein and breast cancer resistance protein at the blood-brain barrier on the predictability of the unbound concentrations of drugs in the brain using cerebrospinal fluid concentration as a surrogate. *The Journal of Pharmacology and Experimental Therapeutics*, 339(3), 935–944. <https://doi.org/10.1124/jpet.111.180398>
- Kodaira, H., Kusuhara, H., Fuse, E., Ushiki, J., & Sugiyama, Y. (2014). Quantitative Investigation of the Brain-to-Cerebrospinal Fluid Unbound Drug Concentration Ratio under Steady-State Conditions in Rats Using a Pharmacokinetic Model and Scaling Factors for Active Efflux Transporters. *Drug Metabolism and Disposition*, 42(6), 983–989. <https://doi.org/10.1124/dmd.113.056606>
- Kolodny, A., Courtwright, D. T., Hwang, C. S., Kreiner, P., Eadie, J. L., Clark, T. W., & Alexander, G. C. (2015). The Prescription Opioid and Heroin Crisis: A Public Health Approach to an Epidemic of Addiction. *Annual Review of Public Health*, 36(1), 559–574. <https://doi.org/10.1146/annurev-publhealth-031914-122957>
- Kolson, D. L. (2022). Developments in Neuroprotection for HIV-Associated Neurocognitive Disorders (HAND). *Current HIV/AIDS Reports*, 19(5), 344–357. <https://doi.org/10.1007/s11904-022-00612-2>

- Kruman, I. I., Nath, A., & Mattson, M. P. (1998). HIV-1 Protein Tat Induces Apoptosis of Hippocampal Neurons by a Mechanism Involving Caspase Activation, Calcium Overload, and Oxidative Stress. *Experimental Neurology*, *154*(2), 276–288. <https://doi.org/10.1006/exnr.1998.6958>
- Kumar, R., Orsoni, S., Norman, L., Verma, A. S., Tirado, G., Giavedoni, L. D., Staprans, S., Miller, G. M., Buch, S. J., & Kumar, A. (2006). Chronic morphine exposure causes pronounced virus replication in cerebral compartment and accelerated onset of AIDS in SIV/SHIV-infected Indian rhesus macaques. *Virology*, *354*(1), 192–206. <https://doi.org/10.1016/j.virol.2006.06.020>
- Lambotte, O., Deiva, K., & Tardieu, M. (2006). HIV-1 Persistence, Viral Reservoir, and the Central Nervous System in the HAART Era. *Brain Pathology*, *13*(1), 95–103. <https://doi.org/10.1111/j.1750-3639.2003.tb00010.x>
- Langford, D., Kim, B. oh, Zou, W., Fan, Y., Rahimain, P., Liu, Y., & He, J. J. (2018). Doxycycline-inducible and astrocyte-specific HIV-1 Tat transgenic mice (iTat) as an HIV/neuroAIDS model. *Journal of Neurovirology*, *24*(2), 168–179. <https://doi.org/10.1007/s13365-017-0598-9>
- Leibrand, C. R., Paris, J. J., Ghandour, M. S., Knapp, P. E., Kim, W.-K., Hauser, K. F., & McRae, M. (2017). HIV-1 Tat disrupts blood-brain barrier integrity and increases phagocytic perivascular macrophages and microglia in the dorsal striatum of transgenic mice. *Neuroscience Letters*, *640*, 136–143. <https://doi.org/10.1016/j.neulet.2016.12.073>
- Leibrand, C. R., Paris, J. J., Jones, A. M., Masuda, Q. N., Halquist, M. S., Kim, W.-K., Knapp, P. E., Kashuba, A. D. M., Hauser, K. F., & McRae, M. (2019). HIV-1 Tat and opioids act independently to limit antiretroviral brain concentrations and reduce blood–brain barrier integrity. *Journal of NeuroVirology*, *25*(4), 560–577. <https://doi.org/10.1007/s13365-019-00757-8>
- Leibrand, C. R., Paris, J. J., Jones, A. M., Ohene-Nyako, M., Rademeyer, K. M., Nass, S. R., Kim, W.-K., Knapp, P. E., Hauser, K. F., & McRae, M. (2022). Independent actions by HIV-1 Tat and morphine to increase recruitment of monocyte-derived macrophages into the brain in a region-specific manner. *Neuroscience Letters*, *788*, 136852. <https://doi.org/10.1016/j.neulet.2022.136852>
- Letendre, S. (2008). Validation of the CNS Penetration-Effectiveness Rank for Quantifying Antiretroviral Penetration Into the Central Nervous System. *Archives of Neurology*, *65*(1), 65. <https://doi.org/10.1001/archneurol.2007.31>
- Letendre, S. L., McCutchan, J. A., Childers, M. E., Woods, S. P., Lazzaretto, D., Heaton, R. K., Grant, I., & Ellis, R. J. (2004). Enhancing antiretroviral therapy for human immunodeficiency virus cognitive disorders. *Annals of Neurology*, *56*(3), 416–423. <https://doi.org/10.1002/ana.20198>
- Li, S., Hayden, E. Y., Garcia, V. J., Fuchs, D.-T., Sheyn, J., Daley, D. A., Rentsendorj, A., Torbati, T., Black, K. L., Rutishauser, U., Teplow, D. B., Koronyo, Y., & Koronyo-Hamaoui, M. (2020). Activated Bone Marrow-Derived Macrophages Eradicate Alzheimer’s-Related A β 42 Oligomers and Protect Synapses. *Frontiers in Immunology*, *11*. <https://www.frontiersin.org/articles/10.3389/fimmu.2020.00049>

- Lindl, K. A., Marks, D. R., Kolson, D. L., & Jordan-Sciutto, K. L. (2010). HIV-Associated Neurocognitive Disorder: Pathogenesis and Therapeutic Opportunities. *Journal of Neuroimmune Pharmacology*, 5(3), 294–309. <https://doi.org/10.1007/s11481-010-9205-z>
- Lopes, G. S., Bielinski, S., Moyer, A. M., Jacobson, D. J., Wang, L., Jiang, R., Larson, N. B., Miller, V. M., Zhu, Y., Cavanaugh, D. C., & Sauver, J. S. (2021). Sex differences in type and occurrence of adverse reactions to opioid analgesics: A retrospective cohort study. *BMJ Open*, 11(6), e044157. <https://doi.org/10.1136/bmjopen-2020-044157>
- Lopresti, N. M., Esguerra, M., & Mermelstein, P. G. (2020). Sex Differences in Animal Models of Opioid Reward. *Current Sexual Health Reports*, 12(3), 186–194. <https://doi.org/10.1007/s11930-020-00266-4>
- Lorenc, A., Ananthavarathan, P., Lorigan, J., Jowata, M., Brook, G., & Banarsee, R. (2014). The prevalence of comorbidities among people living with HIV in Brent: A diverse London Borough. *London Journal of Primary Care*, 6(4), 84–90.
- Loyd, D. R., Wang, X., & Murphy, A. Z. (2008). Sex Differences in μ -Opioid Receptor Expression in the Rat Midbrain Periaqueductal Gray Are Essential for Eliciting Sex Differences in Morphine Analgesia. *The Journal of Neuroscience*, 28(52), 14007–14017. <https://doi.org/10.1523/JNEUROSCI.4123-08.2008>
- Lu, T., & Wang, K.-H. (2020). The effect of opioid abuse on HIV infected nervous system. *Ibrain*, 6(3), 34–40. <https://doi.org/10.1002/j.2769-2795.2020.tb00051.x>
- MacLean, A. g., Belenchia, G. e., Bieniemy, D. n., Moroney-Rasmussen, T. a., & Lackner, A. a. (2005). Simian immunodeficiency virus disrupts extended lengths of the blood–brain barrier. *Journal of Medical Primatology*, 34(5–6), 237–242. <https://doi.org/10.1111/j.1600-0684.2005.00121.x>
- Mahajan, S. D., Aalinkeel, R., Sykes, D. E., Reynolds, J. L., Bindukumar, B., Fernandez, S. F., Chawda, R., Shanahan, T. C., & Schwartz, S. A. (2008). Tight Junction Regulation by Morphine and HIV-1 Tat Modulates Blood–Brain Barrier Permeability. *Journal of Clinical Immunology*, 28(5), 528. <https://doi.org/10.1007/s10875-008-9208-1>
- Mahajan, S. D., Ordain, N. S., Kutscher, H., Karki, S., & Reynolds, J. L. (2021). HIV Neuroinflammation: The Role of Exosomes in Cell Signaling, Prognostic and Diagnostic Biomarkers and Drug Delivery. *Frontiers in Cell and Developmental Biology*, 9. <https://www.frontiersin.org/articles/10.3389/fcell.2021.637192>
- Marban, C., Forouzanfar, F., Ait-Ammar, A., Fahmi, F., El Mekdad, H., Daouad, F., Rohr, O., & Schwartz, C. (2016). Targeting the Brain Reservoirs: Toward an HIV Cure. *Frontiers in Immunology*, 7, 397. <https://doi.org/10.3389/fimmu.2016.00397>
- Marks, J. H. (2020). Lessons from Corporate Influence in the Opioid Epidemic: Toward a Norm of Separation. *Journal of Bioethical Inquiry*, 17(2), 173–189. <https://doi.org/10.1007/s11673-020-09982-x>
- Marks, W. D., Paris, J. J., Schier, C. J., Denton, M. D., Fitting, S., McQuiston, A. R., Knapp, P. E., & Hauser, K. F. (2016). HIV-1 Tat causes cognitive deficits and selective loss of parvalbumin, somatostatin, and neuronal nitric oxide synthase expressing hippocampal CA1

interneuron subpopulations. *Journal of Neurovirology*, 22(6), 747–762.
<https://doi.org/10.1007/s13365-016-0447-2>

Marsden, M. D. (2020). Benefits and limitations of humanized mice in HIV persistence studies. *Retrovirology*, 17(1), 7. <https://doi.org/10.1186/s12977-020-00516-2>

Mathers, B. M., Degenhardt, L., Phillips, B., Wiessing, L., Hickman, M., Strathdee, S. A., Wodak, A., Panda, S., Tyndall, M., Toufik, A., & Mattick, R. P. (2008). Global epidemiology of injecting drug use and HIV among people who inject drugs: A systematic review. *The Lancet*, 372(9651), 1733–1745. [https://doi.org/10.1016/S0140-6736\(08\)61311-2](https://doi.org/10.1016/S0140-6736(08)61311-2)

Maung, R., Hoefer, M. M., Sanchez, A. B., Sejbuk, N. E., Medders, K. E., Desai, M. K., Catalan, I. C., Dowling, C. C., de Rozieres, C. M., Garden, G. A., Russo, R., Roberts, A. J., Williams, R., & Kaul, M. (2014). CCR5 Knockout Prevents Neuronal Injury and Behavioral Impairment Induced in a Transgenic Mouse Model by a CXCR4-using HIV-1 Glycoprotein 120. *Journal of Immunology (Baltimore, Md. : 1950)*, 193(4), 1895–1910.
<https://doi.org/10.4049/jimmunol.1302915>

May, M. T., Gompels, M., Delpech, V., Porter, K., Orkin, C., Kegg, S., Hay, P., Johnson, M., Palfreeman, A., Gilson, R., Chadwick, D., Martin, F., Hill, T., Walsh, J., Post, F., Fisher, M., Ainsworth, J., Jose, S., Leen, C., ... Study, for the U. C. H. C. (UK C. (2014). Impact on life expectancy of HIV-1 positive individuals of CD4+ cell count and viral load response to antiretroviral therapy. *AIDS*, 28(8), 1193. <https://doi.org/10.1097/QAD.0000000000000243>

McArthur, J. C. (2004). HIV dementia: An evolving disease. *Journal of Neuroimmunology*, 157(1), 3–10. <https://doi.org/10.1016/j.jneuroim.2004.08.042>

McArthur, J. C., & Brew, B. J. (2010). HIV-associated neurocognitive disorders: Is there a hidden epidemic? *AIDS*, 24(9), 1367–1370. <https://doi.org/10.1097/QAD.0b013e3283391d56>

McArthur, J. C., Steiner, J., Sacktor, N., & Nath, A. (2010). Human immunodeficiency virus-associated neurocognitive disorders: Mind the gap. *Annals of Neurology*, 67(6), 699–714.
<https://doi.org/10.1002/ana.22053>

McCarthy, L., Wetzell, M., Sliker, J. K., Eisenstein, T. K., & Rogers, T. J. (2001). Opioids, opioid receptors, and the immune response. *Drug and Alcohol Dependence*, 62(2), 111–123.
[https://doi.org/10.1016/S0376-8716\(00\)00181-2](https://doi.org/10.1016/S0376-8716(00)00181-2)

McCarty, J. H. (2005). Cell Biology of the Neurovascular Unit: Implications for Drug Delivery Across the Blood–Brain Barrier. *ASSAY and Drug Development Technologies*, 3(1), 89–95.
<https://doi.org/10.1089/adt.2005.3.89>

McKenzie, J. A. G., & Ridley, A. J. (2007). Roles of Rho/ROCK and MLCK in TNF- α -induced changes in endothelial morphology and permeability. *Journal of Cellular Physiology*, 213(1), 221–228. <https://doi.org/10.1002/jcp.21114>

McLane, V. D., Cao, L., & Willis, C. L. (2014). Morphine increases hippocampal viral load and suppresses frontal lobe CCL5 expression in the LP-BM5 AIDS model. *Journal of Neuroimmunology*, 269(0), 44–51. <https://doi.org/10.1016/j.jneuroim.2014.02.010>

- McLane, V. D., Kumar, S., Leeming, R., Rau, S., Willis, C. L., & Cao, L. (2018). Morphine-potentiated cognitive deficits correlate to suppressed hippocampal iNOS RNA expression and an absent type 1 interferon response in LP-BM5 murine AIDS. *Journal of Neuroimmunology*, *319*, 117–129. <https://doi.org/10.1016/j.jneuroim.2018.02.017>
- McLaurin, K. A., Booze, R. M., & Mactutus, C. F. (2016). Progression of temporal processing deficits in the HIV-1 transgenic rat. *Scientific Reports*, *6*(1), Article 1. <https://doi.org/10.1038/srep32831>
- McLaurin, K. A., Booze, R. M., & Mactutus, C. F. (2018). Evolution of the HIV-1 Transgenic Rat: Utility in Assessing the Progression of HIV-1 Associated Neurocognitive Disorders. *Journal of Neurovirology*, *24*(2), 229–245. <https://doi.org/10.1007/s13365-017-0544-x>
- Meijerink, H., Wisaksana, R., Iskandar, S., den Heijer, M., van der Ven, A. J. A. M., Alisjahbana, B., & van Crevel, R. (2014). Injecting drug use is associated with a more rapid CD4 cell decline among treatment naïve HIV-positive patients in Indonesia. *Journal of the International AIDS Society*, *17*(1), 18844. <https://doi.org/10.7448/IAS.17.1.18844>
- Merlin, J. S., Long, D., Becker, W. C., Cachay, E. R., Christopoulos, K. A., Claborn, K., Crane, H. M., Edelman, E. J., Harding, R., Kertesz, S. G., Liebschutz, J. M., Mathews, W. C., Mugavero, M. J., Napravnik, S., O’Cleirigh, C. C., Saag, M. S., Starrels, J. L., & Gross, R. (2018). THE ASSOCIATION OF CHRONIC PAIN AND LONG-TERM OPIOID THERAPY WITH HIV TREATMENT OUTCOMES. *Journal of Acquired Immune Deficiency Syndromes (1999)*, *79*(1), 77–82. <https://doi.org/10.1097/QAI.0000000000001741>
- Merlin, J. S., Westfall, A. O., Raper, J. L., Zinski, A., Norton, W. E., Willig, J. H., Gross, R., Ritchie, C. S., Saag, M. S., & Mugavero, M. J. (2012). Pain, Mood, and Substance Abuse in HIV: Implications for Clinic Visit Utilization, ART Adherence, and Virologic Failure. *Journal of Acquired Immune Deficiency Syndromes (1999)*, *61*(2), 164–170. <https://doi.org/10.1097/QAI.0b013e3182662215>
- Meyer, V. J., Rubin, L. H., Martin, E., Weber, K. M., Cohen, M. H., Golub, E. T., Valcour, V., Young, M. A., Crystal, H., Anastos, K., Aouizerat, B. E., Milam, J., & Maki, P. M. (2013). HIV and Recent Illicit Drug Use Interact to Affect Verbal Memory in Women. *Journal of Acquired Immune Deficiency Syndromes (1999)*, *63*(1), 67–76. <https://doi.org/10.1097/QAI.0b013e318289565c>
- Moore, D. J., Masliah, E., Rippeth, J. D., Gonzalez, R., Carey, C. L., Cherner, M., Ellis, R. J., Achim, C. L., Marcotte, T. D., Heaton, R. K., Grant, I., & Group, the H. (2006). Cortical and subcortical neurodegeneration is associated with HIV neurocognitive impairment. *AIDS*, *20*(6), 879. <https://doi.org/10.1097/01.aids.0000218552.69834.00>
- Moore, D. J., Montoya, J. L., Casaletto, K. B., & Hampton Atkinson, J. (2018). Medication Adherence and HIV-Associated Neurocognitive Disorders (HAND). In T. J. Hope, D. D. Richman, & M. Stevenson (Eds.), *Encyclopedia of AIDS* (pp. 1312–1318). Springer. https://doi.org/10.1007/978-1-4939-7101-5_466
- Moore, R. D., & Chaisson, R. E. (1999). Natural history of HIV infection in the era of combination antiretroviral therapy. *AIDS*, *13*(14), 1933.

- Morone, N. E., & Weiner, D. K. (2013). PAIN AS THE 5TH VITAL SIGN: EXPOSING THE VITAL NEED FOR PAIN EDUCATION. *Clinical Therapeutics*, 35(11), 1728–1732. <https://doi.org/10.1016/j.clinthera.2013.10.001>
- Morris, M. E., Rodriguez-Cruz, V., & Felmler, M. A. (2017). SLC and ABC Transporters: Expression, Localization, and Species Differences at the Blood-Brain and the Blood-Cerebrospinal Fluid Barriers. *The AAPS Journal*, 19(5), 1317–1331. <https://doi.org/10.1208/s12248-017-0110-8>
- Mosha, F., Muchunguzi, V., Matee, M., Sangeda, R. Z., Vercauteren, J., Nsubuga, P., Lyamuya, E., & Vandamme, A.-M. (2013). Gender differences in HIV disease progression and treatment outcomes among HIV patients one year after starting antiretroviral treatment (ART) in Dar es Salaam, Tanzania. *BMC Public Health*, 13, 38. <https://doi.org/10.1186/1471-2458-13-38>
- Murphy, A., Barbaro, J., Martínez-Aguado, P., Chilunda, V., Jaureguiberry-Bravo, M., & Berman, J. W. (2019). The Effects of Opioids on HIV Neuropathogenesis. *Frontiers in Immunology*, 10, 2445. <https://doi.org/10.3389/fimmu.2019.02445>
- Nabha, L., Duong, L., & Timpone, J. (2013). HIV-Associated Neurocognitive Disorders: Perspective on Management Strategies. *Drugs*, 73(9), 893–905. <https://doi.org/10.1007/s40265-013-0059-6>
- Nass, S. R., Hahn, Y. K., McLane, V. D., Varshneya, N. B., Damaj, M. I., Knapp, P. E., & Hauser, K. F. (2020). Chronic HIV-1 Tat exposure alters anterior cingulate cortico-basal ganglia-thalamocortical synaptic circuitry, associated behavioral control, and immune regulation in male mice. *Brain, Behavior, & Immunity - Health*, 5, 100077. <https://doi.org/10.1016/j.bbih.2020.100077>
- Nath, A. (2015). Eradication of Human Immunodeficiency Virus from Brain Reservoirs. *Journal of Neurovirology*, 21(3), 227–234. <https://doi.org/10.1007/s13365-014-0291-1>
- Nath, A., Anderson, C., Jones, M., Maragos, W., Booze, R., Mactutus, C., Bell, J., Hauser, K. F., & Mattson, M. (2000). Neurotoxicity and dysfunction of dopaminergic systems associated with AIDS dementia. *Journal of Psychopharmacology (Oxford, England)*, 14(3), 222–227. <https://doi.org/10.1177/026988110001400305>
- Nath, A., Hauser, K. F., Wojna, V., Booze, R. M., Maragos, W., Prendergast, M., Cass, W., & Turchan, J. T. (2002). Molecular Basis for Interactions of HIV and Drugs of Abuse. *JAIDS Journal of Acquired Immune Deficiency Syndromes*, 31, S62.
- National Academies of Sciences, E., Division, H. and M., Policy, B. on H. S., Abuse, C. on P. M. and R. S. to A. P. O., Phillips, J. K., Ford, M. A., & Bonnie, R. J. (2017). Trends in Opioid Use, Harms, and Treatment. In *Pain Management and the Opioid Epidemic: Balancing Societal and Individual Benefits and Risks of Prescription Opioid Use*. National Academies Press (US). <https://www.ncbi.nlm.nih.gov/books/NBK458661/>
- Nau, R., Sörgel, F., & Eiffert, H. (2010). Penetration of Drugs through the Blood-Cerebrospinal Fluid/Blood-Brain Barrier for Treatment of Central Nervous System Infections. *Clinical Microbiology Reviews*, 23(4), 858–883. <https://doi.org/10.1128/CMR.00007-10>

- Nicol, M. R., & McRae, M. (2021). Treating viruses in the brain: Perspectives from NeuroAIDS. *Neuroscience Letters*, 748, 135691. <https://doi.org/10.1016/j.neulet.2021.135691>
- Nicol, M. R., Pastick, K. A., Taylor, J., Namuju, O. C., Rhein, J., Williams, D. A., Meya, D. B., Boulware, D. R., & Lukande, R. (2019). Cerebrospinal Fluid and Brain Tissue Penetration of Tenofovir, Lamivudine, and Efavirenz in Postmortem Tissues with Cryptococcal Meningitis. *Clinical and Translational Science*, 12(5), 445–449. <https://doi.org/10.1111/cts.12661>
- Niu, F., Liao, K., Hu, G., Moidunny, S., Roy, S., & Buch, S. (2021). HIV Tat-Mediated Induction of Monocyte Transmigration Across the Blood–Brain Barrier: Role of Chemokine Receptor CXCR3. *Frontiers in Cell and Developmental Biology*, 9. <https://www.frontiersin.org/articles/10.3389/fcell.2021.724970>
- Norman, J. P., Perry, S. W., Kasischke, K. A., Volsky, D. J., & Gelbard, H. A. (2007). HIV-1 Trans Activator of Transcription Protein Elicits Mitochondrial Hyperpolarization and Respiratory Deficit, with Dysregulation of Complex IV and Nicotinamide Adenine Dinucleotide Homeostasis in Cortical Neurons¹. *The Journal of Immunology*, 178(2), 869–876. <https://doi.org/10.4049/jimmunol.178.2.869>
- Ntshangase, S., Mdanda, S., Singh, S. D., Naicker, T., Kruger, H. G., Baijnath, S., & Govender, T. (2019). Mass Spectrometry Imaging Demonstrates the Regional Brain Distribution Patterns of Three First-Line Antiretroviral Drugs. *ACS Omega*, 4(25), 21169–21177. <https://doi.org/10.1021/acsomega.9b02582>
- Okoye, A. A., & Picker, L. J. (2013). CD4+ T cell depletion in HIV infection: Mechanisms of immunological failure. *Immunological Reviews*, 254(1), 54–64. <https://doi.org/10.1111/imr.12066>
- Opportunistic Infections | Living with HIV | HIV Basics | HIV/AIDS | CDC.* (2022, March 30). <https://www.cdc.gov/hiv/basics/livingwithhiv/opportunisticinfections.html>
- Parashar, S., Collins, A. B., Montaner, J. S. G., Hogg, R. S., & Milloy, M.-J. (2016). REDUCING RATES OF PREVENTABLE HIV/AIDS-ASSOCIATED MORTALITY AMONG PEOPLE LIVING WITH HIV WHO INJECT DRUGS. *Current Opinion in HIV and AIDS*, 11(5), 507–513. <https://doi.org/10.1097/COH.0000000000000297>
- Parker, C. M., Hirsch, J. S., Hansen, H. B., Branas, C., & Martins, S. (2019). Facing Opioids in the Shadow of the HIV Epidemic. *The New England Journal of Medicine*, 380(1), 1–3. <https://doi.org/10.1056/NEJMp1813836>
- Parker, R., Stein, D. J., & Jelsma, J. (2014). Pain in people living with HIV/AIDS: A systematic review. *Journal of the International AIDS Society*, 17(1), 18719. <https://doi.org/10.7448/IAS.17.1.18719>
- Pasternak, G. W. (2014). Opiate Pharmacology and Relief of Pain. *Journal of Clinical Oncology*, 32(16), 1655–1661. <https://doi.org/10.1200/JCO.2013.53.1079>
- Patel, S. H., Ismaiel, O. A., Mylott, W. R., Yuan, M., McClay, J. L., Paris, J. J., Hauser, K. F., & McRae, M. (2019). Cell-type specific differences in antiretroviral penetration and the effects of HIV-1 Tat and morphine among primary human brain endothelial cells, astrocytes, pericytes, and microglia. *Neuroscience Letters*, 712, 134475. <https://doi.org/10.1016/j.neulet.2019.134475>

Peng, X., Mosser, D. M., Adler, M. W., Rogers, T. J., Meissler, J. J., & Eisenstein, T. K. (2000). Morphine enhances interleukin-12 and the production of other pro-inflammatory cytokines in mouse peritoneal macrophages. *Journal of Leukocyte Biology*, 68(5), 723–728.

Persidsky, Y., & Gendelman, H. E. (2003). Mononuclear phagocyte immunity and the neuropathogenesis of HIV-1 infection. *Journal of Leukocyte Biology*, 74(5), 691–701. <https://doi.org/10.1189/jlb.0503205>

Persidsky, Y., Ghorpade, A., Rasmussen, J., Limoges, J., Liu, X. J., Stins, M., Fiala, M., Way, D., Kim, K. S., Witte, M. H., Weinand, M., Carhart, L., & Gendelman, H. E. (1999). Microglial and Astrocyte Chemokines Regulate Monocyte Migration through the Blood-Brain Barrier in Human Immunodeficiency Virus-1 Encephalitis. *The American Journal of Pathology*, 155(5), 1599–1611.

Persidsky, Y., Limoges, J., McComb, R., Bock, P., Baldwin, T., Tyor, W., Patil, A., Nottet, H. S., Epstein, L., Gelbard, H., Flanagan, E., Reinhard, J., Pirruccello, S. J., & Gendelman, H. E. (1996). Human immunodeficiency virus encephalitis in SCID mice. *The American Journal of Pathology*, 149(3), 1027–1053.

Peters, F. T., & Steuer, A. E. (2019). Antemortem and postmortem influences on drug concentrations and metabolite patterns in postmortem specimens. *WIREs Forensic Science*, 1(1), e1297. <https://doi.org/10.1002/wfs2.1297>

Peterson, P. K., Sharp, B. M., Gekker, G., Portoghese, P. S., Sannerud, K., & Balfour, H. H. J. (1990). Morphine promotes the growth of HIV-1 in human peripheral blood mononuclear cell cocultures. *AIDS*, 4(9), 869–874.

Poorolajal, J., Hooshmand, E., Mahjub, H., Esmailnasab, N., & Jenabi, E. (2016). Survival rate of AIDS disease and mortality in HIV-infected patients: A meta-analysis. *Public Health*, 139, 3–12. <https://doi.org/10.1016/j.puhe.2016.05.004>

Potash, M. J., Chao, W., Bentsman, G., Paris, N., Saini, M., Nitkiewicz, J., Belem, P., Sharer, L., Brooks, A. I., & Volsky, D. J. (2005). A mouse model for study of systemic HIV-1 infection, antiviral immune responses, and neuroinvasiveness. *Proceedings of the National Academy of Sciences*, 102(10), 3760–3765. <https://doi.org/10.1073/pnas.0500649102>

Prinz, M., Masuda, T., Wheeler, M. A., & Quintana, F. J. (2021). Microglia and Central Nervous System—Associated Macrophages—From Origin to Disease Modulation. *Annual Review of Immunology*, 39, 251–277. <https://doi.org/10.1146/annurev-immunol-093019-110159>

Programs, N. R. C. (US) and I. of M. (US) P. on N. E. and B. D., Normand, J., Vlahov, D., & Moses, L. E. (1995). The Effects of Needle Exchange Programs. In *Preventing HIV Transmission: The Role of Sterile Needles and Bleach*. National Academies Press (US). <https://www.ncbi.nlm.nih.gov/books/NBK232343/>

Race, A. M., Styles, I. B., & Bunch, J. (2012). Inclusive sharing of mass spectrometry imaging data requires a converter for all. *Journal of Proteomics*, 75(16), 5111–5112. <https://doi.org/10.1016/j.jprot.2012.05.035>

Rahimy, E., Li, F.-Y., Hagberg, L., Fuchs, D., Robertson, K., Meyerhoff, D. J., Zetterberg, H., Price, R. W., Gisslén, M., & Spudich, S. (2017). Blood-Brain Barrier Disruption Is Initiated

During Primary HIV Infection and Not Rapidly Altered by Antiretroviral Therapy. *The Journal of Infectious Diseases*, 215(7), 1132–1140. <https://doi.org/10.1093/infdis/jix013>

Rappaport, J., & Volsky, D. J. (2015). Role of the Macrophage in HIV-Associated Neurocognitive Disorders and Other Comorbidities in Patients on Effective Antiretroviral Treatment. *Journal of Neurovirology*, 21(3), 235–241. <https://doi.org/10.1007/s13365-015-0346-y>

Reddy, P. V. B., Pilakka-Kanthikeel, S., Saxena, S. K., Saiyed, Z., & Nair, M. P. N. (2012). Interactive Effects of Morphine on HIV Infection: Role in HIV-Associated Neurocognitive Disorder. *AIDS Research and Treatment*, 2012, 953678. <https://doi.org/10.1155/2012/953678>

Roberts, D. J., & Goralski, K. B. (2008). A critical overview of the influence of inflammation and infection on P-glycoprotein expression and activity in the brain. *Expert Opinion on Drug Metabolism & Toxicology*, 4(10), 1245–1264. <https://doi.org/10.1517/17425255.4.10.1245>

Robichaud, G., Barry, J. A., Garrard, K. P., & Muddiman, D. C. (2013). Infrared Matrix-Assisted Laser Desorption Electrospray Ionization (IR-MALDESI) Imaging Source Coupled to a FT-ICR Mass Spectrometer. *Journal of the American Society for Mass Spectrometry*, 24(1), 92–100. <https://doi.org/10.1007/s13361-012-0505-9>

Robinson-Papp, J., Gelman, B. B., Grant, I., Singer, E., Gensler, G., & Morgello, S. (2012). Substance abuse increases the risk of neuropathy in an HIV-infected cohort. *Muscle & Nerve*, 45(4), 471–476. <https://doi.org/10.1002/mus.23231>

Ronaldson, P. T., & Davis, T. P. (2015). Targeting Transporters: Promoting Blood-Brain Barrier Repair in Response to Oxidative Stress Injury. *Brain Research*, 1623, 39–52. <https://doi.org/10.1016/j.brainres.2015.03.018>

Roomaney, R. A., van Wyk, B., & Pillay-van Wyk, V. (2022). Aging with HIV: Increased Risk of HIV Comorbidities in Older Adults. *International Journal of Environmental Research and Public Health*, 19(4), 2359. <https://doi.org/10.3390/ijerph19042359>

Rosenblum, A., Marsch, L. A., Joseph, H., & Portenoy, R. K. (2008). Opioids and the Treatment of Chronic Pain: Controversies, Current Status, and Future Directions. *Experimental and Clinical Psychopharmacology*, 16(5), 405–416. <https://doi.org/10.1037/a0013628>

Rowson, S. A., Harrell, C. S., Bekhbat, M., Gangavelli, A., Wu, M. J., Kelly, S. D., Reddy, R., & Neigh, G. N. (2016). Neuroinflammation and Behavior in HIV-1 Transgenic Rats Exposed to Chronic Adolescent Stress. *Frontiers in Psychiatry*, 7. <https://www.frontiersin.org/articles/10.3389/fpsy.2016.00102>

Roy, S., Ninkovic, J., Banerjee, S., Charboneau, R., Das, S., Dutta, R., Kirchner, V., Koodie, L., Ma, J., & Meng, J. (2011). Opioid Drug Abuse and Modulation of Immune Function: Consequences in the Susceptibility to Opportunistic Infections. *Journal of Neuroimmune Pharmacology: The Official Journal of the Society on Neuroimmune Pharmacology*, 6(4), 442–465. <https://doi.org/10.1007/s11481-011-9292-5>

Royal, W., Cherner, M., Burdo, T. H., Umlauf, A., Letendre, S. L., Jumare, J., Abimiku, A., Alabi, P., Alkali, N., Bwala, S., Okwuasaba, K., Eyzaguirre, L. M., Akolo, C., Guo, M., Williams, K. C., & Blattner, W. A. (2016). Associations between Cognition, Gender and Monocyte Activation

among HIV Infected Individuals in Nigeria. *PLoS ONE*, 11(2), e0147182.
<https://doi.org/10.1371/journal.pone.0147182>

Ru, W., & Tang, S.-J. (2017). HIV-associated synaptic degeneration. *Molecular Brain*, 10(1), 40.
<https://doi.org/10.1186/s13041-017-0321-z>

Rudd, R. A. (2016). Increases in Drug and Opioid-Involved Overdose Deaths—United States, 2010–2015. *MMWR. Morbidity and Mortality Weekly Report*, 65.
<https://doi.org/10.15585/mmwr.mm6505051e1>

Rumbaugh, J. A., & Tyor, W. (2015). HIV-associated neurocognitive disorders. *Neurology: Clinical Practice*, 5(3), 224–231. <https://doi.org/10.1212/CPJ.0000000000000117>

Ryan, L. A., Brester, M., Bohac, D., Morgello, S., & Zheng, J. (2004). Up-regulation of Soluble Tumor Necrosis Factor Receptor Two in Plasma of HIV-Seropositive Individuals Who Use Opiates. *AIDS Research and Human Retroviruses*, 20(1), 41–45.
<https://doi.org/10.1089/088922204322749486>

Sacktor, N., McDermott, M. P., Marder, K., Schifitto, G., Selnes, O. A., McArthur, J. C., Stern, Y., Albert, S., Palumbo, D., Kieburtz, K., Marcaida, J. A. D., Cohen, B., & Epstein, L. (2002). HIV-associated cognitive impairment before and after the advent of combination therapy. *Journal of Neurovirology*, 8(2), 136–142. <https://doi.org/10.1080/13550280290049615>

Sarton, E., Olofsen, E., Romberg, R., den Hartigh, J., Kest, B., Nieuwenhuijs, D., Burm, A., Teppema, L., & Dahan, A. (2000). Sex Differences in Morphine Analgesia: An Experimental Study in Healthy Volunteers. *Anesthesiology*, 93(5), 1245–1254.
<https://doi.org/10.1097/00000542-200011000-00018>

Saylor, D., Dickens, A. M., Sacktor, N., Haughey, N., Slusher, B., Pletnikov, M., Mankowski, J. L., Brown, A., Volsky, D. J., & McArthur, J. C. (2016). HIV-associated neurocognitive disorder—Pathogenesis and prospects for treatment. *Nature Reviews. Neurology*, 12(4), 234–248.
<https://doi.org/10.1038/nrneurol.2016.27>

Scanlan, A., Zhang, Z., Koneru, R., Reece, M., Gavegnano, C., Anderson, A. M., & Tyor, W. (2022). A Rationale and Approach to the Development of Specific Treatments for HIV Associated Neurocognitive Impairment. *Microorganisms*, 10(11), 2244.
<https://doi.org/10.3390/microorganisms10112244>

Schuetz, E. G., Furuya, K. N., & Schuetz, J. D. (1995). Interindividual variation in expression of P-glycoprotein in normal human liver and secondary hepatic neoplasms. *Journal of Pharmacology and Experimental Therapeutics*, 275(2), 1011–1018.

Scorziello, A., Florio, T., Bajetto, A., & Schettini, G. (1998). Intracellular Signalling Mediating HIV-1 gp120 Neurotoxicity. *Cellular Signalling*, 10(2), 75–84. [https://doi.org/10.1016/S0898-6568\(97\)00093-4](https://doi.org/10.1016/S0898-6568(97)00093-4)

Scully, E. P. (2018). Sex Differences in HIV Infection. *Current HIV/AIDS Reports*, 15(2), 136–146. <https://doi.org/10.1007/s11904-018-0383-2>

Sharp, P. M., & Hahn, B. H. (2011). Origins of HIV and the AIDS Pandemic. *Cold Spring Harbor Perspectives in Medicine*, 1(1), a006841. <https://doi.org/10.1101/cshperspect.a006841>

- Shen, D. D., Artru, A. A., & Adkison, K. K. (2004). Principles and applicability of CSF sampling for the assessment of CNS drug delivery and pharmacodynamics. *Advanced Drug Delivery Reviews*, 56(12), 1825–1857. <https://doi.org/10.1016/j.addr.2004.07.011>
- Shultz, L. D., Brehm, M. A., Garcia-Martinez, J. V., & Greiner, D. L. (2012). Humanized mice for immune system investigation: Progress, promise and challenges. *Nature Reviews Immunology*, 12(11), 786–798. <https://doi.org/10.1038/nri3311>
- Sidebotham, D., Dijkhuizen, M. R. J., & Schug, S. A. (1997). The safety and utilization of patient-controlled analgesia. *Journal of Pain and Symptom Management*, 14(4), 202–209. [https://doi.org/10.1016/S0885-3924\(97\)00182-6](https://doi.org/10.1016/S0885-3924(97)00182-6)
- Silverberg, M. J., Ray, G. T., Saunders, K., Rutter, C. M., Campbell, C. I., Merrill, J. O., Sullivan, M. D., J. Banta-Green, C., Von Korff, M., & Weisner, C. (2012). Prescription Long-term Opioid Use in HIV-infected Patients. *The Clinical Journal of Pain*, 28(1), 39–46. <https://doi.org/10.1097/AJP.0b013e3182201a0f>
- Sindberg, G. M., Sharma, U., Banerjee, S., Anand, V., Dutta, R., Gu, C.-J., Volsky, D. J., & Roy, S. (2015). An infectious murine model for studying the systemic effects of opioids on early HIV pathogenesis in the gut. *Journal of Neuroimmune Pharmacology: The Official Journal of the Society on NeuroImmune Pharmacology*, 10(1), 74–87. <https://doi.org/10.1007/s11481-014-9574-9>
- Smith, M. Z., Wightman, F., & Lewin, S. R. (2012). HIV Reservoirs and Strategies for Eradication. *Current HIV/AIDS Reports*, 9(1), 5–15. <https://doi.org/10.1007/s11904-011-0108-2>
- Smith, R. X., Guha, A., Vaida, F., Paul, R. H., & Ances, B. (2018). Prefrontal Recruitment Mitigates Risk-Taking Behavior in Human Immunodeficiency Virus-Infected Young Adults. *Clinical Infectious Diseases*, 66(10), 1595–1601. <https://doi.org/10.1093/cid/cix1031>
- Soldin, O., & Mattison, D. (2009). Sex Differences in Pharmacokinetics and Pharmacodynamics. *Clinical Pharmacokinetics*, 48(3), 143–157. <https://doi.org/10.2165/00003088-200948030-00001>
- Soldin, O. P., Chung, S. H., & Mattison, D. R. (2011). Sex Differences in Drug Disposition. *Journal of Biomedicine and Biotechnology*, 2011, 187103. <https://doi.org/10.1155/2011/187103>
- South, S. M., Edwards, S. R., & Smith, M. T. (2009). Antinociception Versus Serum Concentration Relationships Following Acute Administration of Intravenous Morphine in Male and Female Sprague-Dawley Rats: Differences Between the Tail Flick and Hot Plate Nociceptive Tests. *Clinical and Experimental Pharmacology and Physiology*, 36(1), 20–28. <https://doi.org/10.1111/j.1440-1681.2008.05019.x>
- Spudich, S., & González-Scarano, F. (2012). HIV-1-related central nervous system disease: Current issues in pathogenesis, diagnosis, and treatment. *Cold Spring Harbor Perspectives in Medicine*, 2(6), a007120. <https://doi.org/10.1101/cshperspect.a007120>
- Stamatovic, S. M., Johnson, A. M., Keep, R. F., & Andjelkovic, A. V. (2016). Junctional proteins of the blood-brain barrier: New insights into function and dysfunction. *Tissue Barriers*, 4(1), e1154641. <https://doi.org/10.1080/21688370.2016.1154641>

Strazza, M., Pirrone, V., Wigdahl, B., Dampier, W., Lin, W., Feng, R., Maubert, M. E., Weksler, B., Romero, I. A., Couraud, P.-O., & Nonnemacher, M. R. (2016). Prolonged Morphine Exposure Induces Increased Firm Adhesion in an in Vitro Model of the Blood–Brain Barrier. *International Journal of Molecular Sciences*, *17*(6). <https://doi.org/10.3390/ijms17060916>

Stretcher, B. N., Pesce, A. J., Frame, P. T., & Stein, D. S. (1994). Pharmacokinetics of zidovudine phosphorylation in peripheral blood mononuclear cells from patients infected with human immunodeficiency virus. *Antimicrobial Agents and Chemotherapy*, *38*(7), 1541–1547.

Tajes, M., Ramos-Fernández, E., Weng-Jiang, X., Bosch-Morató, M., Guivernau, B., Eraso-Pichot, A., Salvador, B., Fernández-Busquets, X., Roquer, J., & Muñoz, F. J. (2014). The blood-brain barrier: Structure, function and therapeutic approaches to cross it. *Molecular Membrane Biology*, *31*(5), 152–167. <https://doi.org/10.3109/09687688.2014.937468>

Tani, M., Glabinski, A. R., Tuohy, V. K., Stoler, M. H., Estes, M. L., & Ransohoff, R. M. (1996). In situ hybridization analysis of glial fibrillary acidic protein mRNA reveals evidence of biphasic astrocyte activation during acute experimental autoimmune encephalomyelitis. *The American Journal of Pathology*, *148*(3), 889–896.

Thaney, V. E., Sanchez, A. B., Fields, J. A., Minassian, A., Young, J., Maung, R., & Kaul, M. (2018). Transgenic Mice Expressing HIV-1 Envelope Protein gp120 in the Brain as an Animal Model in NeuroAIDS Research. *Journal of Neurovirology*, *24*(2), 156–167. <https://doi.org/10.1007/s13365-017-0584-2>

The Stages of HIV Infection | NIH. (n.d.). Retrieved January 9, 2023, from <https://hivinfo.nih.gov/understanding-hiv/fact-sheets/stages-hiv-infection>

Thompson, C. G., Bokhart, M. T., Sykes, C., Adamson, L., Fedoriw, Y., Luciw, P. A., Muddiman, D. C., Kashuba, A. D. M., & Rosen, E. P. (2015). Mass spectrometry imaging reveals heterogeneous efavirenz distribution within putative HIV reservoirs. *Antimicrobial Agents and Chemotherapy*, *59*(5), 2944–2948. <https://doi.org/10.1128/AAC.04952-14>

Thompson, C. G., Rosen, E. P., Prince, H. M. A., White, N., Sykes, C., de la Cruz, G., Mathews, M., Deleage, C., Estes, J. D., Charlins, P., Mulder, L. R., Kovarova, M., Adamson, L., Arora, S., Dellon, E. S., Peery, A. F., Shaheen, N. J., Gay, C., Muddiman, D. C., ... Kashuba, A. D. M. (2019). Heterogeneous antiretroviral drug distribution and HIV/SHIV detection in the gut of three species. *Science Translational Medicine*, *11*(499). <https://doi.org/10.1126/scitranslmed.aap8758>

Thompson, K. A., Cherry, C. L., Bell, J. E., & McLean, C. A. (2011). Brain Cell Reservoirs of Latent Virus in Presymptomatic HIV-Infected Individuals. *The American Journal of Pathology*, *179*(4), 1623–1629. <https://doi.org/10.1016/j.ajpath.2011.06.039>

Thompson, P. M., Dutton, R. A., Hayashi, K. M., Toga, A. W., Lopez, O. L., Aizenstein, H. J., & Becker, J. T. (2005). Thinning of the cerebral cortex visualized in HIV/AIDS reflects CD4+ T lymphocyte decline. *Proceedings of the National Academy of Sciences of the United States of America*, *102*(43), 15647–15652. <https://doi.org/10.1073/pnas.0502548102>

Toborek, M., Lee, Y. W., Flora, G., Pu, H., András, I. E., Wylegala, E., Hennig, B., & Nath, A. (2005). Mechanisms of the Blood–Brain Barrier Disruption in HIV-1 Infection. *Cellular and Molecular Neurobiology*, *25*(1), 181–199. <https://doi.org/10.1007/s10571-004-1383-x>

Toggas, S. M., Masliah, E., Rockenstein, E. M., Rall, G. F., Abraham, C. R., & Mucke, L. (1994). Central nervous system damage produced by expression of the HIV-1 coat protein gp120 in transgenic mice. *Nature*, *367*(6459), 188–193. <https://doi.org/10.1038/367188a0>

Triant, V. A., Lee, H., Hadigan, C., & Grinspoon, S. K. (2007). Increased Acute Myocardial Infarction Rates and Cardiovascular Risk Factors among Patients with Human Immunodeficiency Virus Disease. *The Journal of Clinical Endocrinology and Metabolism*, *92*(7), 2506–2512. <https://doi.org/10.1210/jc.2006-2190>

Tsao, J. C. I., Plankey, M. W., & Young, M. A. (2012). Pain, psychological symptoms and prescription drug misuse in HIV: A literature review. *Journal of Pain Management*, *5*(2), 111–118.

Tyor, W. R., & Bimonte-Nelson, H. (2018). A mouse model of HIV associated neurocognitive disorders: A brain-behavior approach to discover disease mechanisms and novel treatments. *Journal of Neurovirology*, *24*(2), 180–184. <https://doi.org/10.1007/s13365-017-0572-6>
UNAIDS. (2022). *Global HIV & AIDS statistics—Fact sheet*. UNAIDS. <https://www.unaids.org/en/resources/fact-sheet>

Valcour, V. G., Ananworanich, J., Agsalda, M., Sailasuta, N., Chalermchai, T., Schuetz, A., Shikuma, C., Liang, C.-Y., Jirajariyavej, S., Sithinamsuwan, P., Tipsuk, S., Clifford, D. B., Paul, R., Fletcher, J. L. K., Marovich, M. A., Slike, B. M., DeGruttola, V., & Shiramizu, B. (2013). HIV DNA Reservoir Increases Risk for Cognitive Disorders in cART-Naïve Patients. *PLoS ONE*, *8*(7), e70164. <https://doi.org/10.1371/journal.pone.0070164>

Van den Hof, M., Blokhuis, C., Cohen, S., Scherpbier, H. J., Wit, F. W. N. M., Pistorius, M. C. M., Kootstra, N. A., Teunissen, C. E., Mathot, R. A. A., & Pajkrt, D. (2018). CNS penetration of ART in HIV-infected children. *Journal of Antimicrobial Chemotherapy*, *73*(2), 484–489. <https://doi.org/10.1093/jac/dkx396>

Van Zee, A. (2009). The Promotion and Marketing of OxyContin: Commercial Triumph, Public Health Tragedy. *American Journal of Public Health*, *99*(2), 221–227. <https://doi.org/10.2105/AJPH.2007.131714>

Wang, M.-R., Wu, D.-D., Luo, F., Zhong, C.-J., Wang, X., Zhu, N., Wu, Y.-J., Hu, H.-T., Feng, Y., Wang, X., Xiong, H.-R., & Hou, W. (2020). Methadone Inhibits Viral Restriction Factors and Facilitates HIV Infection in Macrophages. *Frontiers in Immunology*, *11*, 1253. <https://doi.org/10.3389/fimmu.2020.01253>

Weiss, J. M., Nath, A., Major, E. O., & Berman, J. W. (1999). HIV-1 Tat Induces Monocyte Chemoattractant Protein-1-Mediated Monocyte Transmigration Across a Model of the Human Blood-Brain Barrier and Up-Regulates CCR5 Expression on Human Monocytes. *The Journal of Immunology*, *163*(5), 2953–2959.

Williams, D. W., Calderon, T. M., Lopez, L., Carvallo-Torres, L., Gaskill, P. J., Eugenin, E. A., Morgello, S., & Berman, J. W. (2013). Mechanisms of HIV Entry into the CNS: Increased Sensitivity of HIV Infected CD14+CD16+ Monocytes to CCL2 and Key Roles of CCR2, JAM-A, and ALCAM in Diapedesis. *PLoS ONE*, *8*(7). <https://doi.org/10.1371/journal.pone.0069270>

Wolburg, H., Wolburg-Buchholz, K., & Engelhardt, B. (2005). Diapedesis of mononuclear cells across cerebral venules during experimental autoimmune encephalomyelitis leaves tight

junctions intact. *Acta Neuropathologica*, 109(2), 181–190. <https://doi.org/10.1007/s00401-004-0928-x>

Wong, J. K., & Yukl, S. A. (2016). Tissue Reservoirs of HIV. *Current Opinion in HIV and AIDS*, 11(4), 362–370. <https://doi.org/10.1097/COH.0000000000000293>

World Health Organization. (2016). *Consolidated guidelines on HIV prevention, diagnosis, treatment and care for key populations* (2016 update). World Health Organization. <https://apps.who.int/iris/handle/10665/246200>

Xiao, H., Neuveut, C., Tiffany, H. L., Benkirane, M., Rich, E. A., Murphy, P. M., & Jeang, K.-T. (2000). Selective CXCR4 antagonism by Tat: Implications for in vivo expansion of coreceptor use by HIV-1. *Proceedings of the National Academy of Sciences of the United States of America*, 97(21), 11466–11471.

Xiaojie, Z., Yan, F., H, V. P., M, W. J., Nathalie, S., & J, H. J. (2020). Long-term HIV-1 Tat Expression in the Brain Led to Neurobehavioral, Pathological, and Epigenetic Changes Reminiscent of Accelerated Aging. *Aging and Disease*, 11(1), Article 1. <https://doi.org/10.14336/AD.2019.0323>

Yadav, A., & Collman, R. G. (2009). CNS Inflammation and Macrophage / Microglial Biology Associated with HIV-1 Infection. *Journal of Neuroimmune Pharmacology: The Official Journal of the Society on Neuroimmune Pharmacology*, 4(4), 430–447. <https://doi.org/10.1007/s11481-009-9174-2>

Yu, F., Wang, Y., Stetler, A. R., Leak, R. K., Hu, X., & Chen, J. (2022). Phagocytic microglia and macrophages in brain injury and repair. *CNS Neuroscience & Therapeutics*, 28(9), 1279–1293. <https://doi.org/10.1111/cns.13899>

Zenebe, Y., Necho, M., Yimam, W., & Akele, B. (2022). Worldwide Occurrence of HIV-Associated Neurocognitive Disorders and Its Associated Factors: A Systematic Review and Meta-Analysis. *Frontiers in Psychiatry*, 13, 814362. <https://doi.org/10.3389/fpsy.2022.814362>

Zhang, Y., Chen, Q., & Yu, L.-C. (2008). Morphine: A protective or destructive role in neurons? *The Neuroscientist: A Review Journal Bringing Neurobiology, Neurology and Psychiatry*, 14(6), 561–570. <https://doi.org/10.1177/1073858408314434>

Zlokovic, B. V. (2010). Neurodegeneration and the neurovascular unit. *Nature Medicine*, 16(12), 1370–1371. <https://doi.org/10.1038/nm1210-1370>

Zou, S., Fitting, S., Hahn, Y.-K., Welch, S. P., El-Hage, N., Hauser, K. F., & Knapp, P. E. (2011). Morphine potentiates neurodegenerative effects of HIV-1 Tat through actions at μ -opioid receptor-expressing glia. *Brain*, 134(12), 3613–3628. <https://doi.org/10.1093/brain/awr281>